https://doi.org/10.5194/egusphere-2024-3590
Preprint. Discussion started: 4 December 2024

Aerosol Composition Trends during 2000-2020: In depth insights from model predictions and multiple worldwide observation datasets

Alexandra P. Tsimpidi[1], Susanne M.C. Scholz[1], Alexandros Milousis[1], Nikolaos Mihalopoulos[2], and Vlassis A. Karydis[1]

[1] Forschungszentrum Jülich, Inst. for Energy and Climate Research, IEK-8, Jülich, Germany

[2] National Observatory of Athens, Inst. for Environm. Res. & Sustainable Dev., Athens, 15236, Greece.

Correspondence to: Alexandra P. Tsimpidi (a.tsimpidi@fz-juelich.de)

Abstract

Atmospheric aerosols significantly impact Earth's climate and air quality. In addition to their number and mass concentrations, their chemical composition influences their environmental and health effects. This study examines global trends in aerosol composition from 2000 to 2020, using the EMAC atmospheric chemistry-climate model and a variety of observational datasets. These include $PM_{2.5}$ data from regional networks and 744 PM_1 datasets from AMS field campaigns conducted at 169 sites worldwide. Results show that organic aerosol (OA) is the dominant fine aerosol component in all continental regions, particularly in areas with significant biomass burning and biogenic VOC emissions. EMAC effectively reproduces the prevalence of secondary OA but underestimates the aging of OA in some cases, revealing uncertainties in distinguishing fresh and aged SOA. While sulfate is a major aerosol component in filter-based observations, AMS and model results indicate nitrate predominates in Europe and Eastern Asia. Mineral dust also plays a critical role in specific regions, as highlighted by EMAC. The study identifies substantial declines in sulfate, nitrate, and ammonium concentrations in Europe and North America, attributed to emission controls, with varying accuracy in model predictions. In Eastern Asia, sulfate reductions due to SO_2 controls are partially captured by the model. OA trends differ between methodologies, with filter data showing slight decreases, while AMS data and model simulations suggest slight increases in PM_1 OA across Europe, North America, and Eastern Asia. This research underscores the need for integrating advanced models and diverse datasets to better understand aerosol trends and guide environmental policy.

https://doi.org/10.5194/egusphere-2024-3590
Preprint. Discussion started: 4 December 2024

1. Introduction

Atmospheric aerosols are tiny solid or liquid particulate matter (PM) suspended in the air, ranging in size from a few nanometers to several micrometers. Atmospheric aerosol, especially fine particles with diameters less than 2.5 micrometers ($PM_{2.5}$), poses health risks as it can penetrate deep into the respiratory system (Who, 2003). Long-term exposure to high levels of PM has been associated with respiratory and cardiovascular diseases (Brook et al., 2010; George et al., 2017). Dominici et al. (2006) and Pope et al. (2009) highlight the impact of PM on mortality and morbidity, while more recent studies have determined that the air pollution by $PM_{2.5}$ is responsible for more than 3 million premature deaths per year worldwide (Lelieveld et al., 2015; Who, 2022). As a result, air pollution is recognized as the largest environmental threat to human health in the recent WHO report (Who, 2021). Furthermore, aerosols can directly influence the Earth's climate by scattering and absorbing sunlight, leading to changes in radiation balance (Haywood and Boucher, 2000; Ipcc, 2013). Aerosols can also affect the Earth's energy balance indirectly through interactions with clouds, i.e., by serving as cloud condensation (CCN) and ice (IN) nuclei, affecting cloud formation, cloud properties, and precipitation patterns (Andreae and Rosenfeld, 2008). Beside the number and mass concentrations of atmospheric aerosol, its chemical composition determines its aerosol-related climatic (Klingmuller et al., 2019; Klingmüller et al., 2020; Kok et al., 2023) and health impacts (Lelieveld et al., 2015; Fang et al., 2017; Karydis et al., 2021).

Atmospheric aerosols have various precursors, and they can be categorized into primary and secondary aerosols based on their origin. Primary sources include natural processes such as volcanic eruptions, wildfires, and sea spray, as well as human activities like industrial emissions and transportation. Secondary aerosols are formed through the oxidation of gas phase pollutants in the atmosphere. Sulfate aerosols are formed through the oxidation of sulfur dioxide (SO_2) which is primarily released from the burning of fossil fuels, particularly coal, and natural sources like volcanoes. Nitrate aerosols result from the atmospheric oxidation of nitrogen oxides (NO_x) emitted from combustion processes, such as those in vehicles and power plants. Ammonium is formed by the reaction of ammonia (NH_3), which is emitted from agricultural activities and waste treatment, with an acid. Secondary organic aerosols (SOA) can form through the oxidation of volatile organic compounds (VOCs), which are emitted from vegetation, industrial processes, and vehicle exhaust.

https://doi.org/10.5194/egusphere-2024-3590
Preprint. Discussion started: 4 December 2024

Several measures have been discussed and implemented to mitigate pollutants emitted from specific source sectors including transport, energy (power generation, industries etc.), waste management, urban planning and agriculture. A few of the most prominent global conferences that have taken place for the purpose of combating climate change and air pollution are the Conferences of the Parties (COP) since the early 90s, and the supreme decision-making body of the United Nations' Framework Convention on Climate Change (UNFCCC). Their passed agreements binding the parties to individual emission targets are for instance the Agenda 21 of 1992, the Kyoto Protocol of 1997 and its successor - the Paris Agreement of 2015. Besides these global agreements, the single parties had to implement national or continental plans to meet air quality requirements. The resulting emission trends have been so drastic that aerosol composition has been unevenly altered in different parts of the world. Most European countries are bound by the Gothenburg Protocol targets from 1999 and its amendment from 2012 and have in majority successfully reduced pollutant levels (Emep, 2021). SO_x emissions have declined the most, by more than 80% in the last two decades. NO_x emissions have declined significantly as well (by 50%), but for NH_3 only very small reductions have been achieved (~10%) (Hoesly et al., 2018; Emep, 2021). NMVOCs have also been significantly decreased due to emission controls to the transportation and the solvents sector (Hoesly et al., 2018). In the US, pollutant levels are controlled through regulations imposed by the National Ambient Air Quality Standards (NAAQS), the Regional Haze Rule and the US Clean Air act of 1970. The US and Canada are also part of the Gothenburg protocol. Over Asia, South Korea and China belong to the Newly Industrialized and high-growth economies. Especially from 1980 to the mid-2000s, pollutants emissions grew in China (Hoesly et al., 2018; Zhai et al., 2019). However, in the face of the Beijing Olympic Games in 2008, there have been drastic endeavors of air pollution control in Beijing and neighboring administrative regions (Huang et al., 2010). In 2013, the first consistent and aggressive emission controls started under the Clean Air Action (Zhai et al., 2019). The Clean Air Action has identified three target regions, the megacity clusters of Beijing-Tianjin-Hebei, Yangtze River Delta and the Pearl River Delta, while in 2018, the latter was replaced by the Fenwei Plain (Zhai et al., 2019).

Air pollution concentration levels can vary by time of day, season, across large spans of time, based on meteorological factors, and in connection to climate change. Trends analysis of air pollution concentrations (Guerreiro et al., 2014; Lang et al., 2019) can

https://doi.org/10.5194/egusphere-2024-3590
Preprint. Discussion started: 4 December 2024

allow the assessment of the impact of various factors on air quality including changes in industrial activities, traffic patterns, or energy production. Analyzing trends in air pollutants enables comparisons between different regions or countries (Anttila and Tuovinen, 2010; Chow et al., 2022; Kyllönen et al., 2020) as well as between different datasets that provide information for the same pollutant. This can highlight areas that are successfully addressing air quality issues, provide benchmarks for others to follow but also highlight any kind of inability of each method to reproduce the concentration levels of the pollutants.

In this study, we use the comprehensive atmospheric chemistry-climate model EMAC to present 20-year global composition trends of fine aerosols in different regions of the planet. Here, for the first time, EMAC uses a computationally lite version of the organic aerosol module ORACLE (Tsimpidi et al., 2014) and the new highly computationally efficient module ISORROPIA-lite (Kakavas et al., 2022; Milousis et al., 2024). The large emission trends in our model are considered by employing the Copernicus Atmosphere Monitoring Service (CAMS) inventory for anthropogenic emissions (Granier et al., 2019). Model results are combined with a global observational aerosol composition dataset to provide insights into the large spatiotemporal changes in aerosol composition over the past two decades, driven by changes in aerosol precursor emissions. The dataset includes observations from regional filter-based monitoring networks that routinely collect $PM_{2.5}$ (e.g. EMEP, IMPROVE, EPA, EANET, SPARTAN), and a unique comprehensive compilation of 744 individual Aerosol Mass Spectometer (AMS) field campaigns worldwide that provide in-situ measurements of PM_1 composition.

2. Observational Dataset

2.1 PM_1 Dataset

Since the year 2000, the quadrupole-based Aerodyne aerosol mass spectrometer (Q-AMS) and its successors enjoy great popularity as a method for atmospheric aerosol sampling. A great advantage of AMS is its ability to deliver high-resolved real-time quantitative data on mass concentration of particles between ~ 0.05 - 1 µm (Canagaratna et al., 2007) as a function of their non-refractory chemical composition (i.e., OA and inorganic SO_4^{2-}, NO_3^-, NH_4^+, and Cl^-) (Jayne et al., 2000). Thus, over the years and numerous field campaigns, a lot of valuable chemical and microphysical

https://doi.org/10.5194/egusphere-2024-3590
Preprint. Discussion started: 4 December 2024

information about ambient aerosols has been obtained (Ng et al., 2011). During 2000s, these campaigns did not last more than a month, however, the development of the Aerosol Chemical Speciation Monitor (ACSM), a small and cost-efficient version of AMS, allowed the long-term monitoring of the PM_1 composition over several locations during the 2010s.

2.1.1 AMS factor analysis techniques

The AMS spectra of OA are often further analyzed via factor analysis techniques in order to extract detailed information about the OA composition as well. Among factor analysis techniques (e.g., ME-2 (Paatero, 1999); PCA (Zhang et al., 2013); MCA (Zhang et al., 2007; Cottrell et al., 2008)), the PMF (Paatero and Tapper, 1994; Paatero, 1997) is the most popular technique, occasionally in combination with the ME-2. Overall, a mass spectrum that peaks at m/z = 44 (or f_{44}) and m/z = 43 (or f_{43}) is mostly dominated by the CO_2^+ and $C_2H_3O^+$ ions, respectively. The first is mostly linked to acidic groups (i.e, -COOH), typically associated with chemically aged and oxygenated organic aerosols (OOA), while the latter is dominated by non-acid oxygenates. OOA can be further categorized into different levels of aging and volatility stages. Most commonly, a less oxidized (semi-volatile) OA (L-OOA (Bougiatioti et al., 2014)) and a more oxidized (low-volatile) OA (M-OOA (Bozzetti et al., 2017)) are distinguished (Jimenez et al., 2009; Ng et al., 2010; Crippa et al., 2014; Stavroulas et al., 2019). The two OOA factors could be identified on the basis of the f_{44} to f_{43} ratio: M-OOA component spectra have a higher f_{44}, while L-OOA component spectra have slightly higher f_{43}. Besides these general factors, other oxygenated OA compounds have been resolved in some campaigns. One of the most important is the IEPOX-OA with abundant ions at m/z = 53, 75, or 82. This “isoprene” factor correlates strongly with molecular tracers of SOA that are derived from isoprene epoxydiols (Xu et al., 2015; Budisulistiorini et al., 2013; Budisulistiorini et al., 2016). Several campaigns in North America have found IEPOX-OA, as have campaigns in South America and Australia. Furthermore, methane-sulfonic acid (MSA) is often retrieved from datasets of marine sites (Crippa et al., 2014; Mallet et al., 2019). Some studies could identify a nitrogen-enriched OA-factor, NOA, mainly composed of amino compounds formed from industrial or marine emissions. A more local-SOA factor that is related to humic-like substances, termed as HULIS OA, found in the Netherlands (Schlag et al., 2016) and in Crete (Crippa et al., 2014). In Greece (Bougiatioti et al., 2014; Stavroulas et al., 2019;

https://doi.org/10.5194/egusphere-2024-3590
Preprint. Discussion started: 4 December 2024

Vasilakopoulou et al., 2023), in the Amazonian (De Sá et al., 2019) and often in Asia (Zhang et al., 2015b; Chakraborty et al., 2015; Du et al., 2015) OOA factors directly associated with biomass burning were found, that are processed from fresh biomass burning emissions. Furthermore, OOA compounds that are verifiable only biogenically oxygenated were also derived (Kostenidou et al., 2015).

Apart from the mass spectrum, OA types can also be distinguished by their oxygen to carbon ratio (O:C), which is an indicator of photochemical aging. Primary organic aerosol (POA) is fresh and has a lower oxygen content than OOA, therefore lower O:C ratios. Yet, it sometimes has the same dominant m/z peaks. Some of the most commonly resolved POA factors are the Hydrocarbon-like (HOA) and Biomass Burning (BBOA) OA. HOA has spectra that are distinguished by clear hydrocarbon signatures, dominated by the ion series $C_nH_{2n+1}^+$ and $C_nH_{2n-1}^+$ (Ng et al., 2010). HOA correlates with fossil fuel combustion tracers like NO_x, CO and elemental carbon (Lanz et al., 2008; Tsimpidi et al., 2016), therefore, is very often observed to be traffic-related and a rather dominant POA factor in urban areas (Crippa et al., 2014; Xu et al., 2015; Budisulistiorini et al., 2016). On the other hand, BBOA typically originates from forest and savanna fires as well as from anthropogenically induced agricultural fires (Hoesly et al., 2018) and residential wood burning for heating. This makes the contribution of BBOA to total OA highly episodic (Zhang et al., 2007) and seasonal, and in several cases underestimated due to the rapid physicochemical transformation of these emissions to OOA (Stavroulas et al., 2019; Vasilakopoulou et al., 2023). Typical tracers to identify BBOA in the spectra are gas-phase acetonitrile, particle-phase levoglucosan and potassium (K^+) (Lanz et al., 2010; Crippa et al., 2014). However, its mass spectra are also highly variable since they can be affected by different types of wood and burning conditions (Crippa et al., 2014).

Furthermore, a coal combustion factor (CCOA) is often identified, which presents a dominant contribution to POA during the heating season, mostly in Eastern Asia (Sun et al., 2013; Zhang et al., 2014). In many cases, HOA shows remarkably similar spectral patterns as CCOA, so that these two factors could not be separated and, instead, are combined in a fossil fuel related OA factor (FFOA) (Sun et al., 2018; Xu et al., 2019). Another relatively frequent primary type resolved by the factor analysis is the cooking related OA (COA) (Mohr et al., 2012). Its spectral pattern is governed by OA from fresh cooking emissions and, fittingly, the spectral profiles have a distinct diurnal cycle which corresponds to typical (local) meal hours (Mohr et al., 2012; Sun et al., 2013;

https://doi.org/10.5194/egusphere-2024-3590
Preprint. Discussion started: 4 December 2024

Stavroulas et al., 2019). Occasionally, special types of COA are also resolved, including coffee roastery OA (Timonen et al., 2013) and OA related to charbroiling (Lanz et al., 2007).

2.1.2 AMS Dataset

Here, a collection of AMS and ACSM field campaign datasets during the period of 2000-2020 has been compiled. The dataset covers a wide range of environments and seasons from almost every continental region worldwide (Figure 1), characterized by a variety of atmospheric and climatological conditions as well as sources of pollutants. The selected field campaigns lasted from at least one full week to several months. Individual campaigns lasting more than one month are divided into shorter periods of preferably only one month. All of these individual periods of campaign data (thus covering a maximum of one month) are hereafter referred to as individual datasets.

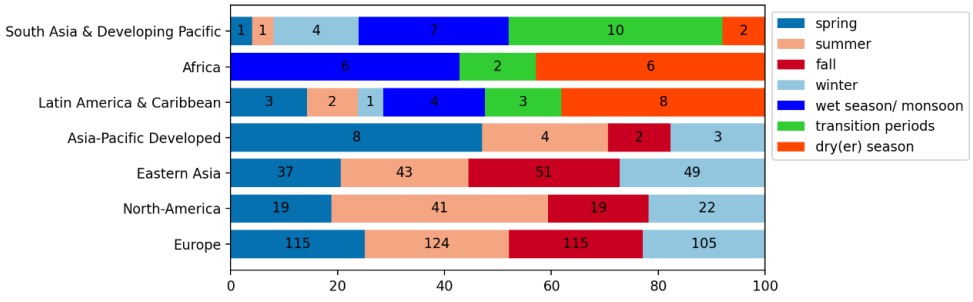

Figure 1: Seasonal distribution of datasets per subcontinent. The colored bars indicate the relative proportions by season. The numbers in the colored boxes indicate the absolute number of field campaigns that occurred in each season.

The number of both PM_1 and OA composition datasets found for each year is increasing significantly for all regions through the years (Figure 2) due to the growing popularity of the AMS devices and the continuous improvement of the analysis

https://doi.org/10.5194/egusphere-2024-3590
Preprint. Discussion started: 4 December 2024

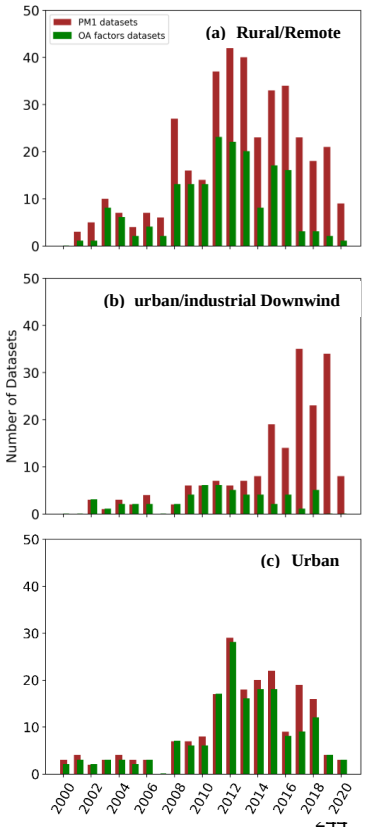

Figure 2: Total AMS (dark red) and factor analysis (green) datasets per year in (a) rural, (b) urban-downwind, and (c) urban regions

techniques. Especially during the second decade, the number of field campaigns increase drastically, supported by the use of ACSM devices since 2010. The long-term campaigns in South Africa (2010-2011; (Tiitta et al., 2014)) and the Southern Great Planes (2010- 2012; (Parworth et al., 2015)) belong to the very first where the ACSM has been utilized. Furthermore, campaigns in regions downwind of urban environments have gotten a growing attention mostly after 2014, primarily in Europe. However, usually these datasets are not factor analyzed and lack information for the OA composition. It is worth mentioning that the small number of downwind datasets available can partially attributed to the ambiguous definition of downwind sites, which might have led instead to the more conventional classifications of rural or urban locations in some cases.

Overall, the compiled dataset includes PM_1 aerosol composition from 744 AMS field campaigns datasets at 169 observational sites around the world, while factor analysis has been used to estimate the OA composition in 398 cases at 140 different observational sites (Table S1). The dataset includes an intermediate level regional breakdown following the sixth assessment report of IPCC working group III (Ipcc, 2022) as shown in Figure 3. The most represented subcontinents are Europe, Eastern Asia and North America. Datasets from these three northern-hemisphere continents are more or less evenly distributed over the seasons with only a little imbalance for North America which is over-represented during summer (Figure 1). The rest of the regions include a significantly lower number of datasets; therefore, the seasonal distribution is often very uneven. As an example, 50% of the data over the Asia-Pacific Developed region has been collected during spring. On the contrary, the

https://doi.org/10.5194/egusphere-2024-3590
Preprint. Discussion started: 4 December 2024

changes between the wet and dry seasons are well represented over Africa where the ACSM has been employed for year-long campaigns (Tiitta et al., 2014).

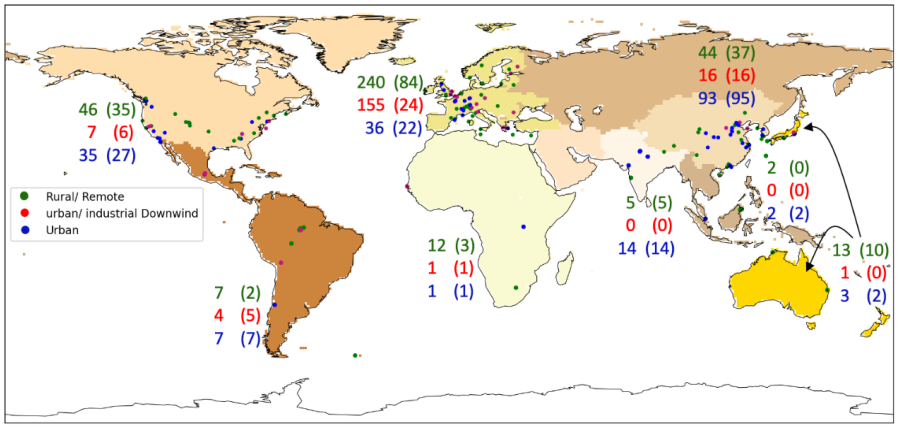

Figure 3: Worldwide distribution of AMS and ACSM datasets for the of period 2000 - 2020. The world map is colored according to the intermediate level regional breakdown of the sixth assessment report of IPCC working group III (IPCC, 2022). The rural (green), downwind (red) and urban (blue) campaign locations and the total number of PM_1 composition (and OA factor analysis in parenthesis) datasets for each region are also shown.

2.1.3 Observed PM_1 Aerosol Composition

The PM_1 aerosol composition derived from AMS field campaigns at 8 regions around the world is depicted in Figure 4. The analysis of the AMS dataset reveals that OA is the dominant component of PM_1 in all continental regions. Campaign data from tropical or subtropical regimes (e.g., Latin America and Southern/Southeast Asia) is strongly affected by biomass burning and biogenic VOC emissions, illustrating remarkably high OA fractions with regional means around 65% and a maximum of 92% in the Amazonian. However, OA concentration shares up to 90% are also found over the Northern Hemisphere regions where the regional average OA contribution to PM_1 concentrations is around 50%. Overall, OA contributes between 17 - 92% (50% on average) of total PM_1. This agrees well with the ranges reported by Kanakidou et al. (2005) (20%-90%) and Zhang et al. (2007) (18%-70% or 45% on average). Sulfate has been the dominant inorganic compound in the aerosol composition in most regions

https://doi.org/10.5194/egusphere-2024-3590
Preprint. Discussion started: 4 December 2024

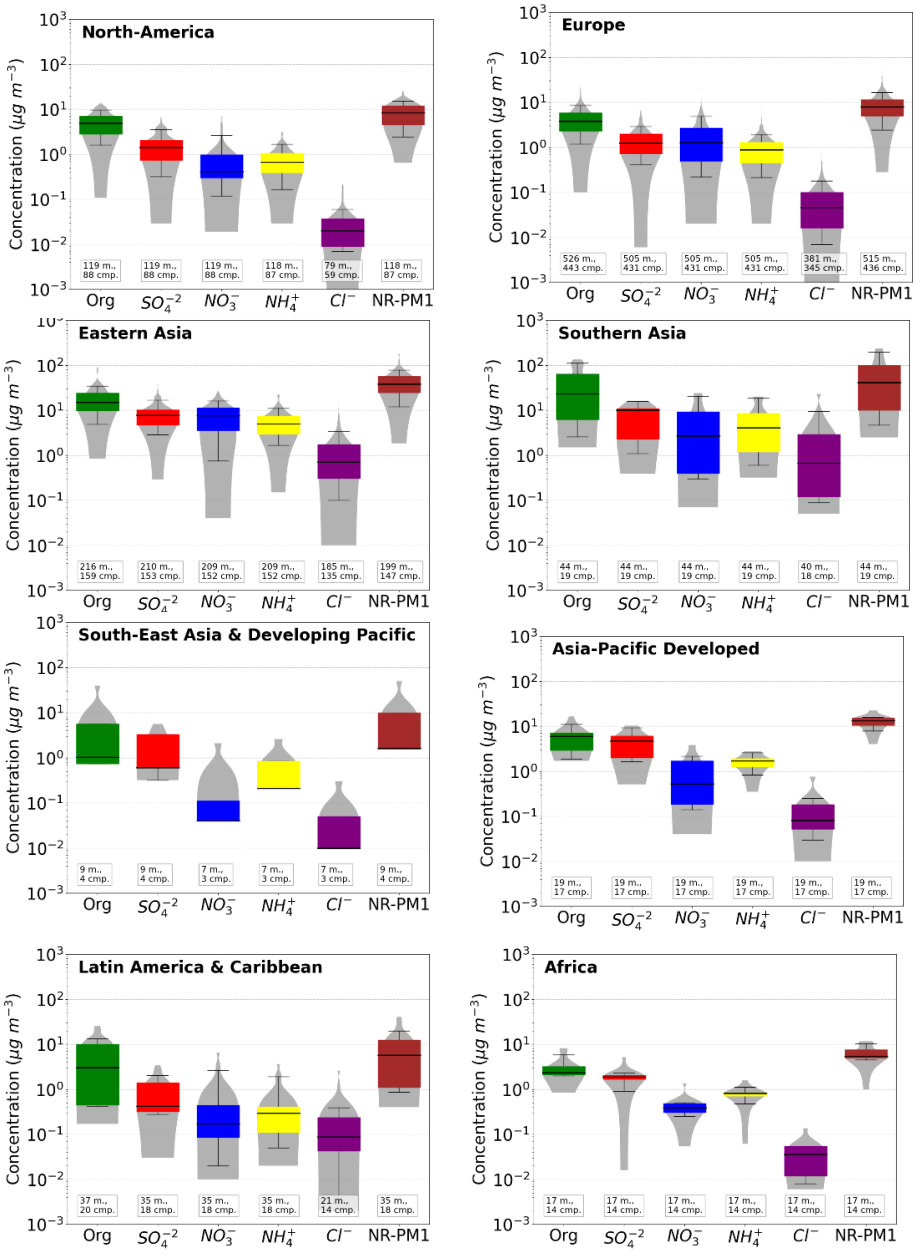

Figure 4: Bar chart plots depicting the distribution (violin) and the 25th, 50th and 75th percentiles (box) of the mass concentration (in μg m^{-3}) for the major PM_1 aerosol components, i.e., organic aerosol (green), sulfate (red), nitrate (blue), ammonium (yellow), chloride (purple), and the total non-refractive PM_1 (dark red). The 10th and 90th percentiles (whiskers) for each aerosol component are also shown. The number of total months (m.) with AMS data and the number of campaigns (cmp.) is written in small boxes under the violins.

275

https://doi.org/10.5194/egusphere-2024-3590
Preprint. Discussion started: 4 December 2024

(Figure 4). The highest regional average share of sulfate is found over Asia-Pacific Developed (37%) while the lowest over Europe (17%) where SO_2 has been drastically reduced due to strict air pollution mitigation strategies. Nitrate dominates over sulfate over Europe and Eastern Asia. However, it is surprising that the PM_1 inorganic composition of North America is dominated by sulfate, even though similar mitigation strategies have been enforced as in Europe. This might be due to an over-representation of summer data in North America (Figure 1) which resulted in lower nitrate concentrations since higher temperatures hinder the condensation of nitric acid in the aerosol phase. At the same time, sulfate concentrations are higher during summer due to the increased photochemical production of H_2SO_4. Overall, nitrate concentrations are highest in winter in Europe and North America, accounting for roughly a quarter of total PM_1 (Figures S1 and S2). A similar proportion is observed in spring, although the absolute concentration is lower. The lowest average nitrate concentrations and shares occur in summer, when sulfate peaks and dominates the inorganic composition. Although both sulfate and nitrate are generated through photochemical reactions, this seasonal shift is due to nitric acid remaining in the gas phase at higher temperatures. Additionally, the increased production of sulfuric acid reduces the amount of free ammonia available for ammonium nitrate formation, further contributing to the summer nitrate decline (Seinfeld and Pandis, 2006). Ammonium concentrations remain relatively stable throughout the seasons, presenting similar shares of PM_1 (Figures S1 and S2). However, in contrast to Europe and North America, sulfate concentrations in East Asia are highest in winter, closely followed by summer (Figure S3). While photochemical reactions still dominate during warmer, sunnier seasons, aqueous phase reactions are more influential in East Asian winter, particularly under high relative humidity (RH) and severe haze conditions. These factors are often present in Chinese winters and likely explain this regional pattern (Zhang et al., 2015a; Zhou et al., 2020a). Over the southern regions, ammonium follows sulfate in the inorganic aerosol composition due to the high agricultural activities. Overall, the global average contribution of the inorganic compounds to total PM_1 concentration is 20%, 18%, and 11%, and 1% by sulfate, nitrate, ammonium, and chloride, respectively. However, Zhang et al. (2007) reported much stronger contribution by sulfate (32%), less by nitrate (10%), and similar values of ammonium (13%) and chloride (1%). Given that Zhang et al. (2007) utilized AMS observations from the early 2000s, this is a first indication that the inorganic aerosol composition has been altered during the last 20 years.

https://doi.org/10.5194/egusphere-2024-3590
Preprint. Discussion started: 4 December 2024

2.1.4 Observed PM_1 Organic Aerosol Composition

HOA concentrations are observed to be higher over North America and Eastern Asia in comparison to Europe (Figure 5). This could be explained by the significant influence of traffic emissions on HOA in the vicinity of urban areas. While urban locations are equally represented with rural sites in the dataset collection of North America and Eastern Asia, in Europe, rural sites are immensely over-represented (3 times more than urban sites), diminishing the importance of HOA. On the other side, the over-representation of rural sites in the European dataset resulted in high concentrations of BBOA which is found to be the dominant primary source of OA in the region (Lanz et al., 2010). Here, BBOA originates mostly from domestic wood burning during the colder seasons in central Europe, including the Alps, rather than from open biomass burning. Even though a few campaigns took place in the European boreal forests, only very few factor analyses have distinguished BBOA as an individual component. Thus, the contribution of European boreal forests to total European BBOA is unfortunately not clear yet. Similarly, biomass burning is an important source of OA in North America and Eastern Asia (Rattanavaraha et al., 2017; Zhou et al., 2020b) but less important than HOA (Figure 5). Biomass burning also presents an especially important source in tropical and subtropical regions (i.e., South Asia and the Developing Pacific, Africa, and Latin America and Caribbean) due to episodic wildfires and harvest related burning (Budisulistiorini et al., 2018; Cash et al., 2021). Overall, the concentration range of BBOA is very high since it varies a lot with season. However, it should be emphasized that the availability of factor analysis datasets in equatorial and southern hemisphere continents is very low and therefore, there is not enough data available for statistically profound statements. The last primary type of OA, COA, is population dependent and therefore is mainly found in urban areas and highly populated regions (Zhou et al., 2020b). Cooking is a very constant and local source throughout the year with low variability and high contributions over Eastern Asia, Europe, North America, and South Asia and developing Pacific, especially in urban campaign sites.

OOA is unequivocally the dominant contributor to total OA with a mean share of 60% in urban and 75% in rural regions. Overall, the OOA contribution range from 19% (urban minimum) to 99% (rural maximum). The extreme shares were both found during European campaigns. The mean OOA share in Europe however lies roughly in the same magnitude as the global mean (~70%). The dominant OOA subfactors resolved are L-OOA and M-OOA, while the more aged M-OOA dominates in the OA composition of

https://doi.org/10.5194/egusphere-2024-3590
Preprint. Discussion started: 4 December 2024

all examined regions (~60% of total OOA). This agrees with the findings of Ng et al. (2010), who stated that OOA component spectra become increasingly similar to each other with atmospheric oxidation, indicating that ambient OA converges towards highly aged M-OOA.

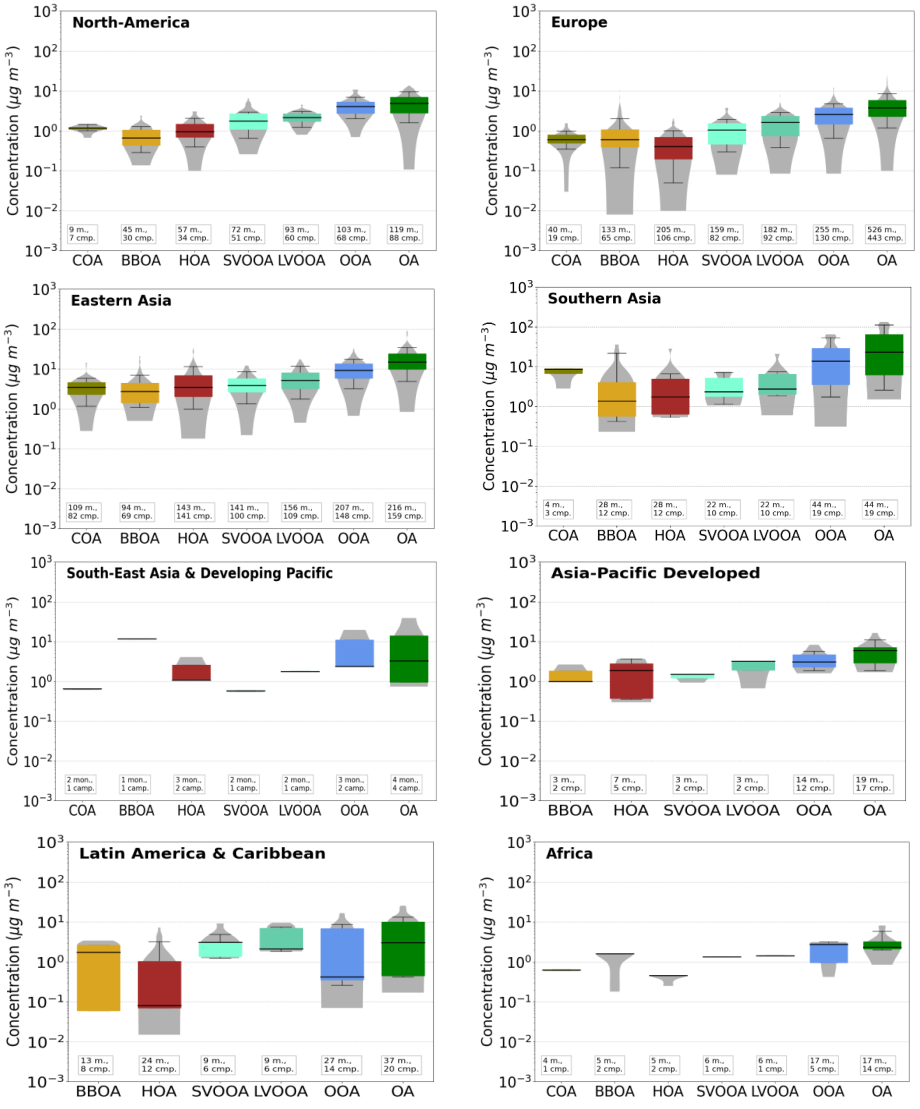

Figure 5: Bar chart plots depicting the distribution (violin) and the 25th, 50th and 75th percentiles (box) of the mass concentration (in μg m^{-3}) for the major PM_1 OA components calculated from the collected factor analysis datasets, i.e., COA (olive green), BBOA (orange), HOA (dark red), L-OOA (light turquoise), M-OOA (dark turquoise), OOA (blue), and total OA (green). The 10th and 90th percentiles (whiskers) for each aerosol component are also shown. The number of datasets (m.) and the number of campaigns (cmp.) is written in small boxes under the violins.

https://doi.org/10.5194/egusphere-2024-3590
Preprint. Discussion started: 4 December 2024

2.2 $PM_{2.5}$ Dataset

Routine filter measurement $PM_{2.5}$ data from large observational networks in East Asia, Europe and North America is used. The filter samplers have three modules that independently collect $PM_{2.5}$ species on a Teflon, a nylon and a quartz filter. The aerosol chemical composition is determined by further analysis of the filters in the laboratory via ion chromatography (inorganic ions), thermal-optical analysis (OC and EC), and X-ray fluorescence (XRF; trace elements) (Solomon et al., 2014). Potential difficulties that could arise when comparing on-line AMS and ACSM PM_1 composition to off-line filter based $PM_{2.5}$ composition, are discussed in section 5. The Environmental Protection Agency (EPA) network includes 211 monitor sites primarily in urban areas of North America. The data used here cover monthly averaged $PM_{2.5}$ aerosol component measurements during 2000-2018 (https://aqs.epa.gov/aqsweb/airdata/download_files.html). The Interagency Monitoring of Protected Visual Environments (IMPROVE) network includes 198 monitoring sites that are representative of the regional haze conditions over North America. IMPROVE samplers collect 24-hour samples, every three days. The data used here cover monthly averaged $PM_{2.5}$ aerosol component measurements during 2000-2018 (http://views.cira.colostate.edu/fed/QueryWizard/Default.aspx). It is worth mentioning that ammonium measurements by IMPROVE are only available until the year 2006. The European Monitoring and Evaluation Programme (EMEP) network monitors the long-range transmission of air pollutants in Europe and Eastern Eurasia (Figure 6). This network includes 70 monitoring sites. The data used here cover monthly averaged $PM_{2.5}$ aerosol component measurements during 2000-2018 (https://www.emep.int/). Finally, the Acid Deposition Monitoring Network in East Asia (EANET) network includes 39 (18 remote, 10 rural, 11 urban) air concentration monitor sites in Eurasia, Eastern Asia, South-East Asia and Developing Pacific, and Asia-Pacific Developed. The data used here cover monthly averaged $PM_{2.5}$ aerosol component measurements during 2001-2017 (https://www.eanet.asia/). The global particulate matter network SPARTAN (Snider et al., 2015; Snider et al., 2016) includes a global federation of ground-level PM2.5 monitors situated primarily in highly populated regions around the word (i.e,, North America, Latin America and Caribbean, Africa, Middle East, Southern Asia, Eastern Asia, South-Eastern Asia and Developing Pacific) (Figure 6). The data used here covers monthly averaged $PM_{2.5}$ aerosol component measurements of sulfate, nitrate, ammonium and sodium during 2013-2019

https://doi.org/10.5194/egusphere-2024-3590
Preprint. Discussion started: 4 December 2024

(https://www.spartan-network.org/). Finally, $PM_{2.5}$ aerosol component measurements from individual observational field campaigns over Latin America and Caribbean, Africa, Europe, Eastern Asia, and Asia-Pacific Developed reported as campaign averages in the literature are used (Wang et al., 2019; Radhi et al., 2010; Favez et al., 2008; Mkoma, 2008; Mkoma et al., 2009; Weinstein et al., 2010; Celis et al., 2004; Bourotte et al., 2007; Fuzzi et al., 2007; Mariani and De Mello, 2007; Martin et al., 2010; Souza et al., 2010; Gioda et al., 2011; Molina et al., 2010; Molina et al., 2007; Kuzu et al., 2020; Aggarwal and Kawamura, 2009; Batmunkh et al., 2011; Cho and Park, 2013; Feng et al., 2006; Li et al., 2010; Pathak et al., 2011; Zhang et al., 2012; Zhao et al., 2013).

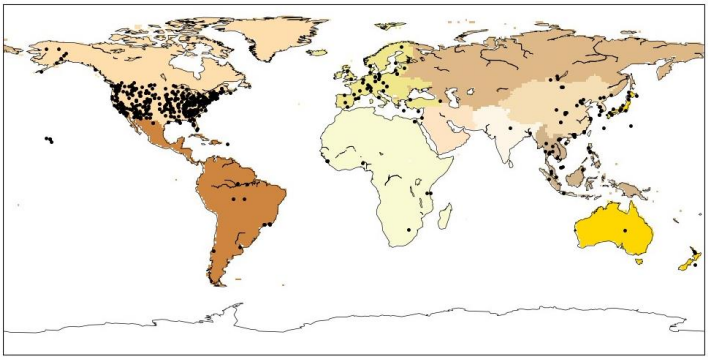

Figure 6: Worldwide distribution of filter-based observations for the period of 2000-2020. The world map is colored following the intermediate level regional breakdown of the sixth assessment report of IPCC working group III (IPCC, 2022). The black dots correspond to the location of the monitor stations.

2.2.1 $PM_{2.5}$ Aerosol Composition

The $PM_{2.5}$ aerosol composition derived from filter observations around the world is depicted in Figure 7. OA is the dominant component of $PM_{2.5}$ in most regions, especially over regions affected by the tropical forests of the southern hemisphere (e.g., Latin America & Caribbean and Africa). Over the Northern Hemisphere, OA and EC dominate the aerosol composition in Eastern Asia (54% and 22% of total $PM_{2.5}$, respectively) and contribute significantly to $PM_{2.5}$ over Europe (30% and 5% of total $PM_{2.5}$, respectively). On the other hand, over North America, OA share is equally important to sulfate over rural areas (28% of total $PM_{2.5}$ each) and less important over urban areas (24% versus 33% of sulfate). Indeed, sulfate is the most important inorganic component of $PM_{2.5}$ around the world (~50% of the inorganic $PM_{2.5}$ mass on average) followed by nitrate and ammonium (~20% each). This contradicts the results from AMS

https://doi.org/10.5194/egusphere-2024-3590
Preprint. Discussion started: 4 December 2024

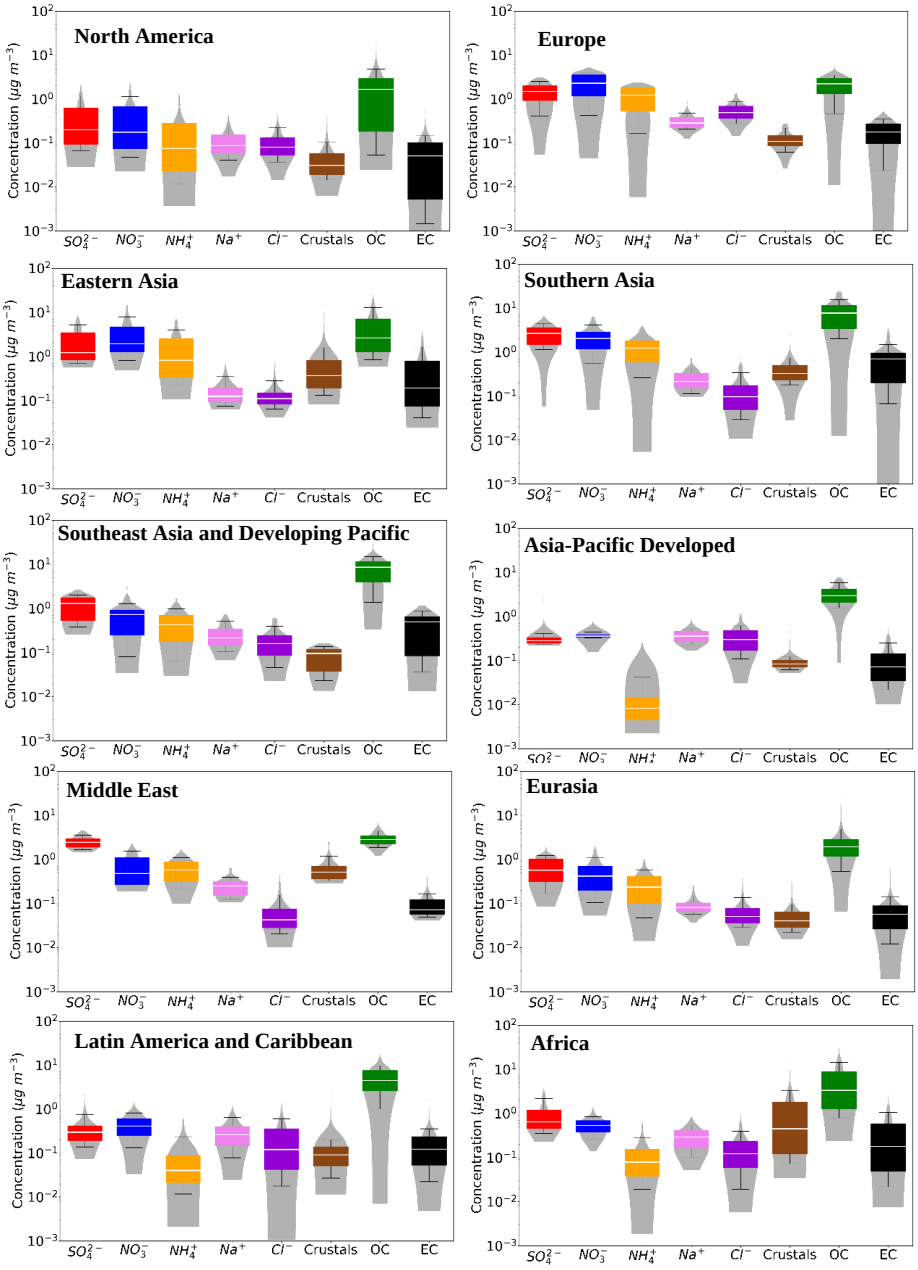

Figure 7: Bar chart plots depicting the distribution (violin) and the 25th, 50th and 75th percentiles (box) of the mass concentration (in μg m^{-3}) for the major $PM_{2.5}$ aerosol components, i.e., sulfate (red), nitrate (blue), ammonium (yellow), sodium (pink), chloride (purple), crustal ions (brown), organic aerosol (green), and elemental carbon (black). The 10th and 90th percentiles (whiskers) for each aerosol component are also shown.

405

https://doi.org/10.5194/egusphere-2024-3590
Preprint. Discussion started: 4 December 2024

campaigns showing that ammonium nitrate surpasses ammonium sulfate in the aerosol composition, especially over Europe and North America. However, filter measurements are prone to negative sampling artifacts due to evaporation losses of the semivolatile ammonium nitrate under warm and dry conditions (Ames and Malm, 2001), in contrast to the nonvolatile sulfate aerosols (Docherty et al., 2011). The contribution of sulfate to the measured inorganic $PM_{2.5}$ aerosol composition is highest over Middle East, while nitrate contributes significantly over Europe (Figure 7). The dominant inorganic ion varies with the season (Figures S1-S3). Nitrate is most important in winter, accounting for about a quarter of total PM2.5, while sulfate is the dominant PM2.5 component in summer and spring. Over the 8 regions where all 7 components are measured, the average contribution of each species to total $PM_{2.5}$ concentration is 21%, 12%, 10%, 2%, 3%, and 40%, and 12% by sulfate, nitrate, ammonium, sodium, chloride, OA, and EC respectively.

3 Model calculated Dataset

The ECHAM/MESSy Atmospheric Chemistry (EMAC) model is used, a numerical chemistry and climate simulation system that includes sub-models describing atmospheric processes from the troposphere to the mesosphere and their interaction with oceans, land, and human influences (Jöckel et al., 2006). EMAC uses the Modular Earth Submodel System (MESSy2) (Jöckel et al., 2010) to link the different sub-models with an atmospheric dynamical core, being an updated version of the 5th generation European Centre - Hamburg general circulation model (ECHAM5) (Roeckner et al., 2006). The EMAC model has been extensively described and evaluated against observations and satellite measurements and can be applied to a range of spatial resolutions (Tsimpidi et al., 2016; Karydis et al., 2016; Janssen et al., 2017; Tsimpidi et al., 2018; Pozzer et al., 2022; Milousis et al., 2024). The spectral resolution used in this study is T63L31, corresponding to a horizontal grid resolution of 1.875°x1.875° and 31 vertical layers extending to 10 hPa at about 25 km from the surface. The presented model simulations cover the period 2000–2020.

3.1 Model configuration

In the model configuration used, EMAC calculates fields of gas phase species online through the Module Efficiently Calculating the Chemistry of the Atmosphere (MECCA) submodel (Sander et al., 2019). MECCA calculates the concentration of a

https://doi.org/10.5194/egusphere-2024-3590
Preprint. Discussion started: 4 December 2024

range of gases, including aerosol precursor species such as SO_2, NH_3, NO_x, DMS, H_2SO_4 and DMSO. The concentrations of the major oxidant species (OH, H_2O_2, NO_3, and O_3) are also calculated online. The loss of gas phase species to the aerosol through heterogeneous reactions (e.g., N_2O_5 to form HNO_3) is treated using the MECCA_KHET submodel (Jöckel et al., 2010). The aqueous phase oxidation of SO_2 and the uptake of HNO_3 and NH_3 in cloud droplets are treated by the SCAV submodel (Tost et al., 2006; Tost et al., 2007).

Aerosol microphysics and gas/aerosol partitioning are calculated by the Global Modal-aerosol eXtension (GMXe) module (Pringle et al., 2010). The aerosol size distribution is described by 7 interacting lognormal modes (4 hydrophilic and 3 hydrophobic modes). The modes cover the aerosol size spectrum (nucleation, Aitken, accumulation and coarse). The aerosol composition within each mode is uniform with size (internally mixed), though can vary between modes (externally mixed). The removal of gas and aerosol species through dry deposition is calculated within the DRYDEP submodel (Kerkweg et al., 2006) based on the big leaf approach. The sedimentation of aerosols is calculated within the SEDI submodel (Kerkweg et al., 2006) using a first order trapezoid scheme. Cloud properties and microphysics are calculated by the CLOUD submodel utilizing the detailed two-moment microphysical scheme of Lohmann and Ferrachat (2010) and considering a physically based treatment of the processes of liquid (Karydis et al., 2017) and ice crystal (Bacer et al., 2018) activation.

3.2 State of the art modules for the inorganic thermodynamics

The inorganic aerosol composition is computed with the ISORROPIA-lite thermodynamic equilibrium model (Kakavas et al., 2022) as implemented in EMAC by Milousis et al. (2024). ISORROPIA-lite is an accelerated and simplified version of the widely used ISORROPIA-II aerosol thermodynamics model which calculates the gas/liquid/solid equilibrium partitioning of the K^+-Ca^{2+}-Mg^{2+}-$NH4^+$-Na^+-$SO4^{2-}$-NO^{3-}-Cl^--H_2O aerosol system. ISORROPIA-lite assumes that the aerosol is always in a metastable state (i.e., it is composed only of a supersaturated aqueous phase) and uses binary activity coefficients from precalculated look-up tables to minimize the computational cost. ISORROPIA-lite provides almost identical results with ISORROPIA-II in a metastable mode and reduces its computational cost by 35% (Kakavas et al., 2022). The application of ISORROPIA-lite in EMAC improved the

https://doi.org/10.5194/egusphere-2024-3590
Preprint. Discussion started: 4 December 2024

computational speed of the model by 4% (Milousis et al., 2024). The assumption of thermodynamic equilibrium is a good approximation for fine mode aerosols which can reach equilibrium within the time frame of one model timestep. However, the equilibrium timescale for large particles is typically larger than the timestep of the model (Meng and Seinfeld, 1996). To account for kinetic limitations, the process of gas/aerosol partitioning is calculated in two stages (Pringle et al., 2010). In the first stage the amount of the gas phase species that are able to kinetically condense onto the aerosol phase within the model timestep is calculated assuming diffusion limited condensation (Vignati et al., 2004). In the second stage ISORROPIA-lite re-distributes the mass between the gas and the aerosol phase assuming instant equilibrium between the two phases.

3.3 State of the art module for organic aerosol

The organic aerosol composition and evolution in the atmosphere is calculated by the ORACLE module (Tsimpidi et al., 2024). ORACLE is a computationally efficient version of the ORACLE module (Tsimpidi et al., 2014) which simulates a wide variety of semi-volatile organic products separating them into bins of logarithmically spaced effective saturation concentrations. ORACLE minimizes the number of surrogate species used to describe POA and SOA formation from different emission sources, while at the same time it reproduces similar total organic aerosol mass concentrations with the ORACLE module (Tsimpidi et al., 2024). In this application ORACLE uses three surrogate species with effective saturation concentration at 298 K of $C^* = 10^{-2}$, 10^{1}, and 10^{4} μg m^{-3} to cover the volatility range of LVOCs, SVOCs and IVOCs emissions from biomass burning and other combustion sources (biofuel and fossil fuel combustion, and other urban sources). These organic compounds are allowed to partition between the gas and aerosol phases resulting in the formation of POA. The least volatile fraction, at 10^{-2} μg m^{-3}, describes the low volatility organics in the atmosphere that are mostly in the particulate phase even in remote locations. The 10 μg m^{-3} volatility bin describes the semivolatile organics in the atmosphere which partition between the particle and gas phase at atmospheric conditions. Finally, even under highly polluted conditions the majority of the material in the 10^{4} μg m^{-3} volatility bin will exist almost exclusively in the vapor phase. Photochemical reactions that modify the volatility of the emitted organic compounds that remain in the gas phase are taken into account and the oxidation products are simulated separately in the module to keep

https://doi.org/10.5194/egusphere-2024-3590
Preprint. Discussion started: 4 December 2024

track of the SOA formation from SVOC and IVOC emissions. LVOCs are not allowed to participate in photochemical reactions since they are already in the lowest volatility bin. A similar approach is followed for SOA formed from VOCs. In the this version of ORACLE, it is assumed that the oxidation of the anthropogenic and biogenic VOC species results in two products for each precursor distributed in two volatility bins with effective saturation concentrations at 298 K equal to 1 and 10^3 μg m^{-3} at 298 K. Overall, we have assumed that functionalization and fragmentation processes after any subsequent photochemical aging as a result of the reaction with OH results in a net average decrease of volatility by a factor of 10^3 for SOA produced by SVOC/IVOC and anthropogenic VOC, without a net average change of volatility for SOA produced by biogenic VOC (Tsimpidi et al., 2024). In total 18 organic compounds are simulated explicitly, i.e., 9 in each of the gas and aerosol phases. Based on the saturation

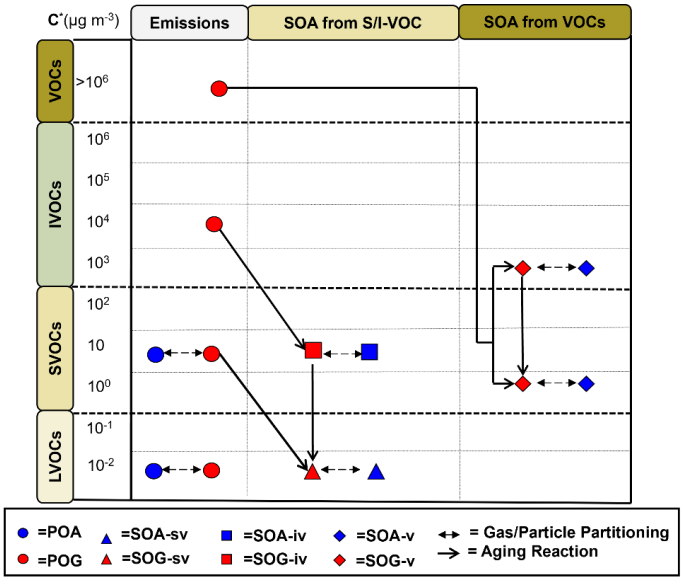

Figure 8: Schematic of the VBS resolution and the formation procedure of POA and SOA from LVOCs, SVOCs, IVOCs and VOCs emissions in ORACLE-lite. Red indicates that the compound is in the vapor phase and blue in the particulate phase. The circles correspond to primary organic material that can be emitted either in the gas or in the aerosol phase. The triangles indicate the formation of SOA from SVOCs by fuel combustion and biomass burning sources, while the squares show SOA from IVOCs by fuel combustion and biomass burning sources, and the diamonds the formation of SOA from anthropogenic and biogenic VOC sources. The partitioning processes, the aging reactions and the names of the species used to track all compounds are also shown.

https://doi.org/10.5194/egusphere-2024-3590
Preprint. Discussion started: 4 December 2024

concentration of each organic compound, ORACLE calculates the partitioning between the gas and particle phases by assuming bulk equilibrium and that all organic compounds form a pseudo-ideal solution. A schematic overview of the ORACLE module and the different aerosol types and chemical processes considered here is provided in Figure 8. More details about ORACLE can be found in Tsimpidi et al. (2024).

3.4 Emissions

Fuel combustion and agriculture related emissions are based on the high resolution (0.1°×0.1°) Copernicus Atmosphere Monitoring Service global anthropogenic emission inventory applied at monthly intervals, CAMSv4.2 (Granier et al., 2019). The emission factors used for the distribution of traditional POA emissions from fuel combustion and open biomass burning sources into the three volatility bins considered by ORACLE are based on the work of Tsimpidi et al. (2024). These emission factors account additionally for IVOC emissions that are not included in the original emission inventories. We assume that the missing IVOC emissions from anthropogenic combustion are 1.5 times the traditional OA emissions included in the inventory. LVOCs and SVOCs are assumed to be emitted in the aerosol phase, while IVOCs are emitted in the gas phase. Then, they are allowed to partition between the gas and particle phase. Figure S4 shows the temporal evolution of anthropogenic emissions of inorganic (SO_2, NH_3, NO_x) and organic (LVOC, SVOC, IVOC, VOC) aerosol precursors over the last 20 years, while Table S5 shows their decadal percentage change between the 2000s and 2010s. Open biomass burning emissions are calculated online based on the dry matter burned from observations (Kaiser et al., 2012) and the fire type which affect the emission factors for the different tracers (Akagi et al., 2011). Similar to POA emissions from fuel combustion, POA from biomass burning is distributed to LVOC, SVOC, and IVOC emissions, however, no additional IVOC emissions are assumed for open biomass burning and therefore the sum for the biomass burning emission factors is unity (Tsimpidi et al., 2016).

Biogenic emissions of isoprene and terpenes are calculated online using the Model of Emissions of Gases and Aerosol from Nature (MEGANv2.04; Guenther et al., 2012) with an average emission flux of 454 and 81.7 Tg yr^{-1}, respectively. The natural emissions of NH_3 are based on the GEIA database (Bouwman et al., 1997) and include excreta from domestic animals, wild animals, synthetic nitrogen fertilizers, oceans,

https://doi.org/10.5194/egusphere-2024-3590
Preprint. Discussion started: 4 December 2024

biomass burning, and emissions from soils under natural vegetation. NOx produced by lightning is calculated online and distributed vertically based on the parameterization of Price and Rind (1992). The emissions of NO from soils are calculated online based on the algorithm of Yienger and Levy (1995). Eruptive and non-eruptive volcanic degassing emissions of SO_2 are based on the AEROCOM data set (Dentener et al., 2006). The oceanic DMS emissions are calculated online by the AIRSEA submodel (Pozzer et al., 2006). Emission fluxes of sea spray aerosols are calculated online (Guelle et al., 2001) assuming a composition of 55% Cl^-, 30.6% Na^+, 7.7% SO_4^{2-}, 3.7% Mg^{2+}, 1.2% Ca^{2+}, 1.1% K^+ (Seinfeld and Pandis, 2006). The average global emission flux of sea spray aerosols is 5910 Tg yr^{-1}. Dust emission fluxes are calculated online by using the meteorological fields calculated by the EMAC model (temperature, pressure, relative humidity, soil moisture and the surface friction velocity) together with specific input fields for soil properties (i.e., the geographical location of the dust sources, the clay fraction of the soils, the rooting depth, and the monthly vegetation area index) (Astitha et al., 2012). The average global emission flux of dust particles is 5684 Tg yr^{-1}. Emissions of individual crustal species (Ca^{2+}, Mg^{2+}, K^+, Na^+) are estimated as a constant fraction of mineral dust emissions. This fraction is determined based on the geological information that exists for the different dust source regions of the planet (Karydis et al., 2016) and is applied online on the calculated mineral dust emission fluxes based on the location of the grid cell (Klingmuller et al., 2018).

3.5 Model calculated aerosol composition

The EMAC simulation corroborates the findings based on filters and AMS observations that OA is the dominant component of fine atmospheric aerosols in all continental regions (Figure 9). The strongest OA contribution to total $PM_{2.5}$ (more than 50%) is calculated over regions affected by biomass burning and biogenic VOC emissions: the tropical forests and savannas of Africa, Latin America and Caribbean, Southern Asia, and Southeast Asia and Developing Pacific, as well as the boreal forests of Eurasia. Considerable OA shares (30-35%) are also calculated over the industrialized regions of the Northern Hemisphere (i.e., North America, Europe, Eastern Asia) and the Middle East, where strong fossil and biofuel combustion related sources are located. OA shares peak in the summer over Europe and North America and in the winter over East Asia (Figures S1-S3). EMAC is also able to reproduce the dominance of SOA (resolved by the AMS as OOA) in all regions, even in regions with strong primary

https://doi.org/10.5194/egusphere-2024-3590
Preprint. Discussion started: 4 December 2024

emissions, e.g., close to tropical forests or industrial areas. However, EMAC cannot reproduce the dominance of aged SOA in many cases (resolved as M-OOA by the AMS), especially over Eastern Asia, revealing weaknesses in the oxidation scheme of its organic module (e.g., including missing sources and formation pathways). POA has the strongest contribution (more than 20%) over heavily forested areas (e.g., Africa and Eurasia) and the lowest (less than 10%) over highly industrialized regions (e.g., Europe

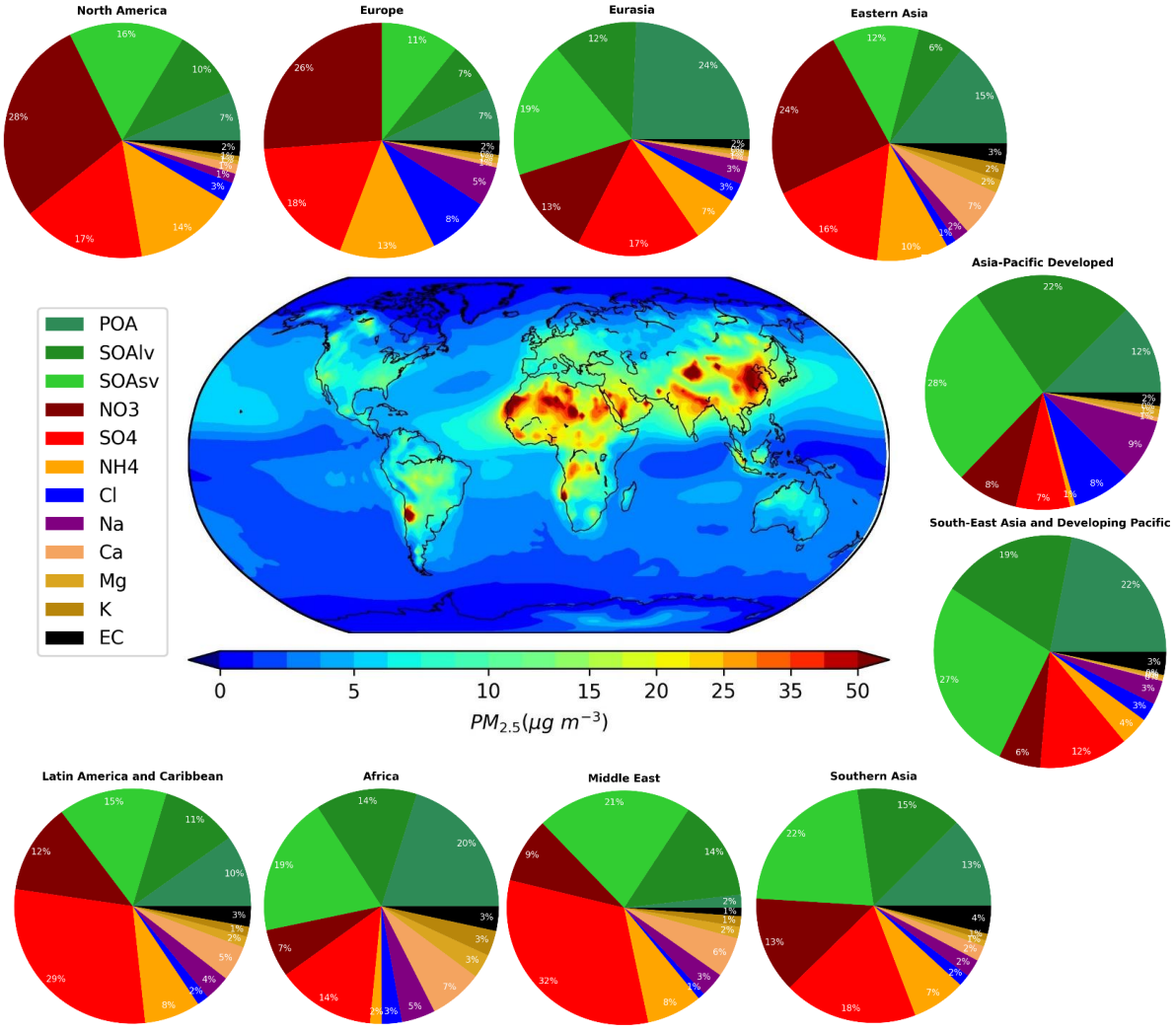

Figure 9: Pie charts showing the simulated 20-year average chemical composition of $PM_{2.5}$ in the 10 regions considered according to WGIII AR6. The central world map shows the simulated average near-surface concentration of $PM_{2.5}$ (in $\mu g\ m^{-3}$) during the period 2000-2020.

https://doi.org/10.5194/egusphere-2024-3590
Preprint. Discussion started: 4 December 2024

and Middle East). Regarding the inorganic aerosol composition, the EMAC model is not always consistent with the filter-based observations since in many regions it reveals that nitrate overpasses sulfate in the aerosol composition, which is also supported by the AMS results. These regions are Europe, North America, and Eastern Asia, where nitrate accounts for 25-30% of total PM2.5, with higher contributions in winter and lower contributions in summer (Figures S1-S3). Sulfate becomes the dominant inorganic aerosol component only during winter over North America (Figures S1-S3). On the other side, sulfate contribution is stronger over the Middle East and Latin America and Caribbean (~30%). Ammonium follows the spatial distribution of sulfate and nitrate with high contributions to $PM_{2.5}$ composition (~10-15%) over the highly populated and agriculturally intensive regions of North America, Europe, Eastern Asia and Southern Asia. Mineral dust is simulated to be a significant natural contributor to aerosol composition in some regions. Here we only focus on the chemically active components of mineral dust, which are the crustal cations of calcium, potassium, sodium, and magnesium. Their total share to $PM_{2.5}$ composition is around 15% in regions affected by desert emissions (e.g., Africa, Middle East, Eastern Asia) while in other areas their contribution is limited (~ 1%). Finally, sodium and chloride from sea salt emissions are found to be high over regions with long coastlines per land area. Most notably, chloride consists of 8% of the total $PM_{2.5}$ over the Asia Pacific Developed region, while sodium is the dominant inorganic component in the same region with a share of 8.5%.

4 In depth model Evaluation

4.1 Sulfate

The EMAC performance for sulfate is best over North America, where the model tends to underpredict its concentrations with a MB of -0.45 μg m-3 (Figure 10a). The model performs better over rural regions with very low NMB (-8%) and worst over urban locations (NMB=-40%). This performance can be attributed to the low spatial resolution used and to possible errors in the assumed injection height of SO_2 (Yang et al., 2019) which can affect sulfate concentrations close to sources. Furthermore, EMAC tends to overestimate sulfate over the Midwest, while underestimating its concentrations over the Eastern states (Figure 10). The coarse resolution of the model cannot reproduce the orography of the mountainous Midwest and therefore overestimates the sulfate concentrations at high altitude sites. On the other hand, due to

https://doi.org/10.5194/egusphere-2024-3590
Preprint. Discussion started: 4 December 2024

its coarse resolution, it underestimates the sulfate concentrations over the urban areas of the densely populated Eastern states. Therefore, the model underpredicts observations over the Eastern US, where sulfate concentrations are high, and overpredicts observations over the Midwest, where sulfate concentrations are low. As a result, the model produces a quite narrow range of concentrations (i.e., 0.3 - 2.5 µg m^{-3}) over the North America in contrast to the AMS observations which cover almost three orders of magnitude, ranging from 0.1 to 10 µg m^{-3}. The seasonal pattern of both measured and observed data shows clear differences between summer and winter. The model calculates the highest sulfate concentrations in autumn, in contrast to the AMS observations which show a peak in summer. The lowest sulfate concentrations are observed in winter which are well captured by the model at most sites (Figure 10a).

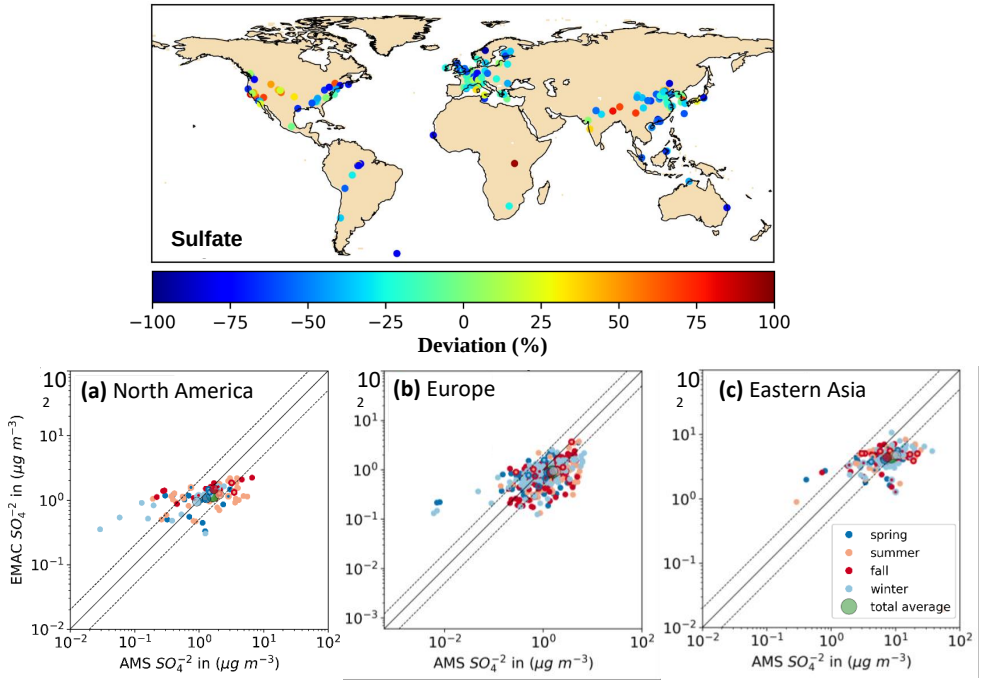

Figure 10: Deviations (in %) between EMAC results and the AMS and ACSM datasets over the period 2000 – 2020 (top). Negative values (blue colors) correspond to underprediction of sulfate concentrations by the model. Scatter plots comparing model results for PM_1 sulfate concentrations (in µg m^{-3}) with AMS and ASCM observations (bottom) over (a) North America, (b) Europe, and (c) Eastern Asia. Each point represents the data set mean and is colored based on the season of the field campaign. Also shown are the 1:1, 2:1, and 1:2 lines.

https://doi.org/10.5194/egusphere-2024-3590
Preprint. Discussion started: 4 December 2024

In Europe, the model underpredicts sulfate in all types of environments and all seasons by about 40% due to errors in emissions and an underestimation of the oxidation capacity of the atmosphere (Emep, 2021). However, a few overpredictions are calculated over Italy and Greece. Around 65% of the simulated sulfate concentrations over Europe are within a factor of 2 compared to measurements (Figure 10b). The performance of the model does not exhibit any clear seasonal pattern except a slight tendency towards higher underpredictions during summer when the observed sulfate concentrations are the highest of the year. Over Asia, sulfate concentrations are significantly higher than over Europe and North America, however, the performance of the model is similar. Sulfate is underpredicted most of the time (Figure 10c, Table 1). The model performs better over rural locations (NME=-38%) and worst over urban areas (50%). Furthermore, while the model underpredicts sulfate concentrations during all seasons, its performance is worst in winter when sulfate exhibits its annual peak concentrations (Figure 10c) due to its multiphase formation during haze events, a pathway not accurately resolved by the model. Furthermore, similar to North America, the concentration range of the simulated sulfate over Eastern Asia is much narrower than the observed, covering little more than one order of magnitude compared to two orders of magnitude reported by the AMS. Over the tropical and subtropical regions, sulfate is underestimated again, mostly over the Asian regions (NME ≈ -45%) and less over Africa and Latin America and Caribbean (NME ≈ -30%) (Table S2, Figure S5).

Table 1: Statistical evaluation of EMAC PM_1 sulphate concentrations against AMS and ACSM datasets over Europe, North America, and Eastern Asia for the period of 2000–2020.

Continent	Region	Number of data sets	Mean observed [μgm^{-3}]	Mean predicted [μgm^{-3}]	MAGE [μgm^{-3}]	MB [μgm^{-3}]	NME [%]	NMB [%]	RMSE [μgm^{-3}]
Europe	all	431	1.54	0.91	0.79	-0.63	51.08	-41.17	1.22
	rural	240	1.41	0.8	0.76	-0.61	53.99	-43.35	1.18
	DW	155	1.71	1.07	0.82	-0.65	47.9	-37.72	1.3
	urban	36	1.71	0.95	0.84	-0.75	48.9	-44.15	1.07
North-America	all	88	1.63	1.18	0.85	-0.45	52.37	-27.72	1.27
	rural	46	1.14	1.05	0.71	-0.09	62.28	-8.25	1.05
	DW	7	1.8	1.29	0.6	-0.5	33.53	-28.05	0.85
	urban	35	2.23	1.32	1.09	-0.91	48.75	-40.74	1.57
Eastern Asia	all	153	8.54	4.52	4.44	-4.02	52.05	-47.12	6.47
	rural	44	7.15	4.44	3.42	-2.71	47.77	-37.93	4.71
	DW	16	7.93	4.31	4.04	-3.61	50.94	-45.58	4.55
	urban	93	9.3	4.59	5.0	-4.71	53.77	-50.69	7.41

https://doi.org/10.5194/egusphere-2024-3590
Preprint. Discussion started: 4 December 2024

4.2 Nitrate

The model is able to capture the observed average nitrate concentrations over the different regions and seasons with very low NMB (below 10%). However, the NME is high over all regions (40-80%) indicating that the discrepancy between model results and observations is highly scattered and not systematically biased (Table 2). The accurate prediction of nitrate concentrations is rather complex. Nitrate is typically formed in areas characterized by high ammonia and nitric acid concentrations and low sulfate concentrations. At the same time, the thermodynamic equilibrium of ammonium nitrate varies several orders of magnitude under typical atmospheric conditions (Seinfeld and Pandis, 2006). This variation causes significant challenges in the calculation of nitrate concentrations since small errors in RH and T can shift the equilibrium of nitric acid to the gas or the aerosol phase. Therefore, even though the scatter is not negligible, it is encouraging that the EMAC model seems to perform surprising well under diverse environments and atmospheric conditions (Figure 11). The scatter is more intense over North America (NME=88%), especially during the summer season where the occurrence of high temperatures and the semi-volatile nature of NH_4NO_3 hinder the model's ability to capture the observations accurately (Figure 11a). However, the model is still able to capture the seasonality of nitrate concentrations well with the highest concentrations calculated during the periods with the lowest temperatures (i.e., winter), when almost all the nitric acid that is available is transferred to the particulate phase.

Over Europe, despite some widely dispersed points, the majority of datapoints (70%) lie within a factor of two compared to observations (Figure 11b). Similar to North America, the seasonality is very well captured, and the model predictions are mostly scattered during the warmer seasons. However, the overall performance is better here with NMB = -4% and NME = 53%. Over Eastern Asia, the overestimation appears to be more systematic, especially during the summer and fall (Figure 11c). However, with an overall NMB of 7.7%, the performance can still be considered very good (Table 2). Nitrate levels are significantly overestimated by the model, especially over the west coast of South Korea and the Chinese inlands (Figure 11). However, Eastern China and especially the coastal regions are well described by the model. The contribution of sea salt to nitrate formation is important in these coastal regions due to their proximity to the Pacific Ocean (Bian et al., 2017). Therefore, the overestimation of nitrate levels on the west coast of Korea, in contrast to the well captured east coast, could be caused by

https://doi.org/10.5194/egusphere-2024-3590
Preprint. Discussion started: 4 December 2024

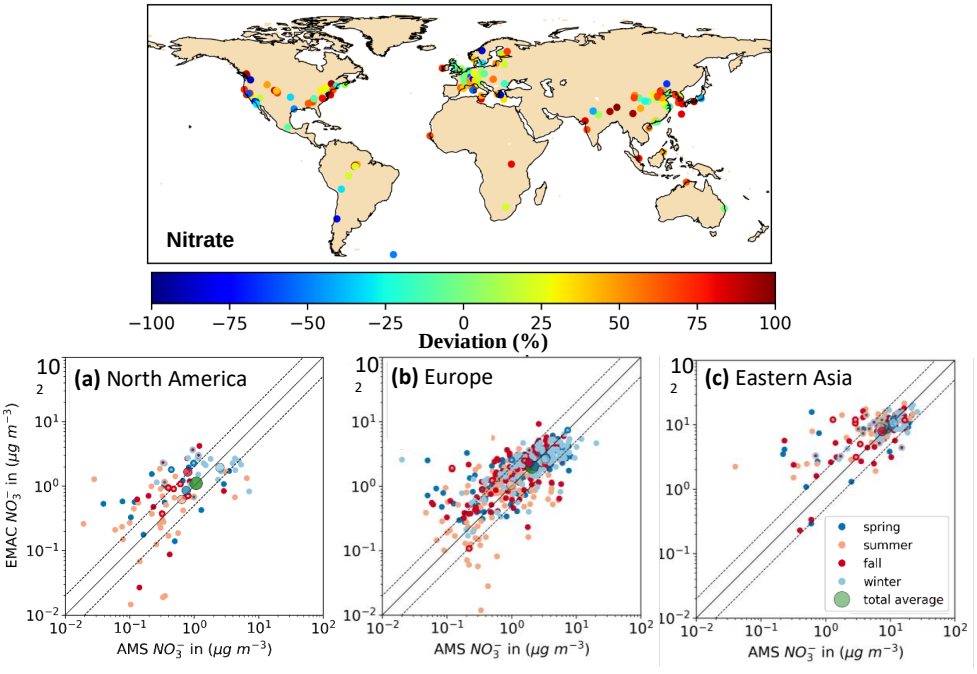

Figure 11: Deviations (in %) between EMAC results and the AMS and ACSM datasets over the period 2000 – 2020 (top). Negative values (blue colors) correspond to underprediction of nitrate concentrations by the model. Scatter plots comparing model results for PM_1 nitrate concentrations (in μg m^{-3}) with AMS and ASCM observations (bottom) over (a) North America, (b) Europe, and (c) Eastern Asia. Each point represents the data set mean and is colored based on the season of the field campaign. Also shown are the 1:1, 2:1, and 1:2 lines.

693 the dominant west-east winds in the Yellow Sea simulated by the model, leading to an
694 overestimation of the sea salt content that can contribute to nitrate formation. Over the
695 tropical and subtropical regions, the discrepancies between the simulated and observed
696 nitrate concentrations are less dispersed with a tendency towards overprediction by the
697 model in most regions (Figure S5; Table S2). Over Latin America and the Caribbean,
698 the model underpredicts nitrate (NMB = -50%) except for a few strong overpredictions,
699 mostly during the wet season, suggesting possible errors in simulated wet deposition
700 (Figure S5). On the other hand, over Africa, the model overpredicts nitrate during the
701 dry season, especially over Welegund, an observation site downwind of Johannesburg.
702 Nitrate is strongly overpredicted over the Asia Pacific Developed region, especially
703 over the industrialized regions of Japan and Australia. On the contrary, the model
704 performance for nitrate is good over the Southeast Asia and the Developing Pacific

https://doi.org/10.5194/egusphere-2024-3590
Preprint. Discussion started: 4 December 2024

(NMB = -3%) with few random over- and underpredictions during the monsoon and the transition periods towards that season.

Table 2: Statistical evaluation of EMAC PM_1 nitrate concentrations against AMS and ACSM datasets over Europe, North America, and Eastern Asia for the period of 2000–2020.

Continent	Region	Number of data sets	Mean observed [μgm^{-3}]	Mean predicted [μgm^{-3}]	MAGE [μgm^{-3}]	MB [μgm^{-3}]	NME [%]	NMB [%]	RMSE [μgm^{-3}]
Europe	all	431	2.07	1.98	1.09	-0.09	52.54	-4.17	1.74
	rural	240	1.57	1.56	1.01	-0.02	64.02	-1.02	1.77
	DW	155	2.88	2.61	1.24	-0.27	42.95	-9.52	1.76
	urban	36	1.86	2.12	0.96	0.26	51.71	13.73	1.36
North-America	all	88	1.07	1.1	0.94	0.04	87.79	3.35	1.45
	rural	46	0.81	0.84	0.66	0.03	81.44	3.59	0.97
	DW	7	0.98	1.18	1.11	0.2	114.09	20.62	1.53
	urban	35	1.43	1.44	1.27	0.01	88.93	0.82	1.88
Eastern Asia	all	152	8.47	9.12	3.58	0.65	42.3	7.67	4.81
	rural	43	6.44	7.36	4.11	0.92	63.8	14.21	5.17
	DW	16	4.74	7.49	3.67	2.75	77.54	58.0	5.08
	urban	93	10.05	10.22	3.33	0.17	33.08	1.65	4.58

4.3 Ammonium

EMAC tends to underpredict ammonium over the three main subcontinents of the Northern Hemisphere, however, its performance is considered satisfactory with relatively low bias and scatter (Table 3). The model evaluation exhibits a large scatter only over North America (NME = 63%), where 50% of the comparison sites are beyond the factor 2 intervals (Figure 12a). Ammonium tends to be overestimated during autumn and underestimated during the rest of the seasons; especially during the summer (Figure 12a). Over Europe, the model exhibits its best performance with low NMB (-9%). The average deviation from the observations is also relatively low (Figure 12) and 75% of the model results diverge less than a factor of two from measurements. Surprisingly, the model performance is best over the Benelux region (Figure 12) where NH_3 emissions are the highest over Europe. While the good model performance for ammonium over Europe indicates an accurate emission inventory for agricultural and livestock NH_3, the overprediction of nitrate and underprediction of sulfate suggest that the model overpredicts the fraction of ammonium that exists as ammonium nitrate (instead of ammonium sulfate). Over Asia, the model strongly underestimates ammonium (NMB = -30%), especially over Eastern China (Figure 12). While this

https://doi.org/10.5194/egusphere-2024-3590
Preprint. Discussion started: 4 December 2024

underestimation can be partially attributed to sulfate underpredictions, the simultaneous overestimation of nitrate over the same areas indicates errors in the NH_3 emission inventory. On the other hand, ammonium is overpredicted close to the deserts of Inland China (e.g., over Tibet) and over South Korea (Figure 12). Over the Tropics and the southern continents, ammonium is underestimated to a higher extent than in the northern continents (with NMB from -40 to -60%). The main problem in model performance is over Asia Pacific Developed and Africa, where the model predicts low ammonium shares that are not supported by AMS observations (Figure S2). On the other hand, EMAC has the largest underprediction and highest NMB over Latin America. Nevertheless, here and over South Asia, EMAC and AMS agree that ammonium has the smallest fraction of PM_1. Overall, deviations in ammonium can be traced back to global livestock emission inventory uncertainties as criticized by Hoesly et al. (2018).

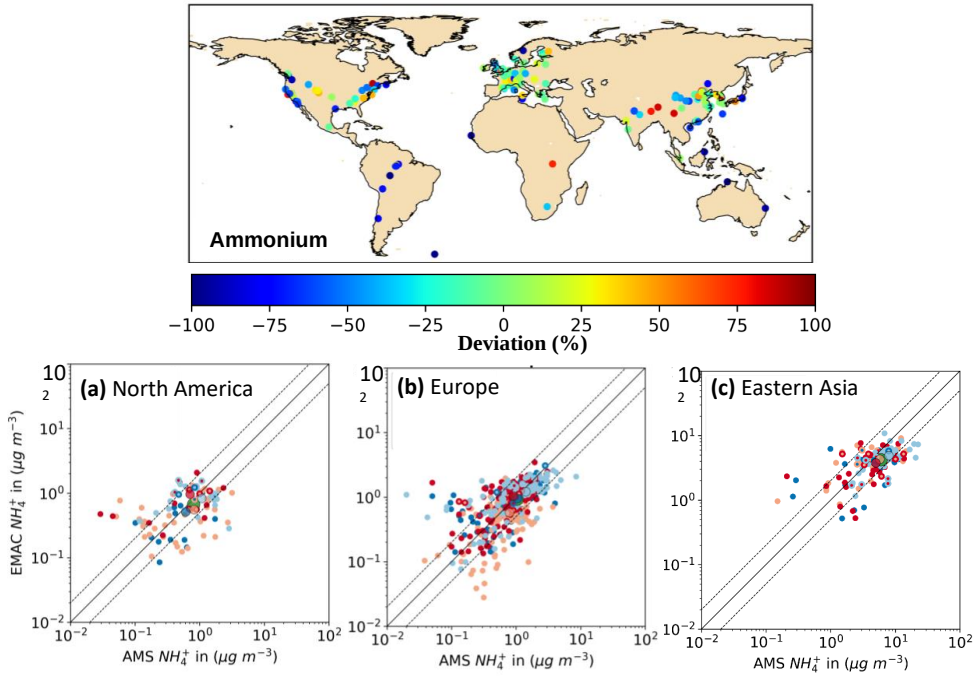

Figure 12: Deviations (in %) between EMAC results and the AMS and ACSM datasets over the period 2000 – 2020 (top). Negative values (blue colors) correspond to underprediction of ammonium concentrations by the model. Scatter plots comparing model results for PM_1 ammonium concentrations (in µg m^{-3}) with AMS and ASCM observations (bottom) over (a) North America, (b) Europe, and (c) Eastern Asia. Each point represents the data set mean and is colored based on the season of the field campaign. Also shown are the 1:1, 2:1, and 1:2 lines.

https://doi.org/10.5194/egusphere-2024-3590
Preprint. Discussion started: 4 December 2024

Table 3: Statistical evaluation of EMAC PM_1 ammonium concentrations against AMS and ACSM datasets over Europe, North America, and Eastern Asia for the period of 2000–2020.

Continent	Region	Number of data sets	Mean observed [μgm^{-3}]	Mean predicted [μgm^{-3}]	MAGE [μgm^{-3}]	MB [μgm^{-3}]	NME [%]	NMB [%]	RMSE [μgm^{-3}]
Europe	all	431	1.03	0.93	0.44	-0.1	42.33	-9.38	0.68
	rural	240	0.8	0.76	0.42	-0.05	52.55	-5.62	0.69
	DW	155	1.36	1.2	0.47	-0.15	34.67	-11.39	0.69
	urban	36	1.13	0.94	0.38	-0.19	33.48	-16.78	0.5
North-America	all	87	0.81	0.67	0.51	-0.14	62.97	-17.29	0.71
	rural	46	0.54	0.49	0.36	-0.05	65.9	-8.6	0.45
	DW	7	0.85	0.74	0.44	-0.11	51.52	-12.93	0.54
	urban	34	1.16	0.89	0.73	-0.27	62.85	-23.41	0.97
Eastern Asia	all	152	5.99	4.21	2.63	-1.78	43.96	-29.76	3.79
	rural	43	4.91	3.64	2.49	-1.27	50.77	-25.83	3.66
	DW	16	3.8	3.51	1.6	-0.29	42.07	-7.51	1.96
	urban	93	6.87	4.59	2.88	-2.28	41.89	-33.18	4.08

4.4 Organic aerosol

The model performance for total OA concentration varies significantly between the three continents. Over North America, the simulated mean OA represents well the observed OA by AMS (NMB = -4%). However, the comparison exhibits a significant scatter (NME = 64%) since the model tends to overpredict OA over rural locations (NMB = 37%) and underpredict it over and downwind of urban sites (NMB = -28%). The model roughly captures the seasonality of OA concentrations over North America, with high OA concentrations in summer and autumn and lower concentrations in spring and winter. OA concentrations peak during summer due to enhanced biogenic VOC emissions and photochemistry (Goldstein and Galbally, 2007; Tsimpidi et al., 2016), however, EMAC tends to overpredict some low OA concentrations measured by AMS over a few rural locations during summertime (Figure 13a). Over Europe, the model tends to underestimate OA during all seasons, except summer (Figure 13b). The model performance is worst during wintertime, where sources from biomass burning, particularly by domestic wood burning, and their dark oxidation have been recently identified as a major source of model bias over Europe during wintertime (Tsimpidi et al., 2016; Kodros et al., 2020). This also affects the simulated OA seasonality over Europe where the model estimates higher OA concentrations during summer over all types of environments, while the AMS observations reveal that this is true only over

https://doi.org/10.5194/egusphere-2024-3590
Preprint. Discussion started: 4 December 2024

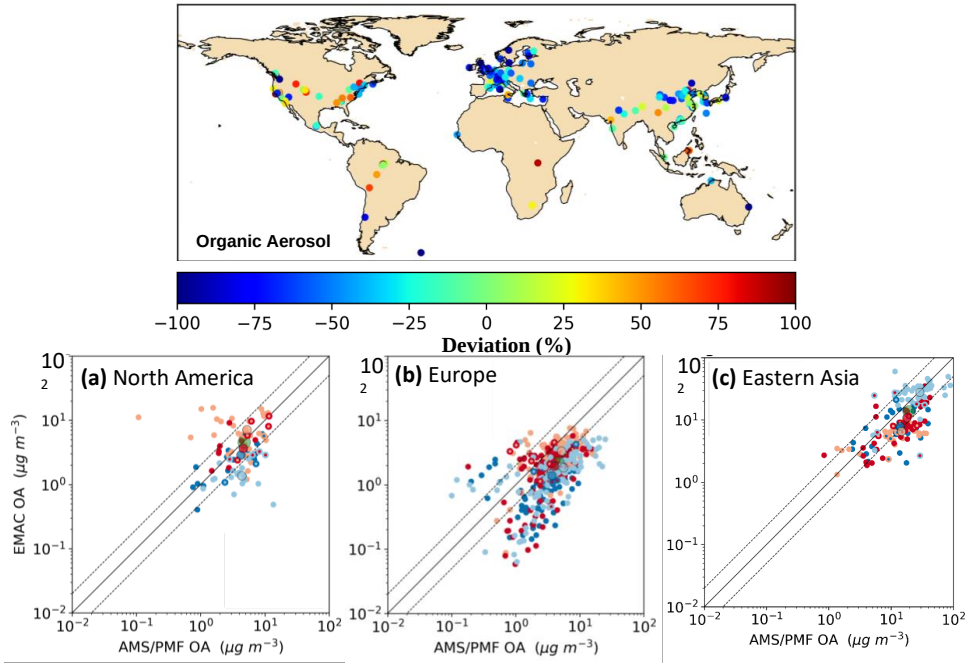

Figure 13: Deviations (in %) between EMAC results and the AMS and ACSM datasets over the period 2000 – 2020 (top). Negative values (blue colors) correspond to underprediction of organic aerosol concentrations by the model. Scatter plots comparing model results for PM_1 organic aerosol concentrations (in μg m^{-3}) with AMS and ASCM observations (bottom) over (a) North America, (b) Europe, and (c) Eastern Asia. Each point represents the data set mean and is colored based on the season of the field campaign. Also shown are the 1:1, 2:1, and 1:2 lines.

rural locations. According to AMS, over and downwind of urban areas, OA concentrations peak during wintertime. Over Eastern Asia, the model exhibits its best performance with relatively low bias (NMB = -29%) and scatter (NME = 49%). In contrast to Europe, the wintertime OA is well captured by the model even over urban locations (Table 4). The model has excellent performance over rural and urban-downwind locations with 75% of the datapoints lying within a factor of two compared to observations. However, as it is typical for every global model (Tsigaridis et al., 2014), the model fails to reproduce some of the high OA concentrations observed over large urban centers due to its limited spatial resolution. Over the rest of the continental regions, the overall performance of the model is satisfying for OA. EMAC tends to underpredict OA over the tropical regions of South Asia and Developing Pacific and over the more urbanized regions of the Asia Pacific Developed, without any clear seasonal pattern (Figure S5). In contrast, simulated OA are overestimated over Africa,

https://doi.org/10.5194/egusphere-2024-3590
Preprint. Discussion started: 4 December 2024

mostly during the dry season. Over Latin America and Caribbean, the evaluation datapoints are more scattered with a few significant overestimations during the Amazonian wet season and underestimations during the dry season.

Table 4: Statistical evaluation of EMAC PM_1 OA concentrations against AMS and ACSM datasets over Europe, North America, and Eastern Asia during 2000–2020.

Continent	Region	Number of data sets	Mean observed [μgm^{-3}]	Mean predicted [μgm^{-3}]	MAGE [μgm^{-3}]	MB [μgm^{-3}]	NME [%]	NMB [%]	RMSE [μgm^{-3}]
Europe	all	442	4.59	2.18	2.73	-2.41	59.54	-52.56	3.95
	rural	247	3.63	1.96	2.11	-1.66	58.16	-45.93	3.08
	DW	156	5.93	2.45	3.65	-3.48	61.58	-58.63	5.08
	urban	39	5.33	2.45	3.01	-2.88	56.39	-54.12	3.73
North-America	all	86	4.77	4.56	3.05	-0.2	64.1	-4.24	4.29
	rural	46	3.29	4.51	2.95	1.22	89.79	37.28	4.52
	DW	7	5.58	4.6	2.29	-0.97	40.98	-17.42	2.92
	urban	33	6.66	4.63	3.36	-2.03	50.53	-30.46	4.2
Eastern Asia	all	159	19.3	13.64	9.41	-5.65	48.74	-29.3	13.19
	rural	44	12.77	10.75	6.72	-2.02	52.64	-15.81	11.55
	DW	16	11.38	9.79	6.0	-1.59	52.73	-13.97	8.87
	urban	99	23.48	15.55	11.15	-7.93	47.49	-33.76	14.41

4.4.1 POA

The simulated POA concentrations are compared with the sum of the AMS HOA and BBOA concentrations. POA concentrations are mostly underestimated by the model over North America and Europe (NMB ≈ -45%) and significantly overestimated over Eastern Asia (NMB = 98%). In North American rural regions, POA simulated concentrations are highest during spring and winter and lowest during fall, consistent with the observed POA levels. However, during summer, most of the observed data is underestimated by the model (Figure 14). Over urban locations, POA is more severely underestimated (NMB = -68%) due to the coarse spatial resolution of the model and the evaporation of organic compounds upon emission. POA concentrations are also underestimated over European urban regions (NMB = -52%), however, to a lesser extent than over North America. Over rural locations, the model performance is scattered during all seasons with a few cases of strong over and under predictions (NME = 62%). Over Eastern Asia, a pronounced overestimation during winter is striking, especially over mega-city clusters (NMB = 106%; Table 5) such as around Hong Kong and Shanghai. This discrepancy can be related to overestimations in the emission inventory (e.g., not including the emission reductions in the frame of the Chinese

https://doi.org/10.5194/egusphere-2024-3590
Preprint. Discussion started: 4 December 2024

control action plans) but also to the overestimated partition of the freshly emitted SVOCs to the aerosol phase during the low winter temperatures. Tsimpidi et al. (2016) has also reported POA overestimations over Eastern Asia due to too high simulated bbPOA transported from the surrounding boreal forests. Since in ORACLE POA do not participate in aqueous phase and other heterogeneous reactions, they do not convert to SOA via these pathways, which can explain part of the positive model bias during winter.

Table 5: Statistical evaluation of EMAC PM_1 POA concentrations against AMS and ACSM datasets over Europe, North America, and Eastern Asia during 2000–2020.

Continent	Region	Number of data sets	Mean observed [μgm^{-3}]	Mean predicted [μgm^{-3}]	MAGE [μgm^{-3}]	MB [μgm^{-3}]	NME [%]	NMB [%]	RMSE [μgm^{-3}]
Europe	all	106	1.18	0.67	0.81	-0.51	68.45	-43.27	1.6
	rural	62	0.9	0.49	0.56	-0.4	62.5	-44.78	1.13
	DW	23	1.7	1.12	1.38	-0.58	81.24	-34.19	2.6
	urban	21	1.45	0.69	0.91	-0.75	62.87	-52.2	1.32
North-America	all	50	1.17	0.63	0.95	-0.54	80.93	-46.2	1.49
	rural	21	0.62	0.64	0.65	0.02	106.18	3.64	1.59
	DW	3	0.41	1.27	1.16	0.86	284.25	212.29	1.76
	urban	26	1.7	0.55	1.16	-1.16	67.93	-67.93	1.38
Eastern Asia	all	129	4.88	9.91	6.89	5.03	141.12	103.18	11.4
	rural	35	5.1	9.28	6.11	4.18	119.82	82.03	11.38
	DW	13	3.68	5.91	3.8	2.23	103.0	60.49	5.82
	urban	81	4.98	10.83	7.72	5.85	155.08	117.62	12.07

Table 6: Statistical evaluation of EMAC PM_1 SOA concentrations against AMS and ACSM datasets over Europe, North America, and Eastern Asia during 2000–2020.

Continent	Region	Number of data sets	Mean observed [μgm^{-3}]	Mean predicted [μgm^{-3}]	MAGE [μgm^{-3}]	MB [μgm^{-3}]	NME [%]	NMB [%]	RMSE [μgm^{-3}]
Europe	all	129	2.77	1.51	1.69	-1.26	61.01	-45.6	2.44
	rural	84	2.53	1.52	1.53	-1.01	60.54	-39.93	2.34
	DW	24	3.43	1.19	2.41	-2.24	70.17	-65.19	3.15
	urban	21	2.98	1.81	1.5	-1.16	50.55	-39.09	1.83
North-America	all	67	3.66	3.83	2.34	0.17	63.89	4.52	3.0
	rural	35	3.16	3.51	2.11	0.35	66.92	11.08	2.79
	DW	6	5.27	4.23	2.33	-1.05	44.25	-19.87	3.05
	urban	26	3.97	4.17	2.65	0.2	66.66	4.97	3.24
Eastern Asia	all	147	10.65	3.54	7.23	-7.11	67.86	-66.74	9.24
	rural	36	8.18	3.38	5.29	-4.8	64.62	-58.69	7.15
	DW	16	7.84	4.03	3.82	-3.82	48.68	-48.68	5.23
	urban	95	12.06	3.52	8.53	-8.53	70.79	-70.79	10.41

https://doi.org/10.5194/egusphere-2024-3590
Preprint. Discussion started: 4 December 2024

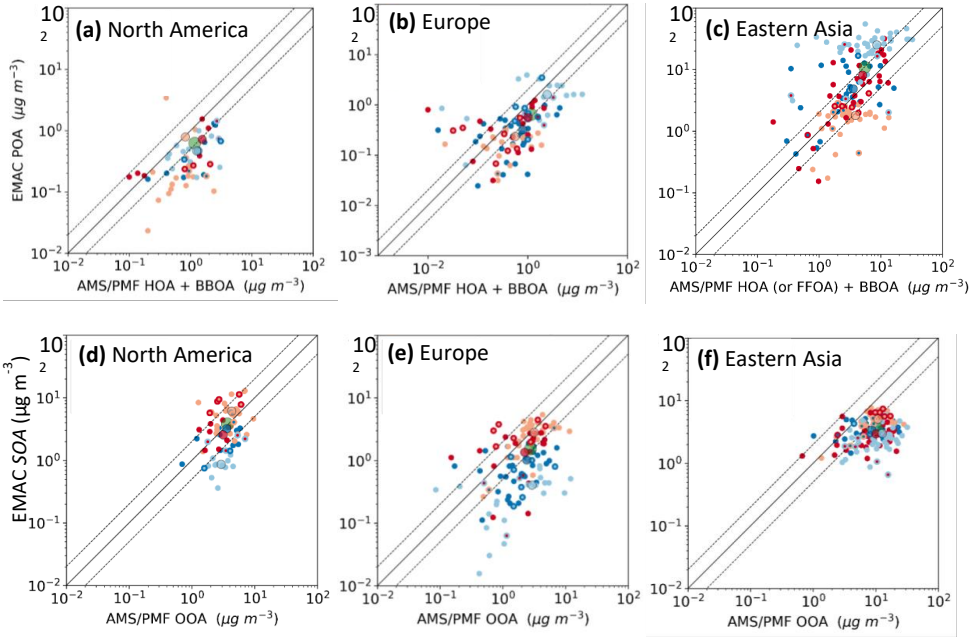

Figure 14: Scatter plots comparing model results for PM_1 primary organic aerosol (a-c) and secondary organic aerosol (d-f) concentrations (in μg m^{-3}) with AMS and ASCM observations of HOA+BOA and OOA, respectively, over North America (a, d), Europe (b, e), and Eastern Asia (c, f). Each point represents the data set mean and is colored based on the season of the field campaign. Also shown are the 1:1, 2:1, and 1:2 lines.

4.4.2 SOA

The model simulated OOA concentrations over North America are in very good agreement with the OOA derived by the PMF analysis of the AMS observations (NMB = 4.5%). The model performs well over both urban and rural areas and during all seasons, except winter when it tends to underpredict the AMS-OOA estimations (Table 6; Figure 14c). L-OOA concentrations are reproduced by the model particularly well (Figure S6a), however, M-OOA concentrations are slightly underestimated during spring and fall and severely underpredicted during winter (Figure S6d). Similarly, the model performance for all OOA types over Europe is best during summer and worst during winter when it underpredicts the AMS estimations, especially for the M-OOA (Figure S6e). During summer, the high temperatures enhance the biogenic VOC emissions from vegetation and, more importantly, the more abundant solar radiation increase the transformation of gas phase organic compounds through photochemical processing into particulate OOA (Seco et al., 2011; Xu et al., 2017; Tsimpidi et al.,

https://doi.org/10.5194/egusphere-2024-3590
Preprint. Discussion started: 4 December 2024

2016). The model performance during summer suggests that the model can accurately represent this process. In winter, however, photochemical processing has lower impact on OOA formation and evolution (Xu et al., 2017). Therefore, in seasons with decreasing temperatures and/or photochemical activity, the model performance is worsening, strongly suggesting that other processes become increasingly more important. Missing SOA formation processes are related to heterogeneous reactions like oligomerization or aqueous phase processing (Hallquist et al., 2009; Tsimpidi et al., 2016). Under high RH, aqueous phase processing can rapidly result in highly oxidized OOA (i.e., M-OOA with high oxygen to carbon ratio, O:C), while the impacts on fresher, less oxygenated OOA (i.e., L-OOA) are minor. For the latter, photochemical aging processes under low RH are more important (Xu et al., 2017). Such processes occur during all seasons, however, the meteorological conditions during winter favor the formation of M-OOA from aqueous phase chemistry against the L-OOA formation from gas-phase photochemical oxidation processes (Xu et al., 2017; Mortier et al., 2020; Pozzer et al., 2022). Therefore, this missing formation pathway becomes gradually more important from spring and fall to winter. Additionally, recent studies have identified high production of SOA during wintertime which can be attributed to the rapid oxidation of biomass burning OA by the NO_3 radical during nighttime (Kodros et al., 2020; Paglione et al., 2020; Liu, 2024). Since residential heating from woodstoves is not included in the model and ORACLE includes only the predominant photochemical processing of BBOA by OH, a non-consideration of dark chemical processing of BBOA can lead to substantial underprediction of OOA during the cold seasons. Over Eastern Asia, OOA is underestimated even during summer (Figure 14f), mainly due to the underestimation of M-OOA since L-OOA is relatively well represented during all seasons (Figure S6). In fact, Eastern Asia is characterized by high RH even during summer, corroborating our hypothesis that aqueous phase processes may be an important missing piece in simulating the SOA formation. Recent studies have provided strong evidence that the uptake of water-soluble gas-phase oxidation products (even small carbonyls like formaldehyde and acetic acid) to the aqueous phase and their subsequent oxidation and oligomerization can lead to significant increases of SOA mass during pollution events (Gkatzelis et al., 2021). Overall, EMAC performs best over the Eastern Asian rural areas during summer and spring and worst in the vicinity of urban regions during fall and winter. Especially during wintertime, while the model simulates well the total OA, it significantly overpredicts POA (Figure 14c) and

https://doi.org/10.5194/egusphere-2024-3590
Preprint. Discussion started: 4 December 2024

at the same time underpredicts SOA (especially M-OOA). This disagreement can be due to an overestimation of the POA formation from the emitted SVOC species, but also due to a missing mechanism that can significantly transform POA to SOA in the aerosol phase during winter.

5 Aerosol Trends

Here, the simulated 20-year global aerosol composition trends of fine aerosols are presented and discussed against trends calculated based on observational data. For this, it is vital to have data well distributed spatially and measured consistently in a comparable way at all observational sites within a region (Tørseth et al., 2012; Hand et al., 2011). These conditions, unfortunately, cannot be satisfied by the available PM_1 datasets (Figure 2). Instead, here we summarize the available observational data from each region for the 1st versus the 2nd decade of the examined period. This allows a rough statistical comparison between the two decades and can give insights on the overall tendency of the observed aerosol composition trends for each region. These trends are compared against the simulated PM_1 trends based on the respective spatiotemporal model data, as well as based on all the available model data for the entire model domain over the complete 20-year period (Figure 15). As the spatial and temporal AMS campaign distribution is much higher for regions in the northern than the southern hemisphere, only PM_1 data of the former is plotted here. $PM_{2.5}$ data from the large monitoring networks is also used to calculate the aerosol composition trends within the regions of North America, Europe, and Eastern Asia. These networks present cooperative measurement efforts that, among others, provide routinely filter based measured data of aerosol composition. Even though not every element is always measured at all sites and despite data gaps for some places, collectively, the networks' datasets provide the consistency and duration requirements mentioned above. The calculated trends are compared against $PM_{2.5}$ simulated results based on the respective spatiotemporal model data. It is worth noting that a comparison of filter $PM_{2.5}$ to AMS detected PM_1 is not completely straightforward. First, as seen in Sections 2.1.3 and 2.2.1, there are expected compositional differences between the two size ranges, especially in polluted regions (Sun et al., 2020; Petit et al., 2015). Second, instrumental differences of the real-time on-line AMS (Decarlo et al., 2006) versus the non-real-time off-line filter instruments (Docherty et al., 2011; Hand et al., 2011) can manipulate the measurements in different ways, as discussed in the following sections.

https://doi.org/10.5194/egusphere-2024-3590
Preprint. Discussion started: 4 December 2024

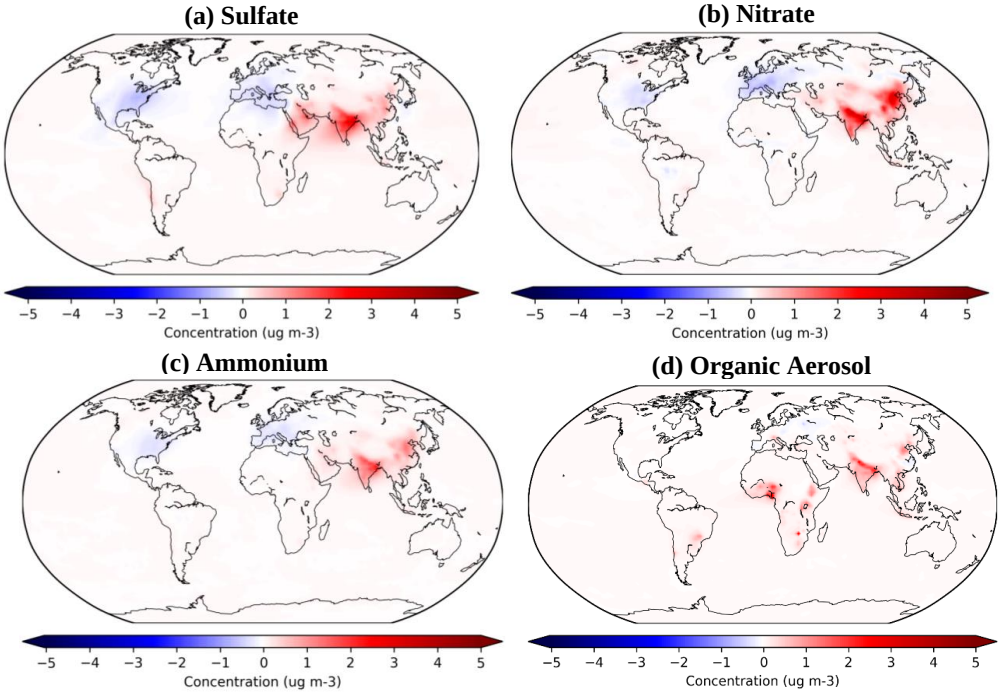

Figure 15: Simulated decadal change in (a) sulfate, (b) nitrate, (c) ammonium, and (d) anthropogenic organic aerosol concentrations between the 2000s and 2010s.

5.1 Europe

Figure 16 depicts the interannual and seasonal concentration change of filter measured $PM_{2.5}$ components with a polynomial fitted trendline, in comparison to the corresponding concentration trends as calculated by the EMAC model. Both observations and the model reveal a concentration decrease for the three main inorganic components of $PM_{2.5}$, following the emission reductions during the last 20 years. Sulfate concentrations have decreased drastically during the last decade (i.e., -46% compared to 2000s). However, the simulated reduction is not so apparent mainly because filter observations show much higher concentrations during the first half of the 2000s than model simulations. Until 2005, observed sulfate concentrations rose during all seasons, however, they rapidly dropped under the 2000 levels in the following years. The average decline rate is -0.15 μg m^{-3} yr^{-1}, compared to the simulated rate of -0.02 μg m^{-3} yr^{-1}. AMS measurements (Figure 17) corroborate the findings of filter observations, revealing a drastic decrease in PM_1 sulfate concentrations during the decade of 2010s (i.e., -18% compared to 2000s). EMAC underestimates European PM_1

https://doi.org/10.5194/egusphere-2024-3590
Preprint. Discussion started: 4 December 2024

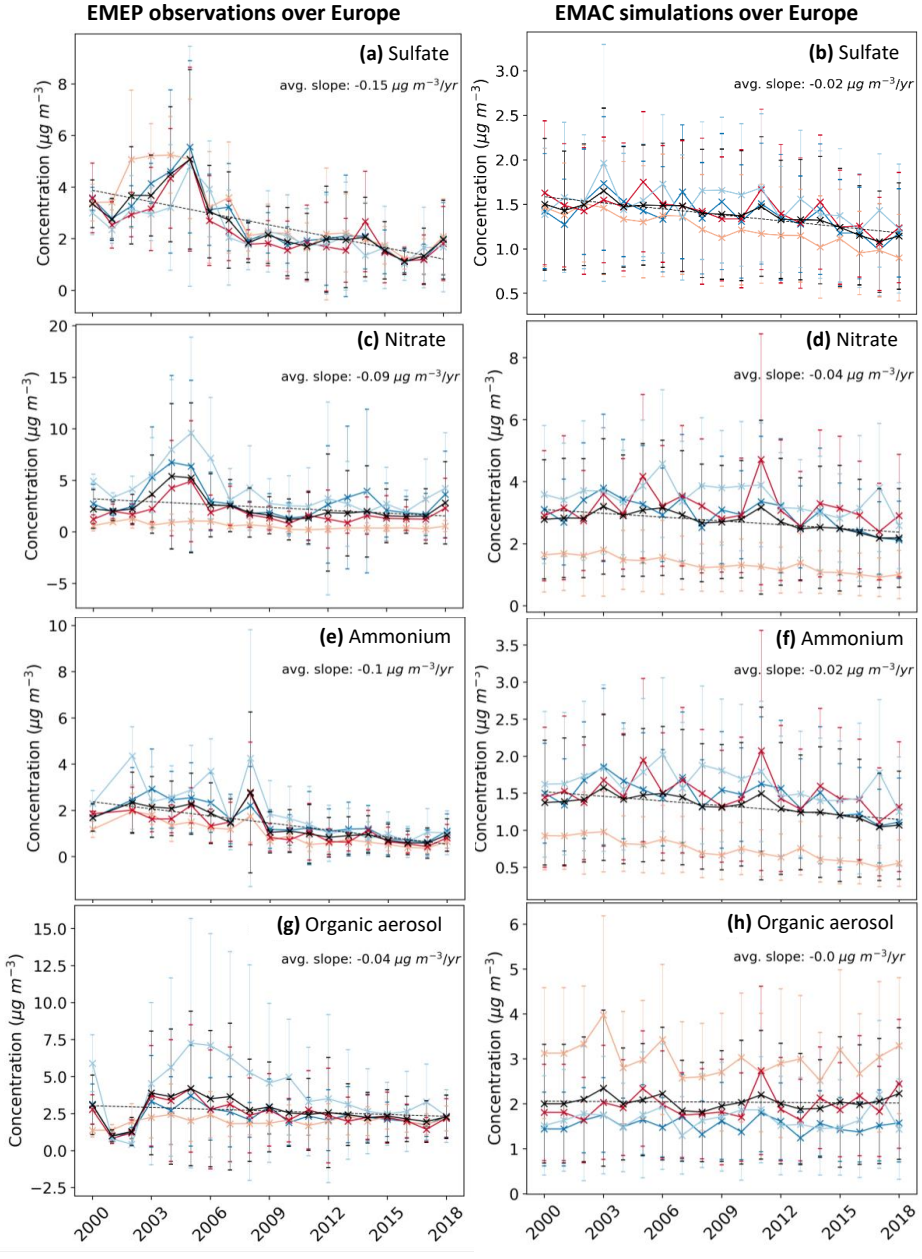

Figure 16: Temporal evolution of the observed (a, c, e, and g subplots on the left) and simulated (b, d, f, h subplots on the right) concentrations of $PM_{2.5}$ sulfate (a, b), nitrate (c, d), ammonium, (e, f), and organic aerosol (g, h) during the period 2000–2018 over Europe. Black lines show the annual trend while the dark blue, light blue, orange, and red lines represent the seasonal trends during winter, spring, summer, and autumn. Ranges represent the 1σ SD (standard deviation).

900

https://doi.org/10.5194/egusphere-2024-3590
Preprint. Discussion started: 4 December 2024

sulfate (Figure 10b) resulting in a less pronounced negative trend in its concentrations (i.e., -11%) since the model underestimation is more pronounced during the 2000s. The average simulated decadal change in sulfate PM_1 concentrations for the entire European domain is -15% (Figure 15). Similar to sulfate, filter measured nitrate concentrations rose until 2005 (except during summer where they remain in low levels) and then quickly dropped again with an average rate of -0.09 µg m^{-3} yr^{-1} (Figure 16c). The high observed nitrate concentrations during the first half of the 2000s results in an average decrease of -35% between the two decades. On the other hand, the calculated change of AMS-PM_1 nitrate concentrations between the 2000s and the 2010s is -10 %, which is similar to the simulated drop of -12%. However, it is worth mentioning that the model significantly overestimates the nitrate concentrations both in comparison to AMS measurements (Figure 11b) and to filter observations, especially during summer (Milousis et al., 2024). The analysis of model simulation and observations (both by AMS and filters) reveal that ammonium concentrations exhibit strong reductions between the decades of 2000s and 2010s. The average concentration reduction between the two decades is -21% based on the AMS observations, -13% based on the EMAC results for PM_1 (or -16% for the entire European domain), and -56% for the $PM_{2.5}$ filter observations. Therefore, the reduction of ammonium is much stronger based on the filter observations (i.e., -0.1 µg m^{-3} yr^{-1}) than based on AMS measurements or modeled data (i.e., -0.02 µg m^{-3} yr^{-1}). It is worth emphasizing that ammonium is clearly declining, even though NH_3 emissions have only been slightly reduced. This apparent inconsistency can be attributed to the strong reductions of SO_2 and NO_x. This results in reduced availability of acids (i.e., H_2SO_4 and HNO_3) preventing the formation of ammonium and allowing the NH_3 to reside in the gas phase. This is also verified by NH_3 observations, where no significant trends, and even statistical increases, have been observed despite reported reductions in NH_3 emissions (Fagerli et al., 2016; Liu et al., 2024).

The downward trend of organic aerosol calculated based on the filter observations (-0.04 µg m^{-3} yr^{-1}) is milder than that of inorganic components and differs between seasons (Figure 16e). During summer, there is no clear trend observed, while in winter, OC concentration soars after 2003 until 2005 when it starts to gradually drop until it reaches the concentration levels of the other seasons during the second half of 2010s. Irregularities in the early first decade could be owed to a lack of OC data (Fagerli et al., 2016). OC data during spring and autumn shows a mild downward trend after 2005 as

https://doi.org/10.5194/egusphere-2024-3590
Preprint. Discussion started: 4 December 2024

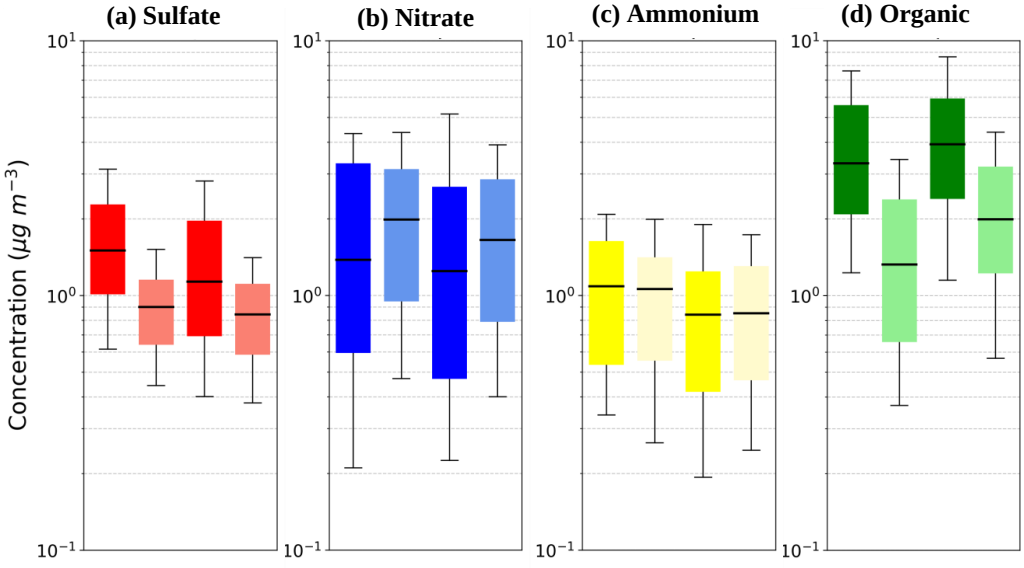

Figure 17: Decadal PM_1 concentration trends in Europe expressed by the bar plots of the mass concentration (in μg m^{-3}) for (a) sulfate, (b) nitrate, (c) ammonium, and (d) OA during the periods 2000 - 2010 (left) and 2011 - 2020 (right) as calculated from the AMS observational dataset (dark colors) and the corresponding simulation values (light colors). The upper and lower whiskers range from 10-90%, the quartiles from 25-75% of the dataset. The black line is the median.

well. Overall, the average difference of OC concentration between the two decades is -22%. However, model data does not corroborate this reduction; on the opposite a slight increase is calculated by the model during the last five years (Figure 16h). This agrees with the AMS observations which predict a positive OA trend (Figure 17d) with an average increase of +0.44 μg m^{-3} (or 10%) from the first to the second decade. Despite the prominent underestimation of PM_1 OA by the model, the simulated PM_1 OA trend is also positive with an average decadal increase of +0.55 μg m^{-3} (or 31%). Overall, inconsistencies between AMS and filter observations can be attributed to instrumental differences. First, is the size of particulate matter observed which is 2.5 μm for filters and up to 1 μm for the AMS. The size distribution of OA can be affected by multiple factors, including RH and chemical composition. Sun et al. (2020) have shown that the $PM_1/PM_{2.5}$ SOA ratio increases when RH is below 60% and the contribution of inorganic components in the aerosol decreases. This increase is related to differences in aerosol water content due to changes in aerosol hygroscopicity and phase state. Simulated data reveals that the frequency of RH dropping below 60% over European locations has marginally increased (by 1%) during the decade of 2010s. However, the

https://doi.org/10.5194/egusphere-2024-3590
Preprint. Discussion started: 4 December 2024

drastic reduction of sulfate and nitrate levels during the same period can explain the increase in PM_1 OA, as measured by the AMS, as opposed to the decrease in $PM_{2.5}$ OA observed by filters. Another important difference between the AMS and the filters is that the latter, in contrast to AMS, only detects the carbonaceous fraction (OC) of OA. Then, the ratio of the total organic mass (OM) to OC must be considered when comparing the measured OC to AMS or simulated OA. However, the OM:OC is broadly debated in literature. OM:OC is closely correlated to the oxygen to carbo ratio (O:C) and therefore it is dependent on the chemical aging degree of OA. For the range of SOA found in the atmosphere, Aiken et al. (2008) calculated the OM/OC ratios between 1.9 to 2.5. Similarly, the ratio for POA varies depending on the source and composition between 1.3 and 1.5 (Aiken et al., 2008). As the EMEP stations in Europe are a mix of urban and rural locations, the measured OC concentrations are typically multiplied by a median OM:OC value of 1.7. However, the oxidation capacity of the atmosphere has increased as anthropogenic emissions such as SO_2 have decreased (Dalsøren et al., 2016), leading to an increased oxidation rate of organic compounds and the formation of SOA. Consequently, a growing SOA fraction over the last 20 years would have been accompanied by a rising OM:OC ratio. It can be assumed that while the OC measured by the filters showed a slight downward trend (Figure 16g), a conversion into OA via adapted gradually increasing OM:OC ratios could have compensated the OC reduction and show a better matching trend compared to the AMS and EMAC OA.

5.2 North America

Over North America, the filter measured inorganic aerosol compound concentrations declined strongly during the last 20 years, following their precursor emission reductions, with higher reductions over urban locations (Figure 18) and less over rural regions (Figure 19). Nitrate reductions are more pronounced over urban regions (-0.07 µg m^{-3} yr^{-1}), especially during winter, while over rural locations, the decline is imperceptible (-0.01 µg m^{-3} yr^{-1}) since the abundance of NH_3 have decelerated the decrease of NH_4NO_3. On the other hand, the drastic decrease of SO_2 emissions (Table S5, Figure S4) resulted in strong reductions of sulfate concentrations primarily over urban areas (-0.16 µg m^{-3} yr^{-1}) but also over remote regions (-0.07 µg m^{-3} yr^{-1}), especially during the summer seasons. Following the reductions of sulfate and

https://doi.org/10.5194/egusphere-2024-3590
Preprint. Discussion started: 4 December 2024

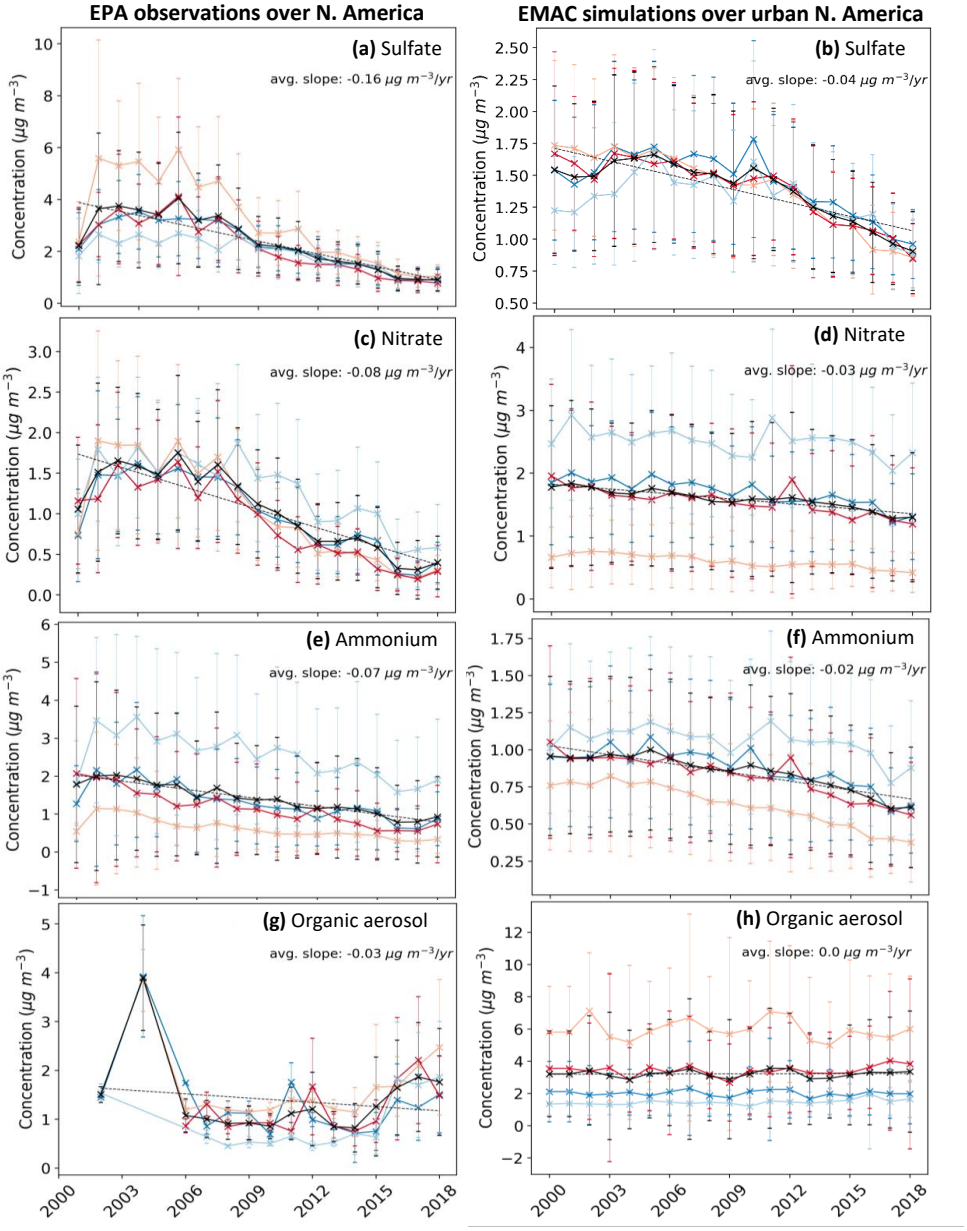

Figure 18: Temporal evolution of the observed (a, c, e, and g subplots on the left) and simulated (b, d, f, h subplots on the right) concentrations of $PM_{2.5}$ sulfate (a, b), nitrate (c, d), ammonium, (e, f), and organic aerosol (g, h) during the period 2000–2018 over urban locations in North America. Black lines show the annual trend while the dark blue, light blue, orange, and red lines represent the seasonal trends during winter, spring, summer, and autumn. Ranges represent the 1σ SD (standard

https://doi.org/10.5194/egusphere-2024-3590
Preprint. Discussion started: 4 December 2024

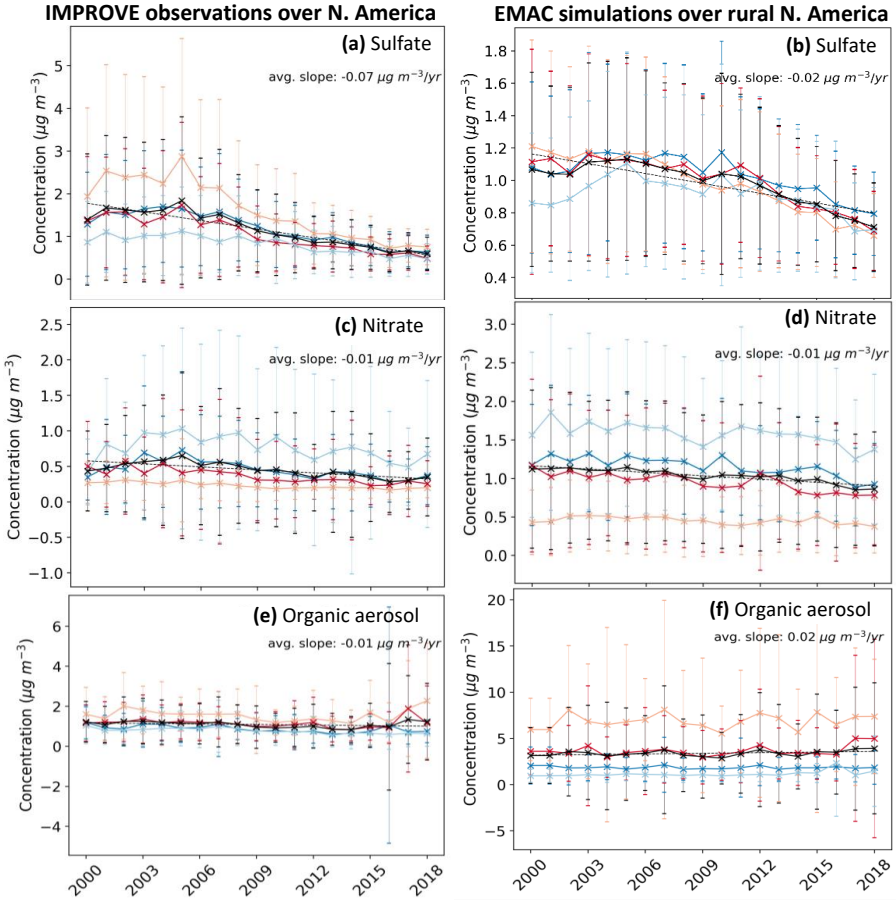

Figure 19: Temporal evolution of the observed (a, c, e, and g subplots on the left) and simulated (b, d, f, h subplots on the right) concentrations of $PM_{2.5}$ sulfate (a, b), nitrate (c, d), and organic aerosol (e, f) during the period 2000–2018 over rural locations in North America. Black lines show the annual trend while the dark blue, light blue, orange, and red lines represent the seasonal trends during winter, spring, summer, and autumn. Ranges represent the 1σ SD (standard deviation).

nitrate, ammonium decrease strongly over urban locations by -0.08 μg m^{-3} yr^{-1}, especially during the 2010s (Figure 18), even though NH_3 emissions remain practically unchanged (Figure S4). Similarly, over Canada, strong reductions in sulfate and nitrate concentrations were observed by the Canadian Air and Precipitation Monitoring Network (CAPMoN), driven by significant decreases in SO_2 and NO_x emissions (Cheng et al., 2022). While $PM_{2.5}$ concentrations decreased in eastern Canada, as observed by the National Air Pollution Surveillance (NAPS), emission reductions were less effective in the west, where large-scale wildfires overwhelmed these improvements and even led to occasional increases in $PM_{2.5}$ concentrations (Yao and Zhang, 2024). These

https://doi.org/10.5194/egusphere-2024-3590
Preprint. Discussion started: 4 December 2024

994 regional differences over Canada are also captured by the EMAC model (Figure 15).
995 Furthermore, EMAC simulates a weaker decline of sulfate concentrations over both
996 rural and urban locations (Figures 18 and 19), mainly due to its tendency to
997 underestimate sulfate concentrations during the 2000s and especially during summer.
998 Reductions on the simulated nitrate and ammonium concentrations are also noticeable
999 but to a lesser extent than on the filter observations (Figures 18 and 19). The observed
1000 OA concentrations over urban regions decrease until 2009, however, they gradually
1001 increase during 2010s by 0.11 μg m^{-3} yr^{-1}. On the other hand, the model calculated OA
1002 concentration levels remain practically unchanged during the simulated period. Both
1003 the simulated and the observed OA concentration trends are also very weak over the
1004 rural and remote regions (Figure 19).

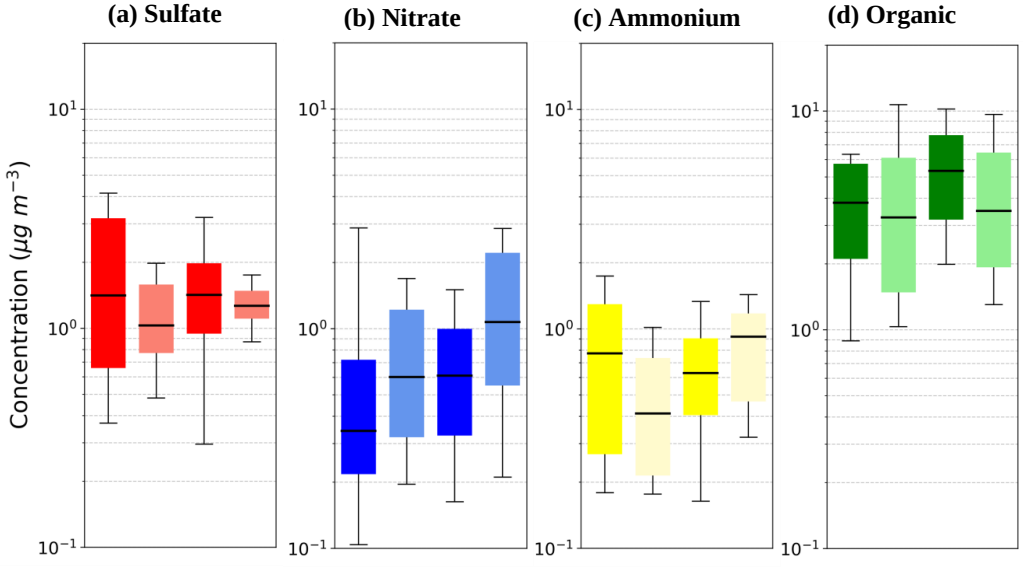

Figure 20: Decadal PM_1 concentration trends in North America expressed by the bar plots of the mass concentration (in μg m^{-3}) for (a) sulfate, (b) nitrate, (c) ammonium, and (d) OA during the periods 2000 - 2010 (left) and 2011 - 2020 (right) as calculated from the AMS observational dataset (dark colors) and the corresponding simulation values (light colors). The upper and lower whiskers range from 10-90%, the quartiles from 25-75% of the dataset. The black line is the median.

1005 Figure 20 depicts the decadal PM_1 concentration trends in North America between
1006 2000s and 2010s. The AMS data for PM_1 aerosol composition is composed of
1007 observational datasets from 30 field campaigns during the 2000s and 58 during the
1008 2010s (Figure 2). This uneven distribution can statistically manipulate the calculations

https://doi.org/10.5194/egusphere-2024-3590
Preprint. Discussion started: 4 December 2024

and hinder the extraction of valid statements for trends over North America. Sulfate concentrations exhibit a tighter distribution during the 2nd decade (Figure 20); however, the mean concentration remains unchanged between the two decades. On the other hand, the simulated sulfate concentrations increase during the 2010s, mainly due to the larger proportion of urban field campaigns during the second decade. Indeed, the model simulates a reduction of the continental average sulfate concentrations by 20%, with maximum differences exceeding 1 μg m^{-3} over the Southeast US (Figure 15). This contradicted behavior is also mirrored on nitrate concentrations where both the AMS dataset and the corresponding simulated results produce a positive trend between the two decades, while the simulated continental average nitrate concentrations decrease (Figure 15). Furthermore, compared to AMS observations, the model tends to underpredict sulfate concentrations and overpredict nitrate. This results in a strong correlation of the simulated ammonium with nitrate exhibiting a significant positive trend, which is not observed in the AMS dataset (Figure 20). Finally, as for $PM_{2.5}$ OA, the observed and, to a lesser extent, the simulated PM_1 OA concentrations increase slightly during the 2010s.

5.3 Eastern Asia

EANET observations of $PM_{2.5}$ sulfate reveal a significant increase of its concentrations until 2007 (Figure 21). However, in view of the upcoming Beijing Olympic Games in 2008, the first SO_2 emission controls have started to be implemented, and sulfate gradually reduced by -0.27 μg m^{-3} yr^{-1}. By the end of 2017, SO_2 emissions have been declined by 59% following the Clean Air Action (Zhai et al., 2019), however, observed sulfate concentrations have decreased by only 23% due to an increased dry deposition and oxidation rate of SO_2 during the same period (Fagerli et al., 2016). EMAC fails to reproduce the reduction of sulfate concentrations after 2008 since the CAMS emission inventory assumes only a stabilization of SO_2 emissions after the year 2013, instead of a strong decline (Figure S4). At the same period, NO_x was reduced by 21% and NH_3 by just 3% (Zhai et al., 2019). This however is not mirrored in the observed nitrate trends (Figure 21), where nitrate reduces by only -0.05 μg m^{-3} yr^{-1} after 2007. The strong SO_2 reduction hinders the decline of nitrate since reductions in $(NH_4)_2SO_4$ release NH_3 to react with HNO_3 and form NH_4NO_3. In contrast to observations, the simulated nitrate and ammonium continues to increase until the end of 2010s following the trends in NO_x emissions used as input in the model (Figure S4).

https://doi.org/10.5194/egusphere-2024-3590
Preprint. Discussion started: 4 December 2024

The frequency of AMS field-campaigns started to grow significantly in Eastern Asia only after 2008, while after 2013, the first consistent and aggressive emission controls started in China under the Clean Air Action (Zhai et al., 2019). Thus, since 2013 marks a significant year for Eastern Asia and due to the lack of AMS campaigns prior to 2006 in the region, the decade comparison for Eastern Asia is done for the periods of 2006-2012 and 2013-2020. Between these two periods, AMS observations reveal a -17% decline for sulfate, while the corresponding simulated sulfate concentrations reduce by just -5% (Figure 22). Similar to $PM_{2.5}$, the average PM_1 nitrate concentrations remain

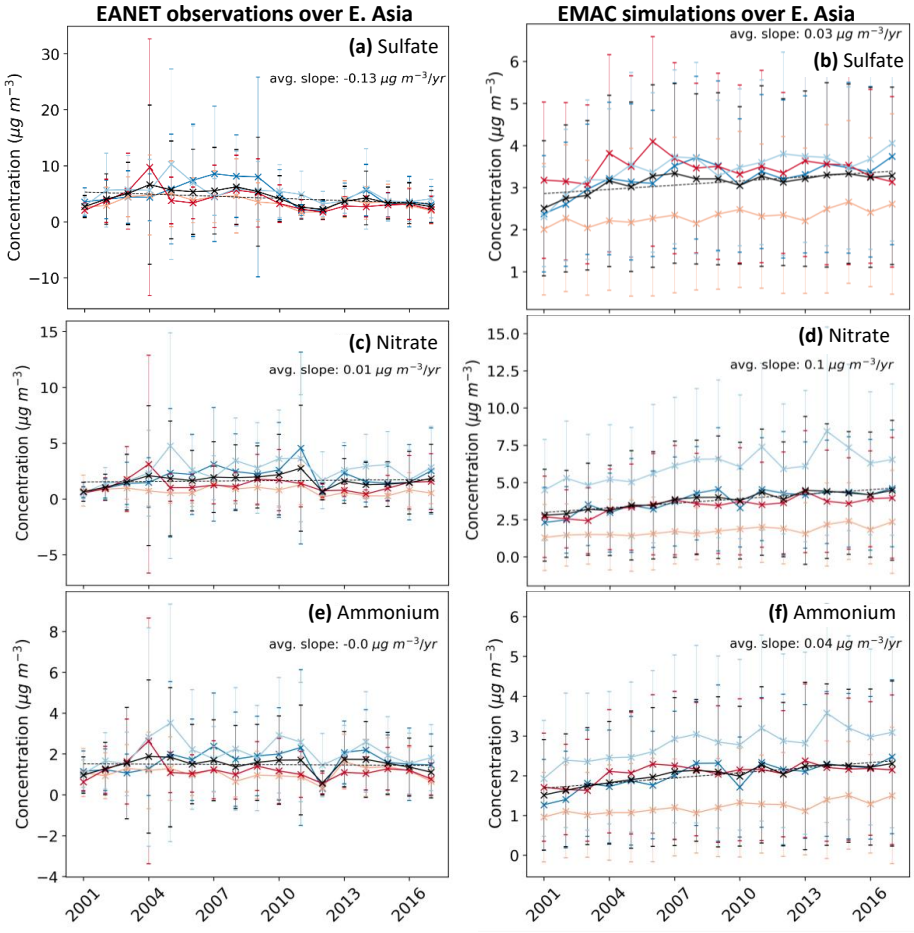

Figure 21: Temporal evolution of the observed (a, c, e, and g subplots on the left) and simulated (b, d, f, h subplots on the right) concentrations of $PM_{2.5}$ sulfate (a, b), nitrate (c, d), and ammonium (e, f) during the period 2000–2018 over Eastern Asia. Black lines show the annual trend while the dark blue, light blue, orange, and red lines represent the seasonal trends during winter, spring, summer, and autumn. Ranges represent the 1σ SD (standard deviation).

https://doi.org/10.5194/egusphere-2024-3590
Preprint. Discussion started: 4 December 2024

the same between the two periods with a marginal decline observed by the AMS and a marginal increase simulated by EMAC, while the observed ammonium reduces by 18% following the reduction in sulfate concentrations (Figure 22). In contrast to inorganic aerosol precursors, the anthropogenic VOC emissions over Eastern Asia continue to increase even after 2013, mostly due to the use of solvents but also due to the energy transformation and industrial sector (Hoesly et al., 2018). Thus, both the observed and the simulated PM_1 OA concentrations increase between the two examined periods by 15% and 33%, respectively (Figure 22).

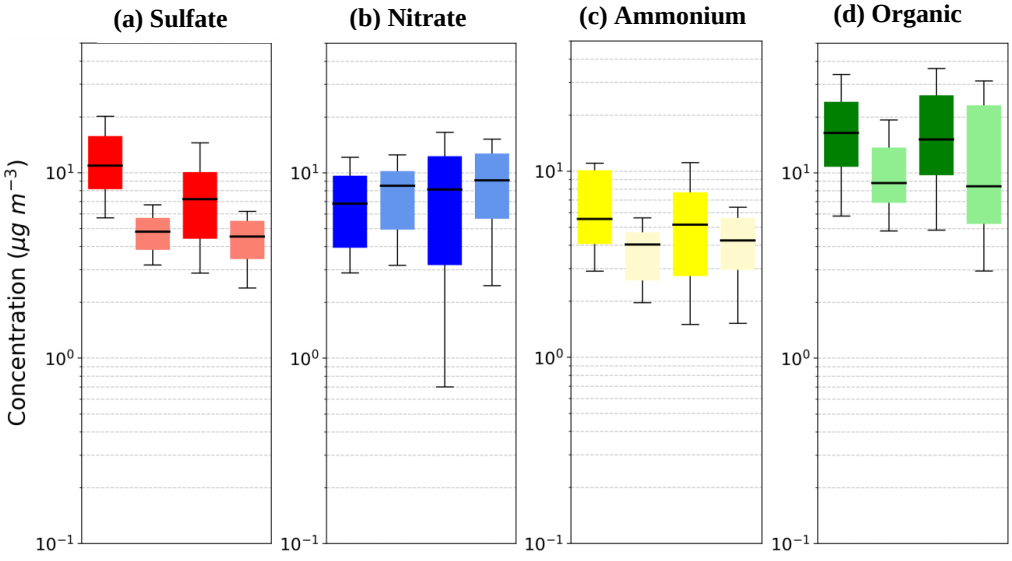

Figure 22: Decadal PM_1 concentration trends in Eastern Asia expressed by the bar plots of the mass concentration (in μg m^{-3}) for (a) sulfate, (b) nitrate, (c) ammonium, and (d) OA during the periods 2006 - 2012 (left) and 2013 - 2020 (right) as calculated from the AMS observational dataset (dark colors) and the corresponding simulation values (light colors). The upper and lower whiskers range from 10-90%, the quartiles from 25-75% of the dataset. The black line is the median.

6 Conclusion

This study investigates global trends in atmospheric aerosol composition over the past two decades, using the EMAC chemistry-climate model and the CAMS anthropogenic emissions inventory. Results integrate model outputs with global observational data from 2000-2020, covering $PM_{2.5}$ composition from regional monitoring networks (e.g., EMEP in Europe) and PM1 composition from 744 AMS observational datasets at 169 sites worldwide. Findings reveal substantial regional

https://doi.org/10.5194/egusphere-2024-3590
Preprint. Discussion started: 4 December 2024

variations in aerosol composition driven by industrial activities, energy production, and air quality regulations, highlighting the complexity of air pollution dynamics and its management.

AMS field campaign data show that OA are the dominant PM_1 component globally, especially in tropical and subtropical regions affected by biomass burning and biogenic VOC emissions. Sulfate is the primary inorganic compound across most areas, though nitrate predominates in Europe and Eastern Asia. Notably, North America shows unexpected sulfate dominance, likely due to seasonal sampling bias. HOA levels are higher in North America and Eastern Asia, while BBOA is prominent in rural Europe and tropical regions. OOA, particularly aged M-OOA, is the largest OA contributor in rural regions across all studied areas.

For $PM_{2.5}$ composition, global filter observations indicate OA as the primary component in most regions, notably in Southern Hemisphere tropical forests. In Eastern Asia, OA and elemental carbon (EC) are prominent, while OA and sulfate have similar importance in rural North America. Globally, sulfate constitutes roughly 50% of the inorganic $PM_{2.5}$ mass, followed by nitrate and ammonium. However, sulfate dominance observed in filter samples contrasts with AMS findings, likely due to sampling artifacts. Regionally, sulfate is highest in the Middle East, while nitrate plays a significant role in Europe. Across eight regions, $PM_{2.5}$ averages are: 21% sulfate, 12% nitrate, 10% ammonium, 2% sodium, 3% chloride, 40% OA, and 12% EC.

The EMAC model confirms OA as the dominant component of fine aerosols globally, with the highest concentrations in regions influenced by biomass burning, such as tropical forests and savannas. Northern industrialized regions exhibit substantial OA levels (30-35%) from fossil and biofuel combustion. While EMAC successfully reproduces the prominence of SOA, it struggles to accurately simulate aged SOA in areas like Eastern Asia. The model further suggests that nitrate surpasses sulfate in $PM_{2.5}$ composition in Europe, North America, and Eastern Asia, consistent with AMS findings but differing from some filter observations. Ammonium mirrors sulfate and nitrate distribution, with significant contributions in populated and agricultural regions. Mineral dust and sea salt emissions also play key roles regionally. Overall, EMAC provides valuable insights into global fine aerosol composition, while indicating areas for model refinement.

This study presents a 20-year analysis of global trends in fine aerosol composition, comparing EMAC model simulations with observed trends. Given limited and

https://doi.org/10.5194/egusphere-2024-3590
Preprint. Discussion started: 4 December 2024

inconsistent PM_1 datasets, the analysis focuses on broad regional trends across the first and second decades, using primarily Northern Hemisphere AMS campaign data and $PM_{2.5}$ data from major monitoring networks in North America, Europe, and East Asia. While these comparisons offer insights, they are complicated by compositional differences between PM_1 and $PM_{2.5}$ and by differences between real-time AMS and non-real-time filter-based methods.

Both filter-based data and EMAC simulations show a major decline in key inorganic components over Europe, especially in sulfate, which dropped by 46% in the last decade. The EMAC model, however, underestimates the sulfate reduction due to initial discrepancies in early 2000s concentrations. Nitrate and ammonium also declined significantly, though the model overestimates nitrate levels. Organic aerosol (OA) trends vary by method: filter data indicate a slight decrease, while AMS data and simulations suggest a mild OA increase in PM_1, likely due to differences in particle size ($PM_{2.5}$ vs. PM_1) and instrument detection capabilities (filter-based OC vs. AMS OA).

In North America, filter-based measurements reveal sharp declines in inorganic aerosol compounds, particularly in urban areas. Nitrate and sulfate concentrations decreased significantly due to lower SO_2 and NO_x precursor emissions, with ammonium levels following this trend, although ammonia itself remained stable in the 2010s. The EMAC model, however, simulates a weaker sulfate and nitrate decline, underestimating sulfate in the early 2000s while overestimating nitrate. Observed OA concentrations in urban North America decreased until 2009, then rose in the 2010s, a trend only partially captured by the model. PM_1 sulfate and nitrate levels from AMS data show inconsistent trends, with the model generally underestimating sulfate and overestimating nitrate, leading to a positive ammonium trend in the model not observed in AMS data.

In Eastern Asia, EANET $PM_{2.5}$ data show rising sulfate concentrations until 2007, followed by a decline as SO_2 emission controls implemented prior to the 2008 Beijing Olympics. Despite a 59% reduction in SO_2 emissions by 2017, sulfate concentrations fell by only 23%, likely due to increased dry deposition and oxidation rates. The EMAC model does not fully capture this trend, as it assumes stable SO_2 emissions post-2013 rather than a steep decline. Similarly, while observed nitrate and ammonium levels show minimal reductions after 2007, the model inaccurately projects continued increases, reflecting discrepancies in NO_x emissions trends. AMS data indicate a 17% reduction in PM_1 sulfate from 2006–2012 to 2013–2020, compared to a 5% reduction

https://doi.org/10.5194/egusphere-2024-3590
Preprint. Discussion started: 4 December 2024

in the model, with observed PM_1 OA concentrations increasing by 15% and model predictions showing a 33% rise, driven by sustained VOC emissions from solvents and industrial sources.

Overall, despite the complexities and inconsistencies in long-term aerosol trend analysis due to instrumental and methodological differences, this study highlights the importance of consistent, long-term global aerosol trend analysis. By integrating model results and observational data over 20 years, the study reveals significant spatiotemporal changes in atmospheric aerosol composition over different regions of the planet, largely driven by recent changes in aerosol precursor emissions.

Code and data availability. The usage of MESSy (Modular Earth Submodel System) and access to the source code is licensed to all affiliates of institutions which are members of the MESSy Consortium. Institutions can become a member of the MESSy Consortium by signing the "MESSy Memorandum of Understanding". More information can be found on the MESSy Consortium website: http://www.messy-interface.org (last access: 8 November 2024). The data produced in the study are available from the author upon request

Authors contribution: APT designed the research with contributions from VAK. APT and VAK developed ORACLE-lite. AM and VAK implemented ISOROPIA-lite in EMAC. SS selected all AMS observations and NM provided specific observations from sites over the Mediterranean. APT performed the simulations. APT and SS analyzed the results. APT, SS and VAK wrote the manuscript with contributions from NM and AM. All co-authors made revisions and corrections.

Competing interests: The authors declare that no competing interests are present

Acknowledgements: The work described in this paper has received funding from the Initiative and Networking Fund of the Helmholtz Association through the project "Advanced Earth System Modelling Capacity (ESM)". The authors gratefully acknowledge the Earth System Modelling Project (ESM) for funding this work by providing computing time on the ESM partition of the supercomputer JUWELS (Alvarez, 2021) at the Jülich Supercomputing Centre (JSC).

Financial support: This research has been supported by the project FORCeS funded from the European Union's Horizon 2020 research and innovation program under grant agreement no. 821205.

References

Aggarwal, S. G. and Kawamura, K.: Carbonaceous and inorganic composition in long-range transported aerosols over northern Japan: Implication for aging of water-soluble organic fraction, Atmospheric Environment, 43, 2532-2540, 10.1016/j.atmosenv.2009.02.032, 2009.

https://doi.org/10.5194/egusphere-2024-3590
Preprint. Discussion started: 4 December 2024

1179 Aiken, A. C., Decarlo, P. F., Kroll, J. H., Worsnop, D. R., Huffman, J. A., Docherty,
1180 K. S., Ulbrich, I. M., Mohr, C., Kimmel, J. R., Sueper, D., Sun, Y., Zhang, Q.,
1181 Trimborn, A., Northway, M., Ziemann, P. J., Canagaratna, M. R., Onasch, T. B.,
1182 Alfarra, M. R., Prevot, A. S. H., Dommen, J., Duplissy, J., Metzger, A.,
1183 Baltensperger, U., and Jimenez, J. L.: O/C and OM/OC ratios of primary, secondary,
1184 and ambient organic aerosols with high-resolution time-of-flight aerosol mass
1185 spectrometry, Environmen. Sci. & Technol., 42, 4478-4485, 2008.
1186 Akagi, S. K., Yokelson, R. J., Wiedinmyer, C., Alvarado, M. J., Reid, J. S., Karl, T.,
1187 Crounse, J. D., and Wennberg, P. O.: Emission factors for open and domestic
1188 biomass burning for use in atmospheric models, Atmos. Chem. Phys., 11, 4039-
1189 4072, 10.5194/acp-11-4039-2011, 2011.
1190 Ames, R. B. and Malm, W. C.: Comparison of sulfate and nitrate particle mass
1191 concentrations measured by IMPROVE and the CDN, Atmospheric Environment,
1192 35, 905-916, 10.1016/s1352-2310(00)00369-1, 2001.
1193 Andreae, M. O. and Rosenfeld, D.: Aerosol-cloud-precipitation interactions. Part 1. The
1194 nature and sources of cloud-active aerosols, Earth-Science Reviews, 89, 13-41,
1195 10.1016/j.earscirev.2008.03.001, 2008.
1196 Anttila, P. and Tuovinen, J. P.: Trends of primary and secondary pollutant
1197 concentrations in Finland in 1994-2007, Atmospheric Environment, 44, 30-41,
1198 10.1016/j.atmosenv.2009.09.041, 2010.
1199 Astitha, M., Lelieveld, J., Kader, M. A., Pozzer, A., and de Meij, A.: Parameterization
1200 of dust emissions in the global atmospheric chemistry-climate model EMAC: impact
1201 of nudging and soil properties, Atmospheric Chemistry and Physics, 12, 11057-
1202 11083, 10.5194/acp-12-11057-2012, 2012.
1203 Bacer, S., Sullivan, S. C., Karydis, V. A., Barahona, D., Kramer, M., Nenes, A., Tost,
1204 H., Tsimpidi, A. P., Lelieveld, J., and Pozzer, A.: Implementation of a
1205 comprehensive ice crystal formation parameterization for cirrus and mixed-phase
1206 clouds in the EMAC model (based on MESSy 2.53), Geoscientific Model
1207 Development, 11, 4021-4041, 10.5194/gmd-11-4021-2018, 2018.
1208 Batmunkh, T., Kim, Y. J., Lee, K. Y., Cayetano, M. G., Jung, J. S., Kim, S. Y., Kim,
1209 K. C., Lee, S. J., Kim, J. S., Chang, L. S., and An, J. Y.: Time-Resolved
1210 Measurements of PM2.5 Carbonaceous Aerosols at Gosan, Korea, J. Air Waste
1211 Manage. Assoc., 61, 1174-1182, 10.1080/10473289.2011.609761, 2011.
1212 Bian, H. S., Chin, M., Hauglustaine, D. A., Schulz, M., Myhre, G., Bauer, S. E., Lund,
1213 M. T., Karydis, V. A., Kucsera, T. L., Pan, X. H., Pozzer, A., Skeie, R. B., Steenrod,
1214 S. D., Sudo, K., Tsigaridis, K., Tsimpidi, A. P., and Tsyro, S. G.: Investigation of
1215 global particulate nitrate from the AeroCom phase III experiment, Atmospheric
1216 Chemistry and Physics, 17, 12911-12940, 10.5194/acp-17-12911-2017, 2017.
1217 Bougiatioti, A., Stavroulas, I., Kostenidou, E., Zarmpas, P., Theodosi, C., Kouvarakis,
1218 G., Canonaco, F., Prevot, A. S. H., Nenes, A., Pandis, S. N., and Mihalopoulos, N.:
1219 Processing of biomass-burning aerosol in the eastern Mediterranean during
1220 summertime, Atmospheric Chemistry and Physics, 14, 4793-4807, 10.5194/acp-14-
1221 4793-2014, 2014.
1222 Bourotte, C., Curl-Amarante, A. P., Forti, M. C., Pereira, L. A. A., Braga, A. L., and
1223 Lotufo, P. A.: Association between ionic composition of fine and coarse aerosol
1224 soluble fraction and peak expiratory flow of asthmatic patients in Sao Paulo city
1225 (Brazil), Atmospheric Environment, 41, 2036-2048,
1226 10.1016/j.atmosenv.2006.11.004, 2007.

https://doi.org/10.5194/egusphere-2024-3590
Preprint. Discussion started: 4 December 2024

Bouwman, A. F., Lee, D. S., Asman, W. A. H., Dentener, F. J., VanderHoek, K. W., and Olivier, J. G. J.: A global high-resolution emission inventory for ammonia, Global Biogeochemical Cycles, 11, 561-587, 10.1029/97gb02266, 1997.

Bozzetti, C., El Haddad, I., Salameh, D., Daellenbach, K. R., Fermo, P., Gonzalez, R., Minguillón, M. C., Iinuma, Y., Poulain, L., Elser, M., Müller, E., Slowik, J. G., Jaffrezo, J. L., Baltensperger, U., Marchand, N., and Prévôt, A. S. H.: Organic aerosol source apportionment by offline-AMS over a full year in Marseille, Atmos. Chem. Phys., 17, 8247-8268, 10.5194/acp-17-8247-2017, 2017.

Brook, R. D., Rajagopalan, S., Pope, C. A., 3rd, Brook, J. R., Bhatnagar, A., Diez-Roux, A. V., Holguin, F., Hong, Y., Luepker, R. V., Mittleman, M. A., Peters, A., Siscovick, D., Smith, S. C., Jr., Whitsel, L., and Kaufman, J. D.: Particulate matter air pollution and cardiovascular disease: An update to the scientific statement from the American Heart Association, Circulation, 121, 2331-2378, 10.1161/CIR.0b013e3181dbece1, 2010.

Budisulistiorini, S. H., Riva, M., Williams, M., Miyakawa, T., Chen, J., Itoh, M., Surratt, J. D., and Kuwata, M.: Dominant contribution of oxygenated organic aerosol to haze particles from real-time observation in Singapore during an Indonesian wildfire event in 2015, Atmos. Chem. Phys., 18, 16481-16498, 10.5194/acp-18-16481-2018, 2018.

Budisulistiorini, S. H., Baumann, K., Edgerton, E. S., Bairai, S. T., Mueller, S., Shaw, S. L., Knipping, E. M., Gold, A., and Surratt, J. D.: Seasonal characterization of submicron aerosol chemical composition and organic aerosol sources in the southeastern United States: Atlanta, Georgia,and Look Rock, Tennessee, Atmos. Chem. Phys., 16, 5171-5189, 10.5194/acp-16-5171-2016, 2016.

Budisulistiorini, S. H., Canagaratna, M. R., Croteau, P. L., Marth, W. J., Baumann, K., Edgerton, E. S., Shaw, S. L., Knipping, E. M., Worsnop, D. R., Jayne, J. T., Gold, A., and Surratt, J. D.: Real-Time Continuous Characterization of Secondary Organic Aerosol Derived from Isoprene Epoxydiols in Downtown Atlanta, Georgia, Using the Aerodyne Aerosol Chemical Speciation Monitor, Environmental Science & Technology, 47, 5686-5694, 10.1021/es400023n, 2013.

Canagaratna, M. R., Jayne, J. T., Jimenez, J. L., Allan, J. D., Alfarra, M. R., Zhang, Q., Onasch, T. B., Drewnick, F., Coe, H., Middlebrook, A., Delia, A., Williams, L. R., Trimborn, A. M., Northway, M. J., DeCarlo, P. F., Kolb, C. E., Davidovits, P., and Worsnop, D. R.: Chemical and microphysical characterization of ambient aerosols with the aerodyne aerosol mass spectrometer, Mass Spectrometry Reviews, 26, 185-222, https://doi.org/10.1002/mas.20115, 2007.

Cash, J. M., Langford, B., Di Marco, C., Mullinger, N. J., Allan, J., Reyes-Villegas, E., Joshi, R., Heal, M. R., Acton, W. J. F., Hewitt, C. N., Misztal, P. K., Drysdale, W., Mandal, T. K., Shivani, Gadi, R., Gurjar, B. R., and Nemitz, E.: Seasonal analysis of submicron aerosol in Old Delhi using high-resolution aerosol mass spectrometry: chemical characterisation, source apportionment and new marker identification, Atmos. Chem. Phys., 21, 10133-10158, 10.5194/acp-21-10133-2021, 2021.

Celis, J. E., Morales, J. R., Zaror, C. A., and Inzunza, J. C.: A study of the particulate matter PM10 composition in the atmosphere of Chillan, Chile, Chemosphere, 54, 541-550, 10.1016/s0045-6535(03)00711-2, 2004.

Chakraborty, A., Bhattu, D., Gupta, T., Tripathi, S. N., and Canagaratna, M. R.: Real-time measurements of ambient aerosols in a polluted Indian city: Sources, characteristics, and processing of organic aerosols during foggy and nonfoggy periods, Journal of Geophysical Research: Atmospheres, 120, 9006-9019, https://doi.org/10.1002/2015JD023419, 2015.

https://doi.org/10.5194/egusphere-2024-3590
Preprint. Discussion started: 4 December 2024

Cheng, I., Zhang, L., He, Z., Cathcart, H., Houle, D., Cole, A., Feng, J., O'Brien, J., Macdonald, A. M., Aherne, J., and Brook, J.: Long-term declines in atmospheric nitrogen and sulfur deposition reduce critical loads exceedances at multiple Canadian rural sites, 2000–2018, Atmos. Chem. Phys., 22, 14631-14656, 10.5194/acp-22-14631-2022, 2022.

Cho, S. Y. and Park, S. S.: Resolving sources of water-soluble organic carbon in fine particulate matter measured at an urban site during winter, Environmental Science-Processes & Impacts, 15, 524-534, 10.1039/c2em30730h, 2013.

Chow, W. S., Liao, K. Z., Huang, X. H. H., Leung, K. F., Lau, A. K. H., and Yu, J. Z.: Measurement report: The 10-year trend of PM_{2.5}major components and source tracers from 2008 to 2017 in an urban site of Hong Kong, China, Atmospheric Chemistry and Physics, 22, 11557-11577, 10.5194/acp-22-11557-2022, 2022.

Cottrell, L. D., Griffin, R. J., Jimenez, J. L., Zhang, Q., Ulbrich, I., Ziemba, L. D., Beckman, P. J., Sive, B. C., and Talbot, R. W.: Submicron particles at Thompson Farm during ICARTT measured using aerosol mass spectrometry, Journal of Geophysical Research-Atmospheres, 113, 10.1029/2007jd009192, 2008.

Crippa, M., Canonaco, F., Lanz, V. A., Aijala, M., Allan, J. D., Carbone, S., Capes, G., Ceburnis, D., Dall'Osto, M., Day, D. A., DeCarlo, P. F., Ehn, M., Eriksson, A., Freney, E., Ruiz, L. H., Hillamo, R., Jimenez, J. L., Junninen, H., Kiendler-Scharr, A., Kortelainen, A. M., Kulmala, M., Laaksonen, A., Mensah, A., Mohr, C., Nemitz, E., O'Dowd, C., Ovadnevaite, J., Pandis, S. N., Petaja, T., Poulain, L., Saarikoski, S., Sellegri, K., Swietlicki, E., Tiitta, P., Worsnop, D. R., Baltensperger, U., and Prevot, A. S. H.: Organic aerosol components derived from 25 AMS data sets across Europe using a consistent ME-2 based source apportionment approach, Atmospheric Chemistry and Physics, 14, 6159-6176, 10.5194/acp-14-6159-2014, 2014.

Dalsøren, S. B., Myhre, C. L., Myhre, G., Gomez-Pelaez, A. J., Søvde, O. A., Isaksen, I. S. A., Weiss, R. F., and Harth, C. M.: Atmospheric methane evolution the last 40 years, Atmos. Chem. Phys., 16, 3099-3126, 10.5194/acp-16-3099-2016, 2016.

de Sá, S. S., Rizzo, L. V., Palm, B. B., Campuzano-Jost, P., Day, D. A., Yee, L. D., Wernis, R., Isaacman-VanWertz, G., Brito, J., Carbone, S., Liu, Y. J., Sedlacek, A., Springston, S., Goldstein, A. H., Barbosa, H. M. J., Alexander, M. L., Artaxo, P., Jimenez, J. L., and Martin, S. T.: Contributions of biomass-burning, urban, and biogenic emissions to the concentrations and light-absorbing properties of particulate matter in central Amazonia during the dry season, Atmos. Chem. Phys., 19, 7973-8001, 10.5194/acp-19-7973-2019, 2019.

DeCarlo, P. F., Kimmel, J. R., Trimborn, A., Northway, M. J., Jayne, J. T., Aiken, A. C., Gonin, M., Fuhrer, K., Horvath, T., Docherty, K. S., Worsnop, D. R., and Jimenez, J. L.: Field-deployable, high-resolution, time-of-flight aerosol mass spectrometer, Analytical Chemistry, 78, 8281-8289, 10.1021/ac061249n, 2006.

Dentener, F., Kinne, S., Bond, T., Boucher, O., Cofala, J., Generoso, S., Ginoux, P., Gong, S., Hoelzemann, J. J., Ito, A., Marelli, L., Penner, J. E., Putaud, J. P., Textor, C., Schulz, M., van der Werf, G. R., and Wilson, J.: Emissions of primary aerosol and precursor gases in the years 2000 and 1750 prescribed data-sets for AeroCom, Atmos. Chem. Phys., 6, 4321-4344, 2006.

Docherty, K. S., Aiken, A. C., Huffman, J. A., Ulbrich, I. M., DeCarlo, P. F., Sueper, D., Worsnop, D. R., Snyder, D. C., Peltier, R. E., Weber, R. J., Grover, B. D., Eatough, D. J., Williams, B. J., Goldstein, A. H., Ziemann, P. J., and Jimenez, J. L.: The 2005 Study of Organic Aerosols at Riverside (SOAR-1): instrumental

https://doi.org/10.5194/egusphere-2024-3590
Preprint. Discussion started: 4 December 2024

intercomparisons and fine particle composition, Atmospheric Chemistry and Physics, 11, 12387-12420, 10.5194/acp-11-12387-2011, 2011.
Dominici, F., Peng, R. D., Bell, M. L., Pham, L., McDermott, A., Zeger, S. L., and Samet, J. M.: Fine particulate air pollution and hospital admission for cardiovascular and respiratory diseases, Jama, 295, 1127-1134, 10.1001/jama.295.10.1127, 2006.
Du, W., Sun, Y. L., Xu, Y. S., Jiang, Q., Wang, Q. Q., Yang, W., Wang, F., Bai, Z. P., Zhao, X. D., and Yang, Y. C.: Chemical characterization of submicron aerosol and particle growth events at a national background site (3295 m a.s.l.) on the Tibetan Plateau, Atmos. Chem. Phys., 15, 10811-10824, 10.5194/acp-15-10811-2015, 2015.
EMEP: EMEP Status Report: Transboundary particulate matter, photo-oxidants, acidifying and eutrophying components., Norwegian Meterological Institute, 2021.
Fagerli, H., Tsyro, S., Denby, B., Olivie, D., Nyiri, A., Gauss, M., Simpson, D., Wind, P., Benedictow, A., Mortier, A., Jonson, J., Schulz, M., Kirkevåg, A., Valdebenito, A., Iversen, T., Seland, Ø., Aas, W., Hjellbrekke, A.-G., Solberg, S., and Varma, V.: Transboundary particulate matter, photo-oxidants, acidifying and eutrophying components. EMEP Status Report 2016, 10.13140/RG.2.2.27632.46088, 2016.
Fang, T., Guo, H. Y., Zeng, L. H., Verma, V., Nenes, A., and Weber, R. J.: Highly Acidic Ambient Particles, Soluble Metals, and Oxidative Potential: A Link between Sulfate and Aerosol Toxicity, Environmental Science & Technology, 51, 2611-2620, 10.1021/acs.est.6b06151, 2017.
Favez, O., Cachler, H., Sciare, J., Alfaro, S. C., El-Araby, T. M., Harhash, M. A., and Abdelwahab, M. M.: Seasonality of major aerosol species and their transformations in Cairo megacity, Atmospheric Environment, 42, 1503-1516, 10.1016/j.atmosenv.2007.10.081, 2008.
Feng, J., Hu, M., Chan, C. K., Lau, P. S., Fang, M., He, L., and Tang, X.: A comparative study of the organic matter in PM2.5 from three Chinese megacities in three different climatic zones, Atmospheric Environment, 40, 3983-3994, 10.1016/j.atmosenv.2006.02.017, 2006.
Fuzzi, S., Decesari, S., Facchini, M. C., Cavalli, F., Emblico, L., Mircea, M., Andreae, M. O., Trebs, I., Hoffer, A., Guyon, P., Artaxo, P., Rizzo, L. V., Lara, L. L., Pauliquevis, T., Maenhaut, W., Raes, N., Chi, X. G., Mayol-Bracero, O. L., Soto-Garcia, L. L., Claeys, M., Kourtchev, I., Rissler, J., Swietlicki, E., Tagliavini, E., Schkolnik, G., Falkovich, A. H., Rudich, Y., Fisch, G., and Gatti, L. V.: Overview of the inorganic and organic composition of size-segregated aerosol in Rondonia, Brazil, from the biomass-burning period to the onset of the wet season, Journal of Geophysical Research-Atmospheres, 112, 10.1029/2005jd006741, 2007.
George, D. T., Howard, K., Isabella, A.-M., John, B., Robert, D. B., Kevin, C., Sara De, M., Francesco, F., Bertil, F., Mark, W. F., Jonathan, G., Dick, H., Frank, J. K., Nino, K., Robert, L., Annette, P., Sanjay, T. R., David, R., Beate, R., Jonathan, M. S., Thomas, S., Torben, S., Jordi, S., and Bert, B.: A joint ERS/ATS policy statement: what constitutes an adverse health effect of air pollution? An analytical framework, European Respiratory Journal, 49, 1600419, 10.1183/13993003.00419-2016, 2017.
Gioda, A., Amaral, B. S., Monteiro, I. L. G., and Saint'Pierre, T. D.: Chemical composition, sources, solubility, and transport of aerosol trace elements in a tropical region, Journal of Environmental Monitoring, 13, 2134-2142, 10.1039/c1em10240k, 2011.
Gkatzelis, G. I., Papanastasiou, D. K., Karydis, V. A., Hohaus, T., Liu, Y., Schmitt, S. H., Schlag, P., Fuchs, H., Novelli, A., Chen, Q., Cheng, X., Broch, S., Dong, H., Holland, F., Li, X., Liu, Y. H., Ma, X. F., Reimer, D., Rohrer, F., Shao, M., Tan, Z.,

https://doi.org/10.5194/egusphere-2024-3590
Preprint. Discussion started: 4 December 2024

Taraborrelli, D., Tillmann, R., Wang, H. C., Wang, Y., Wu, Y. S., Wu, Z. J., Zeng, L. M., Zheng, J., Hu, M., Lu, K. D., Hofzumahaus, A., Zhang, Y. H., Wahner, A., and Kiendler-Scharr, A.: Uptake of Water-soluble Gas-phase Oxidation Products Drives Organic Particulate Pollution in Beijing, Geophysical Research Letters, 48, 10.1029/2020gl091351, 2021.

Goldstein, A. H. and Galbally, I. E.: Known and unexplored organic constituents in the earth's atmosphere, Environmental Science & Technology, 41, 1514-1521, 10.1021/es072476p, 2007.

Granier, C., Darras, S., Gon, H. D. v. d., Doubalova, J., Elguindi, N., Galle, B., Gauss, M., Guevara, M., Jalkanen, J.-P., Kuenen, J., Liousse, C., Quack, B., Simpson, D., and Sindelarova, K.: The Copernicus Atmosphere Monitoring Service global and regional emissions (April 2019 version) 10.24380/d0bn-kx16, 2019.

Guelle, W., Schulz, M., Balkanski, Y., and Dentener, F.: Influence of the source formulation on modeling the atmospheric global distribution of sea salt aerosol, Journal of Geophysical Research: Atmospheres, 106, 27509-27524, https://doi.org/10.1029/2001JD900249, 2001.

Guenther, A. B., Jiang, X., Heald, C. L., Sakulyanontvittaya, T., Duhl, T., Emmons, L. K., and Wang, X.: The Model of Emissions of Gases and Aerosols from Nature version 2.1 (MEGAN2.1): an extended and updated framework for modeling biogenic emissions, Geosci. Model Dev., 5, 1471-1492, 10.5194/gmd-5-1471-2012, 2012.

Guerreiro, C. B. B., Foltescu, V., and de Leeuw, F.: Air quality status and trends in Europe, Atmospheric Environment, 98, 376-384, 10.1016/j.atmosenv.2014.09.017, 2014.

Hallquist, M., Wenger, J. C., Baltensperger, U., Rudich, Y., Simpson, D., Claeys, M., Dommen, J., Donahue, N. M., George, C., Goldstein, A. H., Hamilton, J. F., Herrmann, H., Hoffmann, T., Iinuma, Y., Jang, M., Jenkin, M. E., Jimenez, J. L., Kiendler-Scharr, A., Maenhaut, W., McFiggans, G., Mentel, T. F., Monod, A., Prevot, A. S. H., Seinfeld, J. H., Surratt, J. D., Szmigielski, R., and Wildt, J.: The formation, properties and impact of secondary organic aerosol: current and emerging issues, Atmospheric Chemistry and Physics, 9, 5155-5236, 10.5194/acp-9-5155-2009, 2009.

Hand, J., Copeland, S. A., McDade, C., Day, D., Moore, Jr., Dillner, A., Pitchford, M., Indresand, H., Schichtel, B., Malm, W., and Watson, J.: Spatial and seasonal patterns and temporal variability of haze and its constituents in the United States, IMPROVE Report V, 2011.

Haywood, J. and Boucher, O.: Estimates of the direct and indirect radiative forcing due to tropospheric aerosols: A review, Reviews of Geophysics, 38, 513-543, 10.1029/1999rg000078, 2000.

Hoesly, R. M., Smith, S. J., Feng, L., Klimont, Z., Janssens-Maenhout, G., Pitkanen, T., Seibert, J. J., Vu, L., Andres, R. J., Bolt, R. M., Bond, T. C., Dawidowski, L., Kholod, N., Kurokawa, J. I., Li, M., Liu, L., Lu, Z., Moura, M. C. P., O'Rourke, P. R., and Zhang, Q.: Historical (1750–2014) anthropogenic emissions of reactive gases and aerosols from the Community Emissions Data System (CEDS), Geosci. Model Dev., 11, 369-408, 10.5194/gmd-11-369-2018, 2018.

Huang, X. F., He, L. Y., Hu, M., Canagaratna, M. R., Sun, Y., Zhang, Q., Zhu, T., Xue, L., Zeng, L. W., Liu, X. G., Zhang, Y. H., Jayne, J. T., Ng, N. L., and Worsnop, D. R.: Highly time-resolved chemical characterization of atmospheric submicron particles during 2008 Beijing Olympic Games using an Aerodyne High-Resolution

https://doi.org/10.5194/egusphere-2024-3590
Preprint. Discussion started: 4 December 2024

Aerosol Mass Spectrometer, Atmospheric Chemistry and Physics, 10, 8933-8945, 10.5194/acp-10-8933-2010, 2010.

IPCC: (Intergovernmental Panel on Climate Change): The physical science basis. Contribution of working group I to the fifth assessment report of the intergovernmental panel on climate change. T.F. Stocker, D. Qin, G.-K. Plattner, M. Tignor, S.K. Allen, J. Boschung, A. Nauels, Y. Xia, V. Bex, and P.M. Midgley (eds.). Cambridge University Press, Cambridge, United Kingdom and New York, NY, USA, 2013.

IPCC, P.R. Shukla, J. S., R. Slade, A. Al Khourdajie, R. van Diemen, D. McCollum, M. Pathak, S. Some, P. Vyas, R. Fradera, M. Belkacemi, A. Hasija, G. Lisboa, S. Luz, J. Malley (Ed.): Climate Change 2022: Mitigation of Climate Change. Contribution of Working Group III to the Sixth Assessment Report of the Intergovernmental Panel on Climate Change Cambridge University Press, Cambridge, UK and New York, NY, USA, 10.1017/9781009157926, 2022.

Janssen, R. H. H., Tsimpidi, A. P., Karydis, V. A., Pozzer, A., Lelieveld, J., Crippa, M., Prévôt, A. S. H., Ait-Helal, W., Borbon, A., Sauvage, S., and Locoge, N.: Influence of local production and vertical transport on the organic aerosol budget over Paris, Journal of Geophysical Research: Atmospheres, 122, 8276-8296, https://doi.org/10.1002/2016JD026402, 2017.

Jayne, J. T., Leard, D. C., Zhang, X., Davidovits, P., Smith, K. A., Kolb, C. E., and Worsnop, D. R.: Development of an Aerosol Mass Spectrometer for Size and Composition Analysis of Submicron Particles, Aerosol Science and Technology, 33, 49-70, 10.1080/027868200410840, 2000.

Jimenez, J. L., Canagaratna, M. R., Donahue, N. M., Prevot, A. S. H., Zhang, Q., Kroll, J. H., DeCarlo, P. F., Allan, J. D., Coe, H., Ng, N. L., Aiken, A. C., Docherty, K. S., Ulbrich, I. M., Grieshop, A. P., Robinson, A. L., Duplissy, J., Smith, J. D., Wilson, K. R., Lanz, V. A., Hueglin, C., Sun, Y. L., Tian, J., Laaksonen, A., Raatikainen, T., Rautiainen, J., Vaattovaara, P., Ehn, M., Kulmala, M., Tomlinson, J. M., Collins, D. R., Cubison, M. J., Dunlea, E. J., Huffman, J. A., Onasch, T. B., Alfarra, M. R., Williams, P. I., Bower, K., Kondo, Y., Schneider, J., Drewnick, F., Borrmann, S., Weimer, S., Demerjian, K., Salcedo, D., Cottrell, L., Griffin, R., Takami, A., Miyoshi, T., Hatakeyama, S., Shimono, A., Sun, J. Y., Zhang, Y. M., Dzepina, K., Kimmel, J. R., Sueper, D., Jayne, J. T., Herndon, S. C., Trimborn, A. M., Williams, L. R., Wood, E. C., Middlebrook, A. M., Kolb, C. E., Baltensperger, U., and Worsnop, D. R.: Evolution of organic aerosols in the atmosphere, Science, 326, 1525-1529, 2009.

Jöckel, P., Kerkweg, A., Pozzer, A., Sander, R., Tost, H., Riede, H., Baumgaertner, A., Gromov, S., and Kern, B.: Development cycle 2 of the Modular Earth Submodel System (MESSy2), Geoscientific Model Development, 3, 717-752, 2010.

Jöckel, P., Tost, H., Pozzer, A., Bruehl, C., Buchholz, J., Ganzeveld, L., Hoor, P., Kerkweg, A., Lawrence, M. G., Sander, R., Steil, B., Stiller, G., Tanarhte, M., Taraborrelli, D., Van Aardenne, J., and Lelieveld, J.: The atmospheric chemistry general circulation model ECHAM5/MESSy1: consistent simulation of ozone from the surface to the mesosphere, Atmos. Chem. Phys., 6, 5067-5104, 2006.

Kaiser, J. W., Heil, A., Andreae, M. O., Benedetti, A., Chubarova, N., Jones, L., Morcrette, J. J., Razinger, M., Schultz, M. G., Suttie, M., and van der Werf, G. R.: Biomass burning emissions estimated with a global fire assimilation system based on observed fire radiative power, Biogeosciences, 9, 527-554, 10.5194/bg-9-527-2012, 2012.

https://doi.org/10.5194/egusphere-2024-3590
Preprint. Discussion started: 4 December 2024

Kakavas, S., Pandis, S. N., and Nenes, A.: ISORROPIA-Lite: A Comprehensive Atmospheric Aerosol Thermodynamics Module for Earth System Models, Tellus Series B-Chemical and Physical Meteorology, 74, 1-23, 10.16993/tellusb.33, 2022.

Kanakidou, M., Seinfeld, J. H., Pandis, S. N., Barnes, I., Dentener, F. J., Facchini, M. C., Van Dingenen, R., Ervens, B., Nenes, A., Nielsen, C. J., Swietlicki, E., Putaud, J. P., Balkanski, Y., Fuzzi, S., Horth, J., Moortgat, G. K., Winterhalter, R., Myhre, C. E. L., Tsigaridis, K., Vignati, E., Stephanou, E. G., and Wilson, J.: Organic aerosol and global climate modelling: a review, Atmos. Chem. Phys., 5, 1053-1123, 2005.

Karydis, V. A., Tsimpidi, A. P., Pozzer, A., and Lelieveld, J.: How alkaline compounds control atmospheric aerosol particle acidity, Atmospheric Chemistry and Physics, 21, 14983-15001, 10.5194/acp-21-14983-2021, 2021.

Karydis, V. A., Tsimpidi, A. P., Pozzer, A., Astitha, M., and Lelieveld, J.: Effects of mineral dust on global atmospheric nitrate concentrations, Atmos. Chem. Phys., 16, 1491-1509, 10.5194/acp-16-1491-2016, 2016.

Karydis, V. A., Tsimpidi, A. P., Bacer, S., Pozzer, A., Nenes, A., and Lelieveld, J.: Global impact of mineral dust on cloud droplet number concentration, Atmospheric Chemistry and Physics, 17, 5601-5621, 10.5194/acp-17-5601-2017, 2017.

Kerkweg, A., Buchholz, J., Ganzeveld, L., Pozzer, A., Tost, H., and Jöckel, P.: Technical Note: An implementation of the dry removal processes DRY DEPosition and SEDImentation in the Modular Earth Submodel System (MESSy), Atmos. Chem. Phys., 6, 4617-4632, 2006.

Klingmuller, K., Lelieveld, J., Karydis, V. A., and Stenchikov, G. L.: Direct radiative effect of dust-pollution interactions, Atmospheric Chemistry and Physics, 19, 7397-7408, 10.5194/acp-19-7397-2019, 2019.

Klingmuller, K., Metzger, S., Abdelkader, M., Karydis, V. A., Stenchikov, G. L., Pozzer, A., and Lelieveld, J.: Revised mineral dust emissions in the atmospheric chemistry-climate model EMAC (MESSy 2.52 DU_Astitha1 KKDU2017 patch), Geoscientific Model Development, 11, 989-1008, 10.5194/gmd-11-989-2018, 2018.

Klingmüller, K., Karydis, V. A., Bacer, S., Stenchikov, G. L., and Lelieveld, J.: Weaker cooling by aerosols due to dust-pollution interactions, Atmospheric Chemistry and Physics, 20, 15285-15295, 10.5194/acp-20-15285-2020, 2020.

Kodros, J. K., Papanastasiou, D. K., Paglione, M., Masiol, M., Squizzato, S., Florou, K., Skyllakou, K., Kaltsonoudis, C., Nenes, A., and Pandis, S. N.: Rapid dark aging of biomass burning as an overlooked source of oxidized organic aerosol, Proceedings of the National Academy of Sciences of the United States of America, 117, 33028-33033, 10.1073/pnas.2010365117, 2020.

Kok, J. F., Storelvmo, T., Karydis, V. A., Adebiyi, A. A., Mahowald, N. M., Evan, A. T., He, C. L., and Leung, D. M.: Mineral dust aerosol impacts on global climate and climate change, Nature Reviews Earth & Environment, 4, 71-86, 10.1038/s43017-022-00379-5, 2023.

Kostenidou, E., Florou, K., Kaltsonoudis, C., Tsiflikiotou, M., Vratolis, S., Eleftheriadis, K., and Pandis, S. N.: Sources and chemical characterization of organic aerosol during the summer in the eastern Mediterranean, Atmospheric Chemistry and Physics, 15, 11355-11371, 10.5194/acp-15-11355-2015, 2015.

Kuzu, S. L., Yavuz, E., Akyüz, E., Saral, A., Akkoyunlu, B. O., Özdemir, H., Demir, G., and Ünal, A.: Black carbon and size-segregated elemental carbon, organic carbon compositions in a megacity: a case study for Istanbul, Air Quality, Atmosphere & Health, 13, 827-837, 10.1007/s11869-020-00839-1, 2020.

https://doi.org/10.5194/egusphere-2024-3590
Preprint. Discussion started: 4 December 2024

Kyllönen, K., Vestenius, M., Anttila, P., Makkonen, U., Aurela, M., Wängberg, I., Mastromonaco, M. N., and Hakola, H.: Trends and source apportionment of atmospheric heavy metals at a subarctic site during 1996-2018, Atmospheric Environment, 236, 10.1016/j.atmosenv.2020.117644, 2020.

Lang, P. E., Carslaw, D. C., and Moller, S. J.: A trend analysis approach for air quality network data, Atmospheric Environment-X, 2, 10.1016/j.aeaoa.2019.100030, 2019.

Lanz, V. A., Alfarra, M. R., Baltensperger, U., Buchmann, B., Hueglin, C., and Prevot, A. S. H.: Source apportionment of submicron organic aerosols at an urban site by factor analytical modelling of aerosol mass spectra, Atmospheric Chemistry and Physics, 7, 1503-1522, 2007.

Lanz, V. A., Alfarra, M. R., Baltensperger, U., Buchmann, B., Hueglin, C., Szidat, S., Wehrli, M. N., Wacker, L., Weimer, S., Caseiro, A., Puxbaum, H., and Prevot, A. S. H.: Source attribution of submicron organic aerosols during wintertime inversions by advanced factor analysis of aerosol mass spectra, Environmental Science & Technology, 42, 214-220, 10.1021/es0707207, 2008.

Lanz, V. A., Prevot, A. S. H., Alfarra, M. R., Weimer, S., Mohr, C., DeCarlo, P. F., Gianini, M. F. D., Hueglin, C., Schneider, J., Favez, O., D'Anna, B., George, C., and Baltensperger, U.: Characterization of aerosol chemical composition with aerosol mass spectrometry in Central Europe: an overview, Atmospheric Chemistry and Physics, 10, 10453-10471, 10.5194/acp-10-10453-2010, 2010.

Lelieveld, J., Evans, J. S., Fnais, M., Giannadaki, D., and Pozzer, A.: The contribution of outdoor air pollution sources to premature mortality on a global scale, Nature, 525, 367-371, 10.1038/nature15371, 2015.

Li, L., Wang, W., Feng, J., Zhang, D., Li, H., Gu, Z., Wang, B., Sheng, G., and Fu, J.: Composition, source, mass closure of PM2.5 aerosols for four forests in eastern China, Journal of Environmental Sciences, 22, 405-412, 10.1016/s1001-0742(09)60122-4, 2010.

Liu, L., ; Thorsten Hohaus; Philipp Franke; Anne C. Lange; Ralf Tillmann; Hendrik Fuchs; Zhaofeng Tan; Franz Rohrer; Vlassis Karydis; Quanfu He; Vaishali Vardhan; Stefanie Andres; Birger Bohn; Frank Holland; Benjamin Winter; Sergej Wedel; Anna Novelli; Andreas Hofzumahaus; Andreas Wahner; and Astrid Kiendler-Scharr: Observational evidence reveals the significance of nocturnal chemistry in secondary organic aerosol formation across all seasons, npj Climate and Atmospheric Science, in review, 2024.

Liu, X., Lara, R., Dufresne, M., Wu, L., Zhang, X., Wang, T., Monge, M., Reche, C., Di Leo, A., Lanzani, G., Colombi, C., Font, A., Sheehan, A., Green, D. C., Makkonen, U., Sauvage, S., Salameh, T., Petit, J.-E., Chatain, M., Coe, H., Hou, S., Harrison, R., Hopke, P. K., Petäjä, T., Alastuey, A., and Querol, X.: Variability of ambient air ammonia in urban Europe (Finland, France, Italy, Spain, and the UK), Environment International, 185, 108519, https://doi.org/10.1016/j.envint.2024.108519, 2024.

Lohmann, U. and Ferrachat, S.: Impact of parametric uncertainties on the present-day climate and on the anthropogenic aerosol effect, Atmos. Chem. Phys., 10, 11373-11383, 10.5194/acp-10-11373-2010, 2010.

Mallet, M. D., D'Anna, B., Même, A., Bove, M. C., Cassola, F., Pace, G., Desboeufs, K., Di Biagio, C., Doussin, J. F., Maille, M., Massabò, D., Sciare, J., Zapf, P., di Sarra, A. G., and Formenti, P.: Summertime surface PM1 aerosol composition and size by source region at the Lampedusa island in the central Mediterranean Sea, Atmos. Chem. Phys., 19, 11123-11142, 10.5194/acp-19-11123-2019, 2019.

https://doi.org/10.5194/egusphere-2024-3590
Preprint. Discussion started: 4 December 2024

Mariani, R. L. and de Mello, W. Z.: PM2.5-10, PM2.5 and associated water-soluble inorganic species at a coastal urban site in the metropolitan region of Rio de Janeiro, Atmospheric Environment, 41, 2887-2892, 10.1016/j.atmosenv.2006.12.009, 2007.

Martin, S. T., Andreae, M. O., Artaxo, P., Baumgardner, D., Chen, Q., Goldstein, A. H., Guenther, A., Heald, C. L., Mayol-Bracero, O. L., McMurry, P. H., Pauliquevis, T., Poschl, U., Prather, K. A., Roberts, G. C., Saleska, S. R., Dias, M. A. S., Spracklen, D. V., Swietlicki, E., and Trebs, I.: SOURCES AND PROPERTIES OF AMAZONIAN AEROSOL PARTICLES, Reviews of Geophysics, 48, 10.1029/2008rg000280, 2010.

Meng, Z. Y. and Seinfeld, J. H.: Time scales to achieve atmospheric gas-aerosol equilibrium for volatile species, Atmospheric Environment, 30, 2889-2900, 10.1016/1352-2310(95)00493-9, 1996.

Milousis, A., Tsimpidi, A. P., Tost, H., Pandis, S. N., Nenes, A., Kiendler-Scharr, A., and Karydis, V. A.: Implementation of the ISORROPIA-lite aerosol thermodynamics model into the EMAC chemistry climate model (based on MESSy v2.55): implications for aerosol composition and acidity, Geosci. Model Dev., 17, 1111-1131, 10.5194/gmd-17-1111-2024, 2024.

Mkoma, S. L.: Physico-Chemical Characterisation of Atmospheric Aerosols in Tanzania, with Emphasis on the Carbonaceous Aerosol Components and on Chemical Mass Closure, 2008.

Mkoma, S. L., Maenhaut, W., Chi, X. G., Wang, W., and Raes, N.: Characterisation of PM10 atmospheric aerosols for the wet season 2005 at two sites in East Africa, Atmospheric Environment, 43, 631-639, 10.1016/j.atmosenv.2008.10.008, 2009.

Mohr, C., DeCarlo, P. F., Heringa, M. F., Chirico, R., Slowik, J. G., Richter, R., Reche, C., Alastuey, A., Querol, X., Seco, R., Penuelas, J., Jimenez, J. L., Crippa, M., Zimmermann, R., Baltensperger, U., and Prevot, A. S. H.: Identification and quantification of organic aerosol from cooking and other sources in Barcelona using aerosol mass spectrometer data, Atmospheric Chemistry and Physics, 12, 1649-1665, 10.5194/acp-12-1649-2012, 2012.

Molina, L. T., Kolb, C. E., de Foy, B., Lamb, B. K., Brune, W. H., Jimenez, J. L., Ramos-Villegas, R., Sarmiento, J., Paramo-Figueroa, V. H., Cardenas, B., Gutierrez-Avedoy, V., and Molina, M. J.: Air quality in North America's most populous city – overview of the MCMA-2003 campaign, Atmos. Chem. Phys., 7, 2447-2473, 10.5194/acp-7-2447-2007, 2007.

Molina, L. T., Madronich, S., Gaffney, J. S., Apel, E., de Foy, B., Fast, J., Ferrare, R., Herndon, S., Jimenez, J. L., Lamb, B., Osornio-Vargas, A. R., Russell, P., Schauer, J. J., Stevens, P. S., Volkamer, R., and Zavala, M.: An overview of the MILAGRO 2006 Campaign: Mexico City emissions and their transport and transformation, Atmospheric Chemistry and Physics, 10, 8697-8760, 10.5194/acp-10-8697-2010, 2010.

Mortier, A., Gliß, J., Schulz, M., Aas, W., Andrews, E., Bian, H., Chin, M., Ginoux, P., Hand, J., Holben, B., Zhang, H., Kipling, Z., Kirkevåg, A., Laj, P., Lurton, T., Myhre, G., Neubauer, D., Olivié, D., von Salzen, K., Skeie, R. B., Takemura, T., and Tilmes, S.: Evaluation of climate model aerosol trends with ground-based observations over the last 2 decades – an AeroCom and CMIP6 analysis, Atmos. Chem. Phys., 20, 13355-13378, 10.5194/acp-20-13355-2020, 2020.

Ng, N. L., Canagaratna, M. R., Jimenez, J. L., Zhang, Q., Ulbrich, I. M., and Worsnop, D. R.: Real-Time Methods for Estimating Organic Component Mass Concentrations from Aerosol Mass Spectrometer Data, Environmental Science & Technology, 45, 910-916, 10.1021/es102951k, 2011.

https://doi.org/10.5194/egusphere-2024-3590
Preprint. Discussion started: 4 December 2024

Ng, N. L., Canagaratna, M. R., Zhang, Q., Jimenez, J. L., Tian, J., Ulbrich, I. M., Kroll, J. H., Docherty, K. S., Chhabra, P. S., Bahreini, R., Murphy, S. M., Seinfeld, J. H., Hildebrandt, L., Donahue, N. M., DeCarlo, P. F., Lanz, V. A., Prévôt, A. S. H., Dinar, E., Rudich, Y., and Worsnop, D. R.: Organic aerosol components observed in Northern Hemispheric datasets from Aerosol Mass Spectrometry, Atmos. Chem. Phys., 10, 4625-4641, 10.5194/acp-10-4625-2010, 2010.

Paatero, P.: Least squares formulation of robust non-negative factor analysis, Chemometrics and Intelligent Laboratory Systems, 37, 23-35, 10.1016/s0169-7439(96)00044-5, 1997.

Paatero, P.: The Multilinear Engine—A Table-Driven, Least Squares Program for Solving Multilinear Problems, Including the n-Way Parallel Factor Analysis Model, Journal of Computational and Graphical Statistics, 8, 854-888, 10.1080/10618600.1999.10474853, 1999.

Paatero, P. and Tapper, U.: Positive matrix factorization-A nonnegative factor model with optimal utilization of error-estimates of data values, Environmetrics, 5, 111-126, 10.1002/env.3170050203, 1994.

Paglione, M., Gilardoni, S., Rinaldi, M., Decesari, S., Zanca, N., Sandrini, S., Giulianelli, L., Bacco, D., Ferrari, S., Poluzzi, V., Scotto, F., Trentini, A., Poulain, L., Herrmann, H., Wiedensohler, A., Canonaco, F., Prévôt, A. S. H., Massoli, P., Carbone, C., Facchini, M. C., and Fuzzi, S.: The impact of biomass burning and aqueous-phase processing on air quality: a multi-year source apportionment study in the Po Valley, Italy, Atmos. Chem. Phys., 20, 1233-1254, 10.5194/acp-20-1233-2020, 2020.

Parworth, C., Fast, J., Mei, F., Shippert, T., Sivaraman, C., Tilp, A., Watson, T., and Zhang, Q.: Long-term measurements of submicrometer aerosol chemistry at the Southern Great Plains (SGP) using an Aerosol Chemical Speciation Monitor (ACSM), Atmospheric Environment, 106, 43-55, 10.1016/j.atmosenv.2015.01.060, 2015.

Pathak, R. K., Wang, T., Ho, K. F., and Lee, S. C.: Characteristics of summertime PM2.5 organic and elemental carbon in four major Chinese cities: Implications of high acidity for water-soluble organic carbon (WSOC), Atmospheric Environment, 45, 318-325, 10.1016/j.atmosenv.2010.10.021, 2011.

Petit, J. E., Favez, O., Sciare, J., Crenn, V., Sarda-Estève, R., Bonnaire, N., Močnik, G., Dupont, J. C., Haeffelin, M., and Leoz-Garziandia, E.: Two years of near real-time chemical composition of submicron aerosols in the region of Paris using an Aerosol Chemical Speciation Monitor (ACSM) and a multi-wavelength Aethalometer, Atmos. Chem. Phys., 15, 2985-3005, 10.5194/acp-15-2985-2015, 2015.

Pope, C. A., Ezzati, M., and Dockery, D. W.: Fine-Particulate Air Pollution and Life Expectancy in the United States, New England Journal of Medicine, 360, 376-386, 10.1056/NEJMsa0805646, 2009.

Pozzer, A., Joeckel, P. J., Sander, R., Williams, J., Ganzeveld, L., and Lelieveld, J.: Technical note: the MESSy-submodel AIRSEA calculating the air-sea exchange of chemical species, Atmos. Chem. Phys., 6, 5435-5444, 2006.

Pozzer, A., Reifenberg, S. F., Kumar, V., Franco, B., Kohl, M., Taraborrelli, D., Gromov, S., Ehrhart, S., Jöckel, P., Sander, R., Fall, V., Rosanka, S., Karydis, V., Akritidis, D., Emmerichs, T., Crippa, M., Guizzardi, D., Kaiser, J. W., Clarisse, L., Kiendler-Scharr, A., Tost, H., and Tsimpidi, A.: Simulation of organics in the atmosphere: evaluation of EMACv2.54 with the Mainz Organic Mechanism (MOM)

https://doi.org/10.5194/egusphere-2024-3590
Preprint. Discussion started: 4 December 2024

coupled to the ORACLE (v1.0) submodel, Geoscientific Model Development, 15, 2673-2710, 10.5194/gmd-15-2673-2022, 2022.
Price, C. and Rind, D.: A SIMPLE LIGHTNING PARAMETERIZATION FOR CALCULATING GLOBAL LIGHTNING DISTRIBUTIONS, Journal of Geophysical Research-Atmospheres, 97, 9919-9933, 1992.
Pringle, K. J., Tost, H., Message, S., Steil, B., Giannadaki, D., Nenes, A., Fountoukis, C., Stier, P., Vignati, E., and Leieved, J.: Description and evaluation of GMXe: a new aerosol submodel for global simulations (v1), Geoscientific Model Development, 3, 391-412, 2010.
Radhi, M., Box, M. A., Box, G. P., Mitchell, R. M., Cohen, D. D., Stelcer, E., and Keywood, M. D.: Optical, physical and chemical characteristics of Australian continental aerosols: results from a field experiment, Atmospheric Chemistry and Physics, 10, 5925-5942, 10.5194/acp-10-5925-2010, 2010.
Rattanavaraha, W., Canagaratna, M. R., Budisulistiorini, S. H., Croteau, P. L., Baumann, K., Canonaco, F., Prevot, A. S. H., Edgerton, E. S., Zhang, Z., Jayne, J. T., Worsnop, D. R., Gold, A., Shaw, S. L., and Surratt, J. D.: Source apportionment of submicron organic aerosol collected from Atlanta, Georgia, during 2014–2015 using the aerosol chemical speciation monitor (ACSM), Atmospheric Environment, 167, 389-402, https://doi.org/10.1016/j.atmosenv.2017.07.055, 2017.
Roeckner, E., Brokopf, R., Esch, M., Giorgetta, M., Hagemann, S., Kornblueh, L., Manzini, E., Schlese, U., and Schulzweida, U.: Sensitivity of simulated climate to horizontal and vertical resolution in the ECHAM5 atmosphere model, Journal of Climate, 19, 3771-3791, 10.1175/jcli3824.1, 2006.
Sander, R., Baumgaertner, A., Cabrera-Perez, D., Frank, F., Gromov, S., Grooss, J. U., Harder, H., Huijnen, V., Jockel, P., Karydis, V. A., Niemeyer, K. E., Pozzer, A., Hella, R. B., Schultz, M. G., Taraborrelli, D., and Tauer, S.: The community atmospheric chemistry box model CAABA/MECCA-4.0, Geoscientific Model Development, 12, 1365-1385, 10.5194/gmd-12-1365-2019, 2019.
Schlag, P., Kiendler-Scharr, A., Blom, M. J., Canonaco, F., Henzing, J. S., Moerman, M., Prévôt, A. S. H., and Holzinger, R.: Aerosol source apportionment from 1-year measurements at the CESAR tower in Cabauw, the Netherlands, Atmos. Chem. Phys., 16, 8831-8847, 10.5194/acp-16-8831-2016, 2016.
Seco, R., Peñuelas, J., Filella, I., Llusià, J., Molowny-Horas, R., Schallhart, S., Metzger, A., Müller, M., and Hansel, A.: Contrasting winter and summer VOC mixing ratios at a forest site in the Western Mediterranean Basin: the effect of local biogenic emissions, Atmos. Chem. Phys., 11, 13161-13179, 10.5194/acp-11-13161-2011, 2011.
Seinfeld, J. H. and Pandis, S. N.: Atmospheric Chemistry and Physics: From Air Pollution to Climate Change, Second, John Wiley & Sons, Inc., Hoboken, New Jersey2006.
Snider, G., Weagle, C. L., Martin, R. V., van Donkelaar, A., Conrad, K., Cunningham, D., Gordon, C., Zwicker, M., Akoshile, C., Artaxo, P., Anh, N. X., Brook, J., Dong, J., Garland, R. M., Greenwald, R., Griffith, D., He, K., Holben, B. N., Kahn, R., Koren, I., Lagrosas, N., Lestari, P., Ma, Z., Vanderlei Martins, J., Quel, E. J., Rudich, Y., Salam, A., Tripathi, S. N., Yu, C., Zhang, Q., Zhang, Y., Brauer, M., Cohen, A., Gibson, M. D., and Liu, Y.: SPARTAN: a global network to evaluate and enhance satellite-based estimates of ground-level particulate matter for global health applications, Atmos. Meas. Tech., 8, 505-521, 10.5194/amt-8-505-2015, 2015.
Snider, G., Weagle, C. L., Murdymootoo, K. K., Ring, A., Ritchie, Y., Stone, E., Walsh, A., Akoshile, C., Anh, N. X., Balasubramanian, R., Brook, J., Qonitan, F. D., Dong,

https://doi.org/10.5194/egusphere-2024-3590
Preprint. Discussion started: 4 December 2024

J., Griffith, D., He, K., Holben, B. N., Kahn, R., Lagrosas, N., Lestari, P., Ma, Z., Misra, A., Norford, L. K., Quel, E. J., Salam, A., Schichtel, B., Segev, L., Tripathi, S., Wang, C., Yu, C., Zhang, Q., Zhang, Y., Brauer, M., Cohen, A., Gibson, M. D., Liu, Y., Martins, J. V., Rudich, Y., and Martin, R. V.: Variation in global chemical composition of PM2.5: emerging results from SPARTAN, Atmos. Chem. Phys., 16, 9629-9653, 10.5194/acp-16-9629-2016, 2016.

Solomon, P. A., Crumpler, D., Flanagan, J. B., Jayanty, R. K. M., Rickman, E. E., and McDade, C. E.: US National PM2.5 Chemical Speciation Monitoring Networks-CSN and IMPROVE: Description of networks, J. Air Waste Manage. Assoc., 64, 1410-1438, 10.1080/10962247.2014.956904, 2014.

Souza, P. A. d., Mello, W. Z. d., Mariani, R. L., and Sella, S. M.: Caracterização do material particulado fino e grosso e composição da fração inorgânica solúvel em água em São José dos Campos (SP), Química Nova, 33, 1247-1253, 2010.

Stavroulas, I., Bougiatioti, A., Grivas, G., Paraskevopoulou, D., Tsagkaraki, M., Zarmpas, P., Liakakou, E., Gerasopoulos, E., and Mihalopoulos, N.: Sources and processes that control the submicron organic aerosol composition in an urban Mediterranean environment (Athens): a high temporal-resolution chemical composition measurement study, Atmos. Chem. Phys., 19, 901-919, 10.5194/acp-19-901-2019, 2019.

Sun, Y., Xu, W., Zhang, Q., Jiang, Q., Canonaco, F., Prévôt, A. S. H., Fu, P., Li, J., Jayne, J., Worsnop, D. R., and Wang, Z.: Source apportionment of organic aerosol from 2-year highly time-resolved measurements by an aerosol chemical speciation monitor in Beijing, China, Atmos. Chem. Phys., 18, 8469-8489, 10.5194/acp-18-8469-2018, 2018.

Sun, Y., He, Y., Kuang, Y., Xu, W., Song, S., Ma, N., Tao, J., Cheng, P., Wu, C., Su, H., Cheng, Y., Xie, C., Chen, C., Lei, L., Qiu, Y., Fu, P., Croteau, P., and Worsnop, D. R.: Chemical Differences Between PM1 and PM2.5 in Highly Polluted Environment and Implications in Air Pollution Studies, Geophysical Research Letters, 47, e2019GL086288, https://doi.org/10.1029/2019GL086288, 2020.

Sun, Y. L., Wang, Z. F., Fu, P. Q., Yang, T., Jiang, Q., Dong, H. B., Li, J., and Jia, J. J.: Aerosol composition, sources and processes during wintertime in Beijing, China, Atmos. Chem. Phys., 13, 4577-4592, 10.5194/acp-13-4577-2013, 2013.

Tiitta, P., Vakkari, V., Croteau, P., Beukes, J. P., van Zyl, P. G., Josipovic, M., Venter, A. D., Jaars, K., Pienaar, J. J., Ng, N. L., Canagaratna, M. R., Jayne, J. T., Kerminen, V. M., Kokkola, H., Kulmala, M., Laaksonen, A., Worsnop, D. R., and Laakso, L.: Chemical composition, main sources and temporal variability of PM₁ aerosols in southern African grassland, Atmos. Chem. Phys., 14, 1909-1927, 10.5194/acp-14-1909-2014, 2014.

Timonen, H., Carbone, S., Aurela, M., Saarnio, K., Saarikoski, S., Ng, N. L., Canagaratna, M. R., Kulmala, M., Kerminen, V.-M., Worsnop, D. R., and Hillamo, R.: Characteristics, sources and water-solubility of ambient submicron organic aerosol in springtime in Helsinki, Finland, Journal of Aerosol Science, 56, 61-77, 10.1016/j.jaerosci.2012.06.005, 2013.

Tørseth, K., Aas, W., Breivik, K., Fjæraa, A. M., Fiebig, M., Hjellbrekke, A. G., Lund Myhre, C., Solberg, S., and Yttri, K. E.: Introduction to the European Monitoring and Evaluation Programme (EMEP) and observed atmospheric composition change during 1972–2009, Atmos. Chem. Phys., 12, 5447-5481, 10.5194/acp-12-5447-2012, 2012.

https://doi.org/10.5194/egusphere-2024-3590
Preprint. Discussion started: 4 December 2024

Tost, H., Jockel, P. J., Kerkweg, A., Sander, R., and Lelieveld, J.: Technical note: A new comprehensive SCAVenging submodel for global atmospheric chemistry modelling, Atmos. Chem. Phys., 6, 565-574, 2006.

Tost, H., Joeckel, P., Kerkweg, A., Pozzer, A., Sander, R., and Lelieveld, J.: Global cloud and precipitation chemistry and wet deposition: tropospheric model simulations with ECHAM5/MESSy1, Atmos. Chem. Phys., 7, 2733-2757, 2007.

Tsigaridis, K., Daskalakis, N., Kanakidou, M., Adams, P. J., Artaxo, P., Bahadur, R., Balkanski, Y., Bauer, S. E., Bellouin, N., Benedetti, A., Bergman, T., Berntsen, T. K., Beukes, J. P., Bian, H., Carslaw, K. S., Chin, M., Curci, G., Diehl, T., Easter, R. C., Ghan, S. J., Gong, S. L., Hodzic, A., Hoyle, C. R., Iversen, T., Jathar, S., Jimenez, J. L., Kaiser, J. W., Kirkevag, A., Koch, D., Kokkola, H., Lee, Y. H., Lin, G., Liu, X., Luo, G., Ma, X., Mann, G. W., Mihalopoulos, N., Morcrette, J. J., Mueller, J. F., Myhre, G., Myriokefalitakis, S., Ng, N. L., O'Donnell, D., Penner, J. E., Pozzoli, L., Pringle, K. J., Russell, L. M., Schulz, M., Sciare, J., Seland, O., Shindell, D. T., Sillman, S., Skeie, R. B., Spracklen, D., Stavrakou, T., Steenrod, S. D., Takemura, T., Tiitta, P., Tilmes, S., Tost, H., van Noije, T., van Zyl, P. G., von Salzen, K., Yu, F., Wang, Z., Wang, Z., Zaveri, R. A., Zhang, H., Zhang, K., Zhang, Q., and Zhang, X.: The AeroCom evaluation and intercomparison of organic aerosol in global models, Atmospheric Chemistry and Physics, 14, 10845-10895, 10.5194/acp-14-10845-2014, 2014.

Tsimpidi, A. P., Karydis, V. A., Pandis, S. N., and Lelieveld, J.: Global combustion sources of organic aerosols: model comparison with 84 AMS factor-analysis data sets, Atmos. Chem. Phys., 16, 8939-8962, 10.5194/acp-16-8939-2016, 2016.

Tsimpidi, A. P., Karydis, V. A., Pozzer, A., Pandis, S. N., and Lelieveld, J.: ORACLE (v1.0): module to simulate the organic aerosol composition and evolution in the atmosphere, Geoscientific Model Development, 7, 3153-3172, 10.5194/gmd-7-3153-2014, 2014.

Tsimpidi, A. P., Karydis, V. A., Pozzer, A., Pandis, S. N., and Lelieveld, J.: ORACLE 2-D (v2.0): an efficient module to compute the volatility and oxygen content of organic aerosol with a global chemistry-climate model, Geoscientific Model Development, 11, 3369-3389, 10.5194/gmd-11-3369-2018, 2018.

Vasilakopoulou, C. N., Matrali, A., Skyllakou, K., Georgopoulou, M., Aktypis, A., Florou, K., Kaltsonoudis, C., Siouti, E., Kostenidou, E., Błaziak, A., Nenes, A., Papagiannis, S., Eleftheriadis, K., Patoulias, D., Kioutsioukis, I., and Pandis, S. N.: Rapid transformation of wildfire emissions to harmful background aerosol, npj Climate and Atmospheric Science, 6, 218, 10.1038/s41612-023-00544-7, 2023.

Vignati, E., Wilson, J., and Stier, P.: M7: An efficient size-resolved aerosol microphysics module for large-scale aerosol transport models, J. Geophys. Res.-Atmos., 109, doi: 10.1029/2003jd004485, 2004.

Wang, Y., Li, W., Gao, W., Liu, Z., Tian, S., Shen, R., Ji, D., Wang, S., Wang, L., Tang, G., Song, T., Cheng, M., Wang, G., Gong, Z., Hao, J., and Zhang, Y.: Trends in particulate matter and its chemical compositions in China from 2013–2017, Science China Earth Sciences, 62, 1857-1871, 10.1007/s11430-018-9373-1, 2019.

Weinstein, J. P., Hedges, S. R., and Kimbrough, S.: Characterization and aerosol mass balance of PM2.5 and PM10 collected in Conakry, Guinea during the 2004 Harmattan period, Chemosphere, 78, 980-988, 10.1016/j.chemosphere.2009.12.022, 2010.

WHO: Health aspects of air pollution with particulate matter, ozone and nitrogen dioxide : report on a WHO working group, Bonn, Germany 13-15 January 2003, 2003.

https://doi.org/10.5194/egusphere-2024-3590
Preprint. Discussion started: 4 December 2024

WHO: WHO global air quality guidelines: Particulate matter ($PM_{2.5}$ and PM_{10}), ozone, nitrogen dioxide, sulfur dioxide and carbon monoxide, 2021.

WHO: Ambient (outdoor) air pollution: https://www.who.int/news-room/fact-sheets/detail/ambient-(outdoor)-air-quality-and-health, last access: 15/09/2024.

Xu, L., Suresh, S., Guo, H., Weber, R. J., and Ng, N. L.: Aerosol characterization over the southeastern United States using high-resolution aerosol mass spectrometry: spatial and seasonal variation of aerosol composition and sources with a focus on organic nitrates, Atmos. Chem. Phys., 15, 7307-7336, 10.5194/acp-15-7307-2015, 2015.

Xu, W., Han, T., Du, W., Wang, Q., Chen, C., Zhao, J., Zhang, Y., Li, J., Fu, P., Wang, Z., Worsnop, D. R., and Sun, Y.: Effects of Aqueous-Phase and Photochemical Processing on Secondary Organic Aerosol Formation and Evolution in Beijing, China, Environ Sci Technol, 51, 762-770, 10.1021/acs.est.6b04498, 2017.

Xu, W., Sun, Y., Wang, Q., Zhao, J., Wang, J., Ge, X., Xie, C., Zhou, W., Du, W., Li, J., Fu, P., Wang, Z., Worsnop, D. R., and Coe, H.: Changes in Aerosol Chemistry From 2014 to 2016 in Winter in Beijing: Insights From High-Resolution Aerosol Mass Spectrometry, Journal of Geophysical Research: Atmospheres, 124, 1132-1147, https://doi.org/10.1029/2018JD029245, 2019.

Yang, Y., Smith, S. J., Wang, H., Lou, S., and Rasch, P. J.: Impact of Anthropogenic Emission Injection Height Uncertainty on Global Sulfur Dioxide and Aerosol Distribution, Journal of Geophysical Research: Atmospheres, 124, 4812-4826, https://doi.org/10.1029/2018JD030001, 2019.

Yao, X. and Zhang, L.: Identifying decadal trends in deweathered concentrations of criteria air pollutants in Canadian urban atmospheres with machine learning approaches, Atmos. Chem. Phys., 24, 7773-7791, 10.5194/acp-24-7773-2024, 2024.

Yienger, J. J. and Levy, H.: Empirical-model of global soil-biogenic NOx emissions, Journal of Geophysical Research-Atmospheres, 100, 11447-11464, 10.1029/95jd00370, 1995.

Zhai, S., Jacob, D. J., Wang, X., Shen, L., Li, K., Zhang, Y., Gui, K., Zhao, T., and Liao, H.: Fine particulate matter (PM2.5) trends in China, 2013–2018: separating contributions from anthropogenic emissions and meteorology, Atmos. Chem. Phys., 19, 11031-11041, 10.5194/acp-19-11031-2019, 2019.

Zhang, F., Xu, L., Chen, J., Yu, Y., Niu, Z., and Yin, L.: Chemical compositions and extinction coefficients of PM2.5 in peri-urban of Xiamen, China, during June 2009-May 2010, Atmospheric Research, 106, 150-158, 10.1016/j.atmosres.2011.12.005, 2012.

Zhang, Q., Jimenez, J. L., Canagaratna, M. R., Allan, J. D., Coe, H., Ulbrich, I., Alfarra, M. R., Takami, A., Middlebrook, A. M., Sun, Y. L., Dzepina, K., Dunlea, E., Docherty, K., DeCarlo, P. F., Salcedo, D., Onasch, T., Jayne, J. T., Miyoshi, T., Shimono, A., Hatakeyama, S., Takegawa, N., Kondo, Y., Schneider, J., Drewnick, F., Borrmann, S., Weimer, S., Demerjian, K., Williams, P., Bower, K., Bahreini, R., Cottrell, L., Griffin, R. J., Rautiainen, J., Sun, J. Y., Zhang, Y. M., and Worsnop, D. R.: Ubiquity and dominance of oxygenated species in organic aerosols in anthropogenically-influenced Northern Hemisphere midlatitudes, Geophys. Res. Lett., 34, doi: L13801 10.1029/2007gl029979, 2007.

Zhang, Y., Sun, J., Zhang, X., Shen, X., Wang, T., and Qin, M.: Seasonal characterization of components and size distributions for submicron aerosols in Beijing, Science China Earth Sciences, 56, 890-900, 10.1007/s11430-012-4515-z, 2013.

https://doi.org/10.5194/egusphere-2024-3590
Preprint. Discussion started: 4 December 2024

Zhang, Y., Tang, L., Yu, H., Wang, Z., Sun, Y., Qin, W., Chen, W., Chen, C., Ding, A., Wu, J., Ge, S., Chen, C., and Zhou, H.-c.: Chemical composition, sources and evolution processes of aerosol at an urban site in Yangtze River Delta, China during wintertime, Atmospheric Environment, 123, 339-349, https://doi.org/10.1016/j.atmosenv.2015.08.017, 2015a.

Zhang, Y. J., Tang, L. L., Wang, Z., Yu, H. X., Sun, Y. L., Liu, D., Qin, W., Canonaco, F., Prévôt, A. S. H., Zhang, H. L., and Zhou, H. C.: Insights into characteristics, sources, and evolution of submicron aerosols during harvest seasons in the Yangtze River delta region, China, Atmos. Chem. Phys., 15, 1331-1349, 10.5194/acp-15-1331-2015, 2015b.

Zhang, Y. M., Zhang, X. Y., Sun, J. Y., Hu, G. Y., Shen, X. J., Wang, Y. Q., Wang, T. T., Wang, D. Z., and Zhao, Y.: Chemical composition and mass size distribution of PM₁ at an elevated site in central east China, Atmos. Chem. Phys., 14, 12237-12249, 10.5194/acp-14-12237-2014, 2014.

Zhao, P. S., Dong, F., He, D., Zhao, X. J., Zhang, X. L., Zhang, W. Z., Yao, Q., and Liu, H. Y.: Characteristics of concentrations and chemical compositions for PM2.5 in the region of Beijing, Tianjin, and Hebei, China, Atmospheric Chemistry and Physics, 13, 4631-4644, 10.5194/acp-13-4631-2013, 2013.

Zhou, W., Xu, W., Kim, H., Zhang, Q., Fu, P., Worsnop, D. R., and Sun, Y.: A review of aerosol chemistry in Asia: insights from aerosol mass spectrometer measurements, Environ Sci Process Impacts, 22, 1616-1653, 10.1039/d0em00212g, 2020a.

Zhou, W., Xu, W., Kim, H., Zhang, Q., Fu, P., Worsnop, D. R., and Sun, Y.: A review of aerosol chemistry in Asia: insights from aerosol mass spectrometer measurements, Environmental Science: Processes & Impacts, 22, 1616-1653, 10.1039/D0EM00212G, 2020b.